Genetic Tools for the Analysis of Neural Networks in Flies

Thomas Hendel

München 2008

Genetic Tools for the Analysis of Neural Networks in Flies

Thomas Hendel

Dissertation zur Erlangung des Doktorgrades der

Naturwissenschaften

an der Fakultät für Biologie

der Ludwig–Maximilians–Universität

München

vorgelegt von

Thomas Hendel

aus Buchen im Odenwald

München, den 8.01.2008

Erstgutachter: Prof. Alexander Borst

Zweitgutachter: Prof. Rainer Uhl

Tag der mündlichen Prüfung: 11.02.2008

Contents

List of Figures

List of Tables

Abstract

Motion vision is of fundamental importance for moving animals from arthropods to mammals. In this thesis I lay ground for the functional analysis of the neural circuit underlying visual motion detection in fruit flies by means of genetic tools. In *Drosophila melanogaster* transgenic tools allow for both experimental observation and manipulation of neural activity: genetically encoded calcium indicators (GECIs) can be used for the optophysiological characterization of neural activity and transgenes for the inhibition of neural activity can be used to determine these neurons' function. Combined, yet independent use of both tools is a powerful approach for the functional analysis of a neural network. However, GECI signals *in vivo* generally suffer from poor signal-to-noise ratios and GECI characteristics change dramatically and unpredictably when transfered from the cuvette into neurons of living animals, probably due to interactions with native cellular proteins.

Here, I quantified and compared the *in vivo* response properties of five new (Yellow Cameleon 3.60 & 2.60, D3cpV, TN-XL and TN-XXL) and two more established ratiometric GECIs (Yellow Cameleon 3.3, TN-L15). In addition, I included the single-chromophore probe GCaMP 1.6 in this comparison. The analysis was performed under 2-photon microscopy at presynaptic boutons of neuromuscular junctions in transgenic fly larvae. I quantified action potential induced changes of calcium concentrations by calibrating responses of a synthetic calcium indicator that was microinjected under 2-photon guidance. The observed cytosolic calcium concentration was 31 nM at rest and increased linearly with stimulus frequency by 0.1 to 1.8 μM at sustained activity of 10 and 160 Hz, respectively. This allowed for a quantitative comparison of the responses of GECIs in terms of their steady state response amplitudes, signal-to-noise ratio, response kinetics, calcium affinities and hill coefficients *in vivo*. The results were then compared to *in vitro* properties of GECIs measured in cuvettes.

The data reveal that a new generation of GECIs retain improved signalling characteristics *in vivo*. Maximum fluorescence changes were 2-3 fold increased in new compared to former ratiometric GECI variants. Small calcium changes in response to 10 Hz stimulation

induced fluorescence responses with signal-to-noise ratio above 2 in Yellow Cameleon 2.60 & 3.60, D3cpv and TN-XXL. Kinetics were slowest in Yellow Cameleon 2.60 and fastest in TN-XL. The observed changes between *in vitro* and *in vivo* performance revealed systematic differences between GECIs of different types. GECIs in this study employ different calcium sensing molecules: calmodulin-M13 in Yellow Cameleons and GCaMP, a redesigned calmodulin-M13 in D3cpv, and troponin C in TN-indicators. Those indicators comprising calmodulin-M13 as calcium sensors displayed reduced maximum fluorescence changes and reduced hill coefficients *in vivo*, while troponin-based GECIs and D3cpv showed increased hill coefficients and increased maximum fluorescence changes *in vivo*. Calcium affinity of all GECIs was increased *in vivo*. The results demonstrate that there are now suitable GECIs at hand for experimental questions at differing expected calcium regimes. However, in contrast to a synthetic calcium sensor, none of the tested GECIs reported calcium concentration changes related to single action potentials at presynaptic boutons of the neuromuscular junction.

In the visual system of *Drosophila*, optical recordings from motion sensitive neurons while selectively blocking certain classes of columnar neurons will allow for a network analysis of the motion detection circuit. The Gal4-UAS system can be used to express proteins that block neural activity. A similar two-part expression system, based on bacterial protein-DNA interaction (LexA and LexA-operator), can be used in parallel to drive the expression of GECIs. I generated flies expressing TN-XXL or Yellow Cameleon 3.60 under the control of the LexA-operator and demonstrated GECI expression in olfactory receptor neurons. In parallel, I cloned putative genomic enhancers that can be used to drive LexA expression in motion sensitive cells of the flies visual system.

Finally, adult fixed flies expressing TN-XXL in motion sensitive neurons were visually stimulated by large field moving gratings. Parallel fluorescence measurements from these neurons showed for the first time directional selective calcium responses in *Drosophila*. The next step will now be the combination of calcium imaging in these neurons and functional blocking of their presynaptic partners.
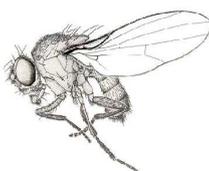
1 Introduction

Animals including humans care for what changes in the world and ignore what does not. For most sensory systems, changes are what matters most. This selective processing of variable input is not under voluntary control. Constant sensory input is suppressed e.g. by adaptation - with the unfortunate exception of nociception [1]. In the human visual system the preferred processing of changing inputs is so prominent, that our eyes perform involuntary microsaccades, drifts and tremors during object fixation. If these movements are suppressed, visual perception usually vanishes. One can experience the consequence in the Troxler's effect [1]. Eye movements keep the visual world stable so to speak. Thus, motion is not merely a feature of visual scenes but a prerequisite of vision. A closer look at eye movements raises an interesting problem: How does a perceiving subject judge whether image motion on its retina is produced by itself or by the external world?

When a small object in the visual scene is moving, like a fly buzzing around in front of us, we perceive the fly as moving and ourselves as stable. From the fly's perspective, the whole visual scene is moving, which is a good indicator of self motion, as the world at large is mostly stable. The same assumption sometimes tricks humans e.g. when we look out of the window of a stagnant train and see a train on the neighbor track starting to move. The large field motion on the retina elicits the impression of self motion. The percept is the stronger, the larger the optic flow field is. When seeing a rotating cylinder from the inside, a test person cannot help perceiving self motion, despite cognitive knowledge about being steady and the cylinder rotating and despite the lack of corresponding signals from the vestibular system. How is this percept generated by a neural circuit in brains?

It turns out that specialized cells involved in processing of large field visual information likely signal self motion in the brains of monkeys [2] and flies [3, 4]. In blowflies, these cells have been extensively studied (reviewed in [5]). However, the neural circuit underlying motion detection remains elusive, because most of the neurons in the brains of blowflies have escaped electrophysiological characterization due to their small size. In our laboratory, we study the even smaller fly *Drosophila melanogaster* in spite of the even smaller cell sizes and

the minor depth of physiological knowledge, because of the genetic tools available. These may allow to dissect the motion detection circuit at a cellular and biophysical level [6] by two types of experiments: First, I want to characterize the responses from various types of cells in the fly's visual system by optical imaging using genetically encoded calcium indicators (GECIs) and second, I want to deactivate cell types presynaptic to motion sensitive cells to assess their functional contribution to motion detection circuits. Yet, in initial imaging experiments we could not detect motion responses using GECIs in cells that are known to be motion sensitive.

In this thesis I therefore focused on a thorough characterization of GECIs that ultimately revealed a new GECI that allowed recordings of motion responses in fruit fly visual interneurons. In parallel I started to adapt a transgene expression system for fruit flies, that can be used together with the well established Gal4-UAS system, to express two different transgenes for the detection and manipulation of activity in independent sets of neurons.

1.1 Motion Vision in Flies

Drosophila's compound or facet eye consists of roughly 800 ommatidia in a hexagonal arrangement. Each ommatidium has a lens and comprises 2 central photoreceptors (R7&8) that are surrounded by 6 peripheral photoreceptors (R1-6). R1-8 gather visual information in the retina. This information is processed in the visual ganglia in three successive neuropils (see Fig 1.1 A): the lamina, the medulla and the lobula complex, that is split into lobula plate and lobula. These neuropils are structurally layered and organized in retinotopic columns [7]. Tangential neurons contact all or subsets of columns, mainly within one layer.

In the third visual neuropil, the lobula plate (lobula plate, see Fig 1.1 A), a group of large, non-columnar interneurons have been characterized that show directional selective responses to large field visual motion, the Lobula Plate Tangential Cells (LPTCs; see Figs 1.1 & 1.2). They have extensive arborizations in the lobula plate and project either to the central brain or the contralateral optic lobe. When a moving grating is presented to a tethered blowfly, electrophysiological recordings from these cells reveal directional selective motion responses: Depolarization in one direction of motion and hyperpolarization in the opposite direction. Different subsets of LPTCs have been classified according to their preferred axis of motion and anatomy [8, 3] (see Figs 1.1 & 1.2). For example, in *Calliphora*
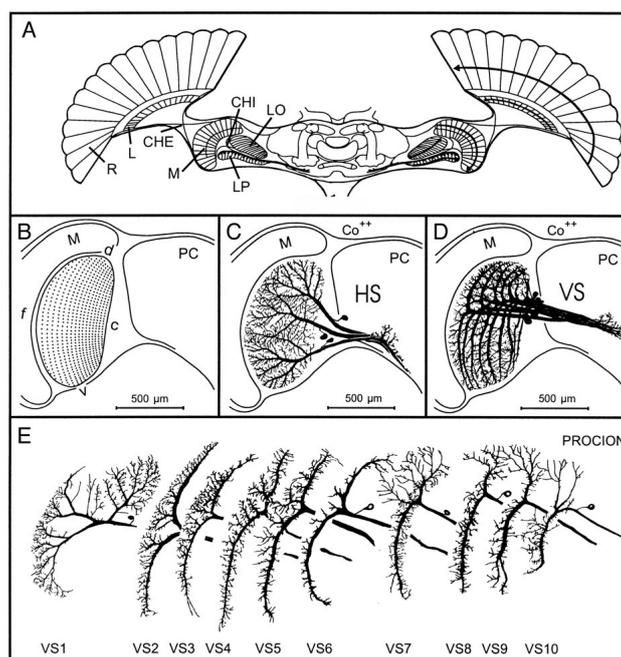
Figure 1.1: Visual system of the blowfly. (A) Schematic horizontal section showing the retina (R) and the 3 visual neuropils: lamina (L), medulla (M), and the lobula complex with lobula (LO) and lobula plate (LP). Fiber tracts (CHE, CHI) connecting the neuropils preserve the retinotopy over chiasms (indicated by inverted arrows in retina and medulla). Output neurons of the lobula plate converge on descending neurons. (B) Retinotopic representation of the right visual hemisphere in the right lobula plate viewed from anterior (f, frontal; c, caudal; d, dorsal; v, ventral). (C) 3 neurons constitute the "horizontal system (HS)". Their dendrites fill the anterior layers of the lobula plate. Each extends over roughly 1/3 of the neuropil. (D) 10 neurons of the "vertical system" (VS) with arborizations mainly in the posterior layers. Their dendritic fields are vertically oriented, stacked from the distal to the proximal margin of the lobula plate. Together they cover retinotopic extent of the neuropil. (E) Individual dendrites of the 10 VS neurons drawn apart to reveal their distinct structures. The fan-shaped dorsal branches of VS1 and VS7-VS10 are located in anterior layers. Picture taken from [4].

cells of the Horizontal System (3 HS cells)(Fig 1.1 C) are most sensitive to horizontal image motion as occurring during rotation around the fly's vertical body axis (see Fig 1.2). Cells of the Vertical System (10 VS cells, Fig 1.1 D&E) are most sensitive to rotation around different axes along the azimuth of the fly [9, 10, 4] (see Fig 1.2). The complex receptive fields of LPTCs are well described. They are shaped by input from columnar elements and from other LPTCs, by electrical coupling via gap junctions and excitatory and inhibitory

synapses [11, 12, 13, 14, 15, 16, 17]. But how is motion information computed from the input to photoreceptors?
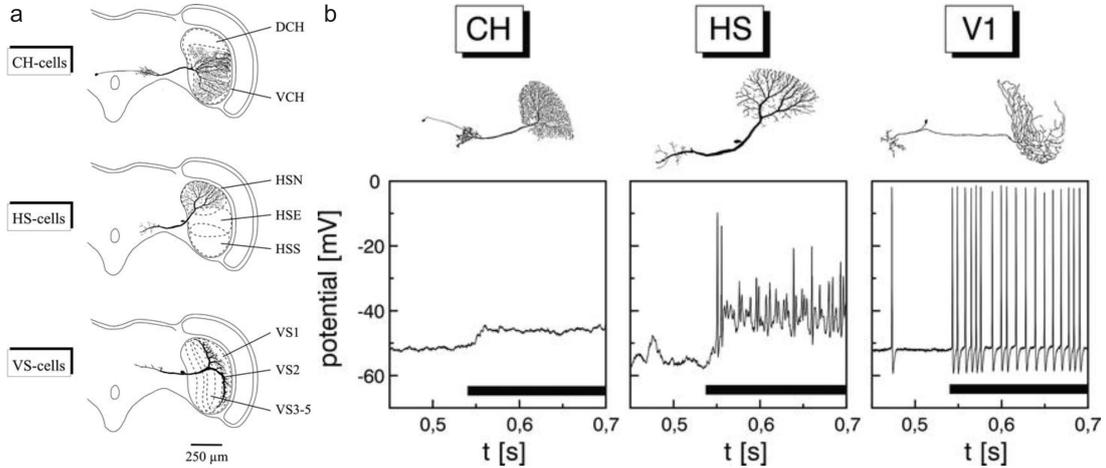
Figure 1.2: Anatomy and preferred direction responses of some lobula plate tangential cells (LPTCs). (a) LPTCs in *Calliphora* as seen from a posterior view of sagittal brain sections. The neuropil to the right is the medulla. Lamina and retina are not shown. From each of three LPTC families, one member is represented. Hatched lines in the lobula plate indicate areas covered by the dendrites of the other family members. (b) LPTCs respond to preferred direction motion (indicated by black bars under voltage traces) in various ways, from purely graded (Centrifugal Horizontal cells), over mixed (Horizontal System cells) to purely spiking (cells sensitive to vertical image motion, V1-cell). Picture taken from [5].

Responses from individual photoreceptors to a moving image, do not encode motion information. At this level, directional information is only represented in temporal relations of signals from neighboring photoreceptors [18]. Thus, comparison of photoreceptor signals at different points in space and time allows the extraction of motion information. A delay between signals from different points can be interpreted as motion. In simple words: if a signal was detected from point A and the same signal appears in point B shortly thereafter, it maybe that the signal source has moved from A to B.

Behavioral studies on the beetle *Clorophanus* led to an influential algorithmic model of a motion detection circuit [18] known as the 'correlation-type of motion detector', also called the 'Reichardt detector'. This model assumes two essential operations to perform the above outlined comparison: First, asymmetrical temporal filtering, i.e. low-pass filtering of one signal, and second a nonlinear interaction, in which the low-pass filtered signal from one image location is multiplied with the signal from the neighboring image location. This

can produce a motion sensitive directional selective output [5]. Predictions derived from this algorithmic model were experimentally shown to hold true in behavioral [19, 20] and physiological experiments (e.g. [21, 12, 22], reviewed in [5]).

Cells postsynaptic to photoreceptors and presynaptic to LPTCs are assumed to perform calculations underlying such a comparison. Each column within one neuropil contains a stereotypic set of neurons, termed 'columnar elements'. These have been described anatomically in detail in several dipteran fly species [23] including *Drosophila melanogaster* [7]. It is uncertain whether these catalog of cells are complete. Columnar neurons ramify in specific layers of neuropils. The sites of ramifications give hints towards possible connectivity of different columnar neurons and importantly towards parallel retinotopic processing channels [7]. However, this remains speculative, as electronmicroscopic studies demonstrating synaptic connections between columnar neurons are lacking. Also, apart from lamina neurons the electrophysiology of columnar neurons in flies is unknown with few exceptions ([24, 25] in the blowfly *Phormia* and [26] in the fleshfly *Sarcophaga*). Anyway, based on the available data possible parallel information processing pathways for motion detection have been proposed [27, 23]: In the retina photoreceptors R7-8 are dispensable for motion vision and necessary for color discrimination, while R1-6 provide input to the motion channel [28] by contacting the large lamina monopolar cells L1 and L2 within the lamina (see Fig 1.3 B). The L1 pathway is thought to activate the intrinsic medulla neuron Mi1 that may synapse onto T4 cells in the proximal medulla (see Fig 1.3 D). T4 cells exist in four types, each connecting the outer-most layer of the medulla to one of 4 layers of the lobula plate (see Fig 1.3 E). Also, they have been shown to contact HS cells [11]. In parallel, the L2 pathway is thought to contact the transmedullary neuron Tm1, that projects to the posterior layer of the lobula (see Fig 1.3 C). There, T5 cells ramify and may relay information to LPTCs (see Fig 1.3 E). Like T4 cells, 4 types of T5 cells ramify each in a different layer of the lobula plate.

Evidence for the involvement of the outlined pathways was based on morphological criteria, that assume connections between cells that ramify within the same layers in the optic lobes of blowflies or fruit flies [23, 7]. Another line of evidence came from activity dependent 2-Deoxy-Glucose labeling, in which specific layers of the lobula, the lobula plate and the medulla were stained after motion stimulation in fruit flies [29, 27]. Mutant analysis of *Drosophila* supported the hypothetical pathways [30, 31]. Recently a transgenic approach in *Drosophila* provided good evidence for L1 and L2 and the amacrine T1 neurons in the Lamina to provide all information to the motion pathways from the lamina [32] (see
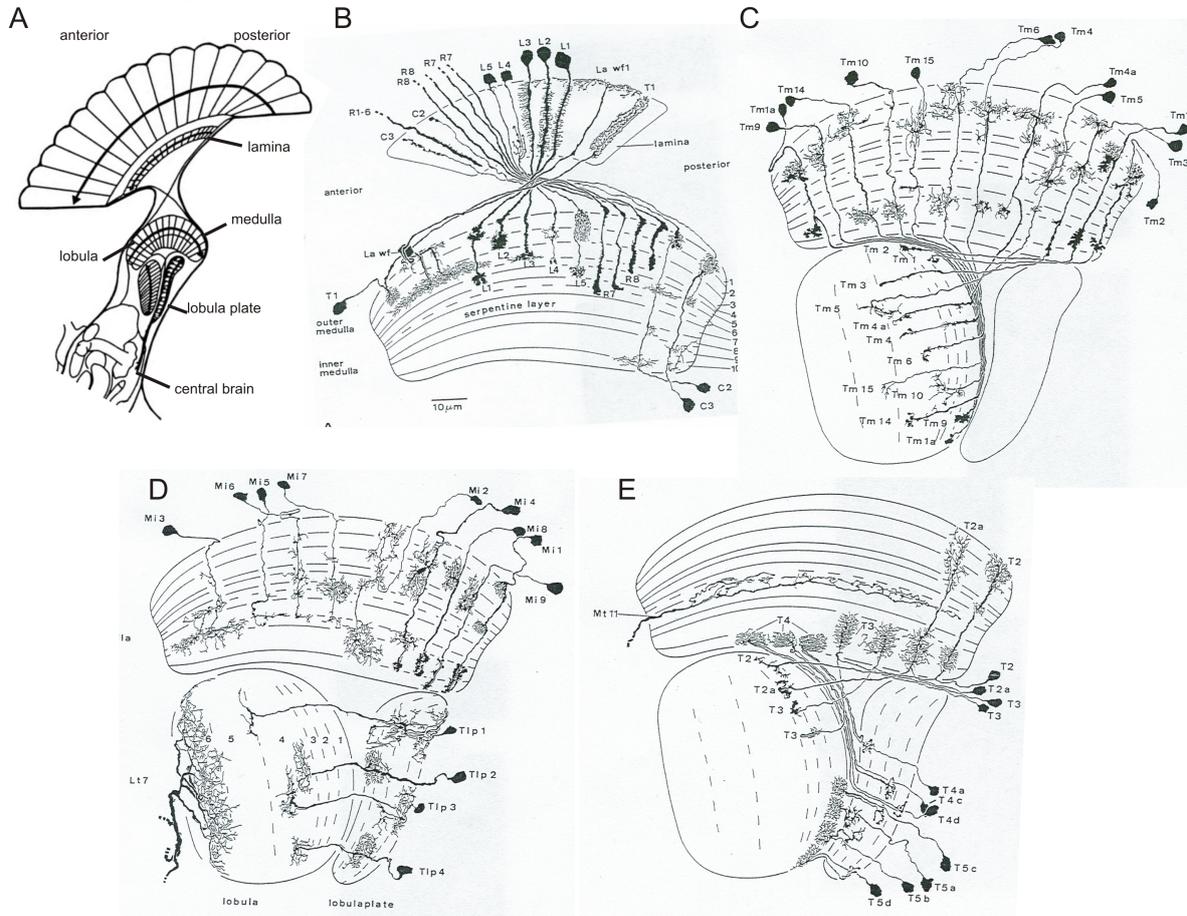
Figure 1.3: Camera lucida drawings of columnar neurons stained by golgi impregnations. (A) Schematic from Fig 1.1 gives orientation for all further images. (B) Outlined are lamina and medulla. L1, L2 and amacrine T1 cells are implicated in motion vision. (C) Outlined are medulla and lobula complex. Tm1 cells are implicated in motion vision via the L2 pathway. (D) Outlined are medulla and lobula complex. Mi1 cells are implicated in motion vision via the L1 pathway. (E) Outlined are medulla and lobula complex. Bushy T4 and T5 cells probably synapse onto LPTCs and are implicated in motion vision via L1 and L2 pathway, respectively. Figures from [4, 7].

Fig 1.4). However, while in mammals a possible mechanism for directional selectivity intrinsic to starburst amacrine cells has been identified [33, 34], in flies the mechanism or cellular network performing these calculations remains unknown.

The neural architecture of the visual systems of different dipteran species has been assumed to be evolutionarily preserved. Even if this is not completely true [7, 35], insights from other dipteran species can at least provide good working hypotheses for experiments
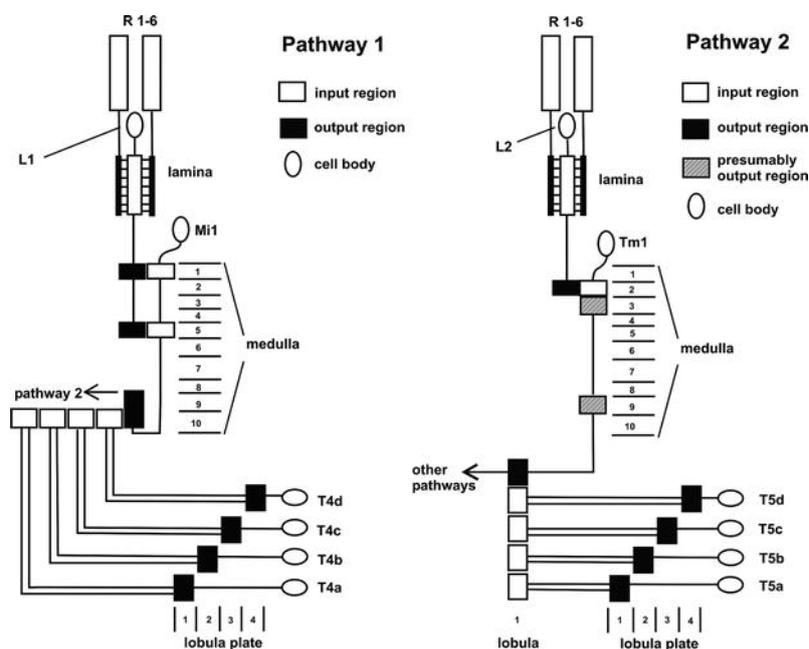
Figure 1.4: Neuronal pathways from photoreceptors to the lobula plate. Two pathways
were suggested based on anatomical studies. Pathway 1 involves L1 from the
lamina to medulla and Mi1 cells feeding into T4 cells, that contact LPTCs in
the 4 different layers of the lobula plate. Pathway 2 involves L2 cells from the
lamina, that feed into Tm1 cells in the medulla. Those synapse onto T5 cells
that contact LPTCs in the 4 layers of the lobula plate. Figure from [5].

on a different species. In fruit flies the small size and correspondingly small neurons com-
plicate electrophysiological characterizations. Only recently, however, the first electrical
recordings from LPTCs have been achieved in our laboratory (Maximilian Joesch-Krotki,
unpublished data). Basic features of the response properties of blowfly VS cells were also
found in VS cell responses of fruit flies. Calcium imaging with GECIs is a promising
alternative method to assess the response profiles of visual interneurons.

1.2 Calcium Imaging

GECI-based imaging [36] in principle allows physiological characterization of individual
neurons. However, available sensor proteins do not provide the signal-to-noise ratios
achieved with synthetic probes yet [37, 38, 39, 40]. Moreover, the choice of the most
promising sensor protein is difficult for two reasons: first, descriptions of sensors from
different laboratories cannot directly be compared due to variable test conditions. Sec-

ond, signal properties of such sensors change dramatically between *in vitro* and *in vivo* conditions. Thus a simple, reproducible test system was established that allows for a quantitative comparison of indicator performance *in vivo*. This was done by 2-photon imaging of calcium activity at the neuromuscular junction of fly larvae.

Measures of Neural Activity   Neuronal activity is most accurately measured with intracellular electrodes, providing greatest possible temporal resolution. Spatial information however is poor in electrophysiology, as only a limited number of intracellular electrodes can be used on one specimen or neuron. Extracellular electrodes and multi electrode arrays provide some spatial information but detect only spiking activity without identifying the recorded cells anatomically.

Spatial distribution of activity in neurons or ensembles of neurons can be acquired by electromagnetic measures: fMRI (functional magnetic resonance imaging) leaves the specimen largely unperturbed. It visualizes the local oxygenation level of hemoglobin, which is associated with neural activity, however, fMRI gives poor spatial (1 mm^3) and temporal (1-4 s) resolution. The same is true for PET (positron emission tomography), which is also based on increased metabolism of active neurons. In PET a radioactive, metabolically active substance is applied and the emitted gamma rays are sampled for reconstruction of 3-dimensional activity maps. PET and fMRI allow visualization of neural activity through the intact skull. Both are suitable for sampling from large volumes of tissue. Intrinsic imaging also measures metabolic activity correlates with poor spatial resolution.

Activity distribution in cellular compartments can be observed with fluorescent sensor molecules that signal correlates of neural activity such as membrane potential [41], synaptic vesicle release [42] or fluxes of the ions chloride [43], sodium [44], potassium [44], magnesium and calcium [45, 46, 47]. In particular, genetic probes for calcium ion concentration have become an important tool in neuroscience over the past ten years. The mechanism of fluorescence is the same in synthetic molecules and proteins.

Fluorescence   Fluorescence microscopy is a form of dark field microscopy. The name stands in contrast to bright field microscopy where the whole specimen is illuminated, while in fluorescence microscopy only the fluorescent molecules inside a specimen are made visible: In fluorescence the molecular absorption of a photon triggers the emission of a photon of longer wavelength (see Fig 1.5). Conceptually this can be described in three steps (see Fig 1.5 A). First, an electron is excited from ground state (S_0) to a singlet state (S_1-S_3) by one or more photons that provide a certain energy. Second, this excited state

lasts for about 1-10 ns. During this time an electron interacts with the environment and
its energy is partly dissipated to state S_1. Third, the electron returns to the ground state
S_0 under emission of a photon. Alternatively an electron can return to S_0 by non-radiative
decay, e.g. by collisional quenching, FRET, and intersystem crossing to triplet states. The
electronic states of a fluorescent molecule are depicted in a Jablonski diagram (see Fig 1.5).
The efficacy of photon absorption is quantified in the extinction coefficient (55.000-57.000
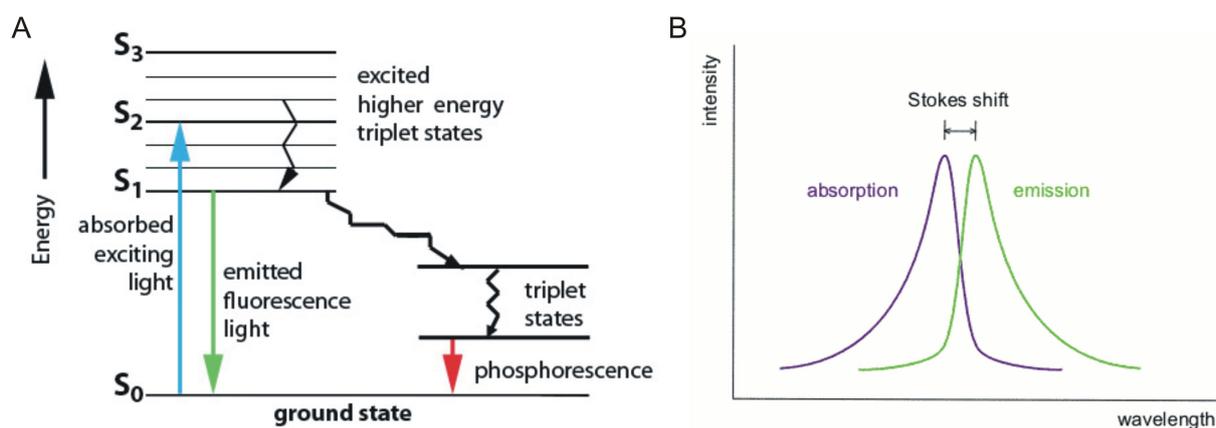
Figure 1.5: Fluorescence mechanism. (A) The Jablonski diagram illustrates electronic
states of a fluorescent molecule. Absorption of a photon can lead to exci-
tation of an electron (blue arrow) from groundstate to excited singlet states
(S1-3). Thick lines indicate more stable states. Transitions back to the ground
state can lead to radiation: Fluorescence occurs when transition from excited
to ground state occurs directly - a photon is emitted (green arrow). Other
transitions can lead to other forms of radiation including phosphorescence. (B)
When the emitted photon has less energy than the absorbed photon, this en-
ergy difference is the Stoke shift. This is apparent in the difference between
the maximum absorption and emission wavelengths.

$molar^{-1}$ cm^{-1} for EGFP). The fluorescence efficacy or quantum yield is defined as the
amount of photons emitted over the amount of photons absorbed, that is, the portion of
electrons that return to the groundstate directly by emission of a photon. It cannot exceed
1 (0.60 for EGFP). The product of absorption and quantum yield define the brightness
of a fluorophore. For EGFP excitation peaks at 488 nm and emission at 509 nm. The
difference between peak excitation and emission wavelengths is called 'Stoke shift' (see Fig
1.5 B). Another characteristic of a fluorescent molecule is its fluorescence lifetime, which
describes the time it stays in the excited state before a photon is emitted (typically 1-10
ns) [48, 49].

1.2.1 Synthetic Calcium Indicators

The first synthetic calcium sensor was originally described as heavy metal ligand in 1959 (ArsenazoIII [50, 51]). Early sensors suffered from several difficulties: (i) insufficient calcium selectivity over magnesium; (ii) complex stoichiometries of calcium binding, e.g. 1 calcium binds 2 indicator molecules; (iii) inflexible molecular design; (iv) impractical excitation wavelength (339 nm for Quin2); (v) low extinction coefficient and quantum yield. These problems were solved stepwise till currently available indicators were developed (e.g. Quin2 and BAPTA [45], Fura and Indo [47], Fluo and Rhod [52]).

1.2.2 Genetically Encoded Calcium Indicators - GECIs

The first protein-based optical calcium sensor used in biological experiments, aequorin, was isolated from the hydromedusa *Aequorea forskalea* [53, 54]. The aequorin protein has several EF-hands. An EF-hand represents a helix-loop-helix motif of $\approx$ 30 amino acids that is capable of coordinating one calcium (or magnesium) ion. EF-hands are the most common calcium binding domains in nature and occur as pairs in proteins so that most EF-hand containing polypeptides have 2, 4, 6 or more EF-hand domains (e.g. parvalbumin or calmodulin). The most important part of the domain is the loop region that gives rise to the coordination space through predominantly negatively charged amino acid residues. Together with the prosthetic group coelenterazine, aequorin emits blue light upon calcium binding. Medusans coexpress a green fluorescent protein (GFP) with aequorin (see Fig 1.6) in the same set of cells [55]. Part of aequorins blue light emission is absorbed by GFP which emits photons of slightly longer wavelengths [49], appearing green.

GFP

The history of discovery, analysis and development of GFPs is in depth reviewed by Roger Tsien in [49]. A brief wrap up: When aequorin and GFP were first described in 1962 scientists' interest focused on aequorin as a tool for sensing intracellular calcium concentrations [54]. In 1992 the GFP sequence was described by Douglas Prasher [56] and it was first used to trace translation of other proteins in 1994 [57]. Although crystallized already in 1974 [58] it took until 1994 to resolve its structure [59, 60] (see Fig 1.6 A). GFP is barrel shaped. The wall consists of 11 beta sheets and an alpha helix runs through the center of the barrel. The chromophore is assembled in the heart of the barrel by a sequence of reactions of the amino acids 64-66, namely Ser, Tyr and Gly (see Fig 1.6 B) [49]. Al-
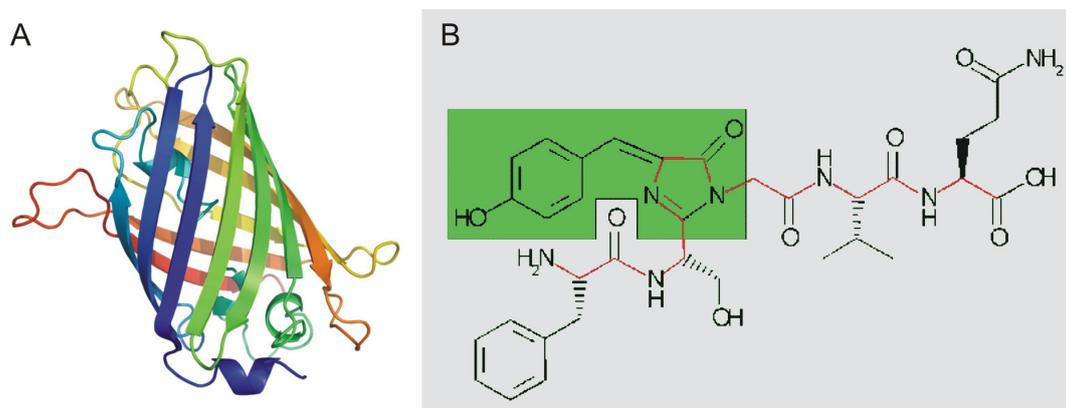
Figure 1.6: Structure of GFP. (A) Schematic structure of the GFP beta barrel. The chromophore is hidden inside the barrel. (From Richard Wheeler free at wikipedia.org) (B) The chemical structure of the chromophore peptide from *Aequorea victoria* GFP. The chromophore itself is a p-hydroxybenzylidene-imidazolidone (green background). It consists of residues 64-66 (Ser - dehydroTyr - Gly) of the protein. The cyclized backbone of these residues forms the imidazolidone ring. The peptide backbone trace is shown in red. (From Silke Jonda's PPS2 project, Birkbeck College, London, UK.)

though this amino acid sequence can be found in a number of other proteins as well, it is neither cyclized in any of these, nor is the tyrosine oxidized, nor are these proteins fluorescent. This implies that the tendency to form such a chromophore is no intrinsic property of this tripeptide. Researchers inserted mutations in various amino acid residues in and around the chromophore to alter and improve protein properties for biological applications (see Table 1.1): the lower of two excitation peaks has been eliminated, different spectral variants were generated and fluorescence was increased [49], environmental sensitivity to pH-changes and chloride ions was decreased [61], folding was enhanced [62] or properties were optimized for FRET [63] (see Fig 1.7 & Table 1.1). A number of other fluorescent proteins from different marine organisms are available for biological applications now [64].

GECIs

In 1997 GFP-based calcium sensors were developed by Atsushi Miyawaki in the laboratory of Roger Y. Tsien [36]. These sensors, named Cameleons because they change color upon calcium binding, were fusion proteins consistent of two spectrally overlapping GFP variants, which sandwich the calcium binding protein calmodulin, a glycylglycine linker and the calmodulin binding peptide of myosin light-chain kinase (M13) (see Fig 1.7). Cal-

XFP[(0)]	**Exc**[(1)]	**Ext**[(2)]	**Em**[(3)]	**QY**[(4)]	**Mut**[(5)]	**GECI**[(6)]
wtGFP	396 & 472	25-30& 9.5-14	504	0.79	- or Q80R [49]	-
EGFP	488	55-57	508	0.60	wtGFP; F64L, S65T [49]	Cameleon-1, cp in GCaMPs
ECFP	433	29	476	0.37	wtGFP; F64L, S65T, Y66W, N146I, M153T, V163A, N164H, N146I, M153T, V163A [49]	YC-2.60,-3.60, D3cpv, TN-L15, TN-XL, TN-XXL
Cerulean	433	43	475	0.62	ECFP; S72A, Y145A, H148D [65]	TN-L15 cerulean
EYFP	516	62	529	0.71	wtGFP; S65G, V68L, Q69K, S72A, T203Y	YC2.0,-3.0 , -4.0, -6.0
Citrine	515	82	527	0.76	wtGFP; S65G, V68L, Q69M, S72A, T203Y [61]	YC3.3, TN-L15
cpCitrine	515	94	527	0.75	Citrine; cp174 [66]	TN-XL, TN-XXL
Venus	515	92	528	0.57	EYFP; F46L, F64L, M153T, V163A, S175G [62]	YC2.12
cpVenus	515	92	528	0.57	Venus; cp173 [67]	YC3.60, -2.60, D3cpv

Table 1.1: Table of selected relevant GFP variants. [(0)] Common name of variant X of GFP. [(1)] Peak excitation wavelength (nm). [(2)] Extinction coefficient ($x10^3$ $molar^{-1}$ cm^{-1}). [(3)] Peak emission wavelength (nm). [(4)] Quantum yield. [(5)] Amino acid substitutions referring to the GFP variant stated first. [(6)] GECIs, the respective GFP variant is employed in. cp - circular permutation, YC - Yellow Cameleon.

cium binding changes fluorescence properties of these fusion molecules. In the same year Romoser and colleagues had described a similar indicator composed of M13, sandwiched between two chromophores [68]. Here, binding of 4-calcium-bound native calmodulin to M13 induces the fluorescence changes. Both sensor protein signals rely on a physical effect known as Fluorescence or Foerster Resonance Energy Transfer (FRET).

FRET In FRET, a donor chromophore in its excited state, transfers energy to an acceptor chromophore in close proximity (typically $< 10\ nm$) by a nonradiative, long-range dipole-dipole coupling mechanism. Although the process does not involve fluorescence emission, overlap of the donors emission and the acceptors excitation spectra is a prerequisite for FRET from the lower wavelength variant e.g. cyan fluorescent protein (CFP, donor fluorophore) to the longer wavelength fluorophore, e.g. yellow fluorescent protein (YFP, acceptor chromophore), as shown in Fig 1.7. The binding of M13 to calmodulin is calcium dependent and changes the relative orientation and position of the two chromophores. Thus, FRET becomes a function of the calcium concentration. The efficiency, E, of FRET drops steeply with increasing distance, R, between the fluorophores, according to the equation $E = [1 + (R/R_0)^6]^{-1}$. The characteristic distance, R_0, at which FRET efficacy is 50 % depends on the quantum yield of the donor fluorophore, the extinction coefficient of the acceptor, and the overlap of the spectra of the donor's emission and the acceptor's excitation. FRET can yield 98 % efficacy in CFP/YFP pairs [69].
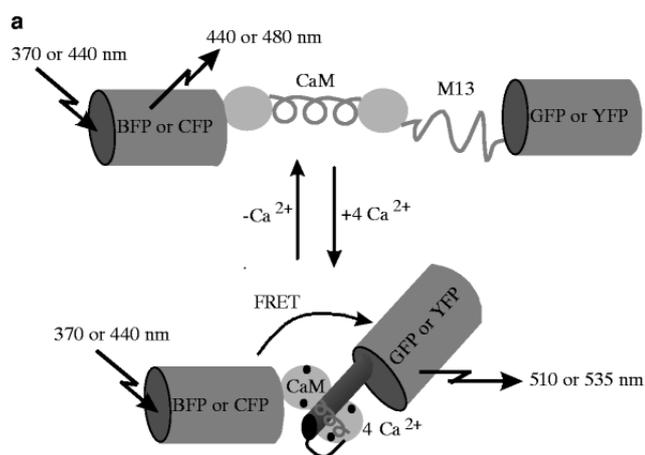
Figure 1.7: Illustration of FRET in Yellow Cameleons. Grey cylinders illustrate GFP barrels. Binding of 4 calcium ions to calmodulin probably changes the relative distance and orientation of both chromophores, and increases FRET between them (Taken from the first description of Cameleon [36])

Traditional Ratiometric GECIs All GECIs used in this study are summarized in Table 1.2 and depicted in Fig 1.8. In practice, ratiometric indicators require the simultaneous measurement of both emission wavelengths for the determination of FRET changes. The ratiometric measurement cancels out imaging artifacts that affect both wavelengths equally, like intensity fluctuations of the excitation light source and motion along the X-, Y- and

GECI	GFP types	Ca sensor	Ref
Yellow Cameleon 3.3	ECFP & Citrine	xl calmodulin (E104Q) & M13	[61]
Yellow Cameleon 3.60	ECFP & cpVenus	xl calmodulin (E104Q) & M13	[67]
Yellow Cameleon 2.60	ECFP & cpVenus	xl calmodulin & M13	[67]
D3cpv	ECFP & cpVenus	xl calmodulin (I14F, F19L, V31Q, M36L, L39) & M13	[71]
TN-L15	ECFP & Citrine	cs troponinC	[72]
TN-XL	ECFP & cpCitrine	cs troponinC	[66]
TN-XXL	ECFP & cpCitrine	cs troponinC	(MM)
TN-XXL SF	ECFP SF & cpCitrine SF	cs troponinC	(MM)
GC1.6	EGFP	xl calmodulin & M13	[73]
GC2	EGFP	xl calmodulin & M13	[74]

Table 1.2: GECIs analyzed *in vivo* in this thesis. Name, Incorporated GFP variants, Calcium sensor proteins with respective mutations and original publication are listed. xl - *Xenopus laevis*, MM - *Marco Mank*, unpublished data.

Z-axis of imaging. However, artifacts like bleaching, which affect the two chromophores differentially, are not canceled. Uncorrelated noise may even be enhanced by the division step in ratiometric analysis. A fundamental problem is bleed-through of emitted light from one channel into the other, which cannot be avoided with the emission spectra and stoke shifts todays chromophores exhibit [70]. However, the benefits and promises of FRET GECIs have led to the development of dozens of variants, the most promising of which will be reviewed and analyzed here.

The confusing nomenclature i.e. numbering of Yellow Cameleons has historical reasons and requires some clarification: The first number refers to the calcium binding protein calmodulin and its interaction domain. E.g. Yellow Cameleons 2 and 3 differ in affinities to calcium ions because of one amino acid exchange in calmodulin, 4 contains a different mutation, 5 has apparently never left the laboratory, 6 contains a different calmodulin interaction peptide (from the calmodulin-dependent kinase kinase). The numbers after the point indicate varied and improved fluorophores. E.g. x.1 indicates the introduction of an EYFP, x.12 the introduction of Venus, x.2 the introduction of a new circularly permutated ECFP (see 1.2.2) and x.3 the introduction of Citrine (see Table 1.1). Cameleons were stepwise developed much like above described for synthetic calcium sensors. The original constructs [36] contained a EBFP/EGFP pair (Cameleon-1) and a CFP/YFP pair

YC3.3	CFP	CaM	M13	Citrine

YC3.60	CFP	CaM	M13	cpVenus

YC2.60	CFP	CaM	M13	cpVenus

D3cpv	CFP	CaM*	M13*	cpVenus

TN-L15	CFP	TnC	Citrine

TN-XL	CFP	TnC	cpCitrine

TN-XXL	CFP	TnC	cpCitrine

TN-XXL SF	CFP SF	TnC	cpCitrineSF

GC1.6	CaM	cpEGFP	M13

GC2	CaM	cpEGFP	M13
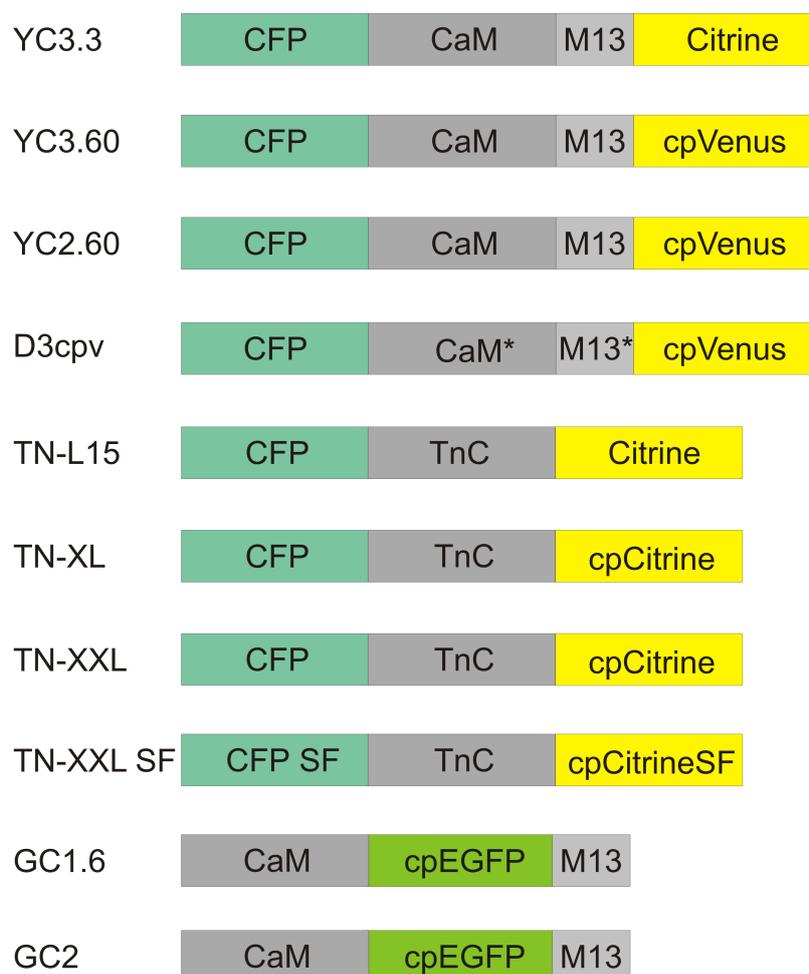
Figure 1.8: Composition of all GECIs used in this study. For details see text. Major differences between variants are: Yellow Cameleon (YC) 3.3 consists of a CFP, calmodulin (CaM) and M13 and Citrine. In variant 3.60 the acceptor chromophore is the circular permuted (cp) Venus. In variant 2.60 calcium affinity is increased due to a mutation in calmodulin. In D3cpv, calmodulin and M13 interaction sites of Yellow Cameleon 3.60 were complementary redesigned. TN-L15 differs from Yellow Cameleon 3.3 in the replacement of calmodulin-M13 with troponin (TnC). In TN-XL magnesium sensitivity and calcium affinity of TnC were reduced, and Citrine was replaced with cp Citrine. In TN-XXL TnC was modified to increase its calcium affinity compared to TN-XL. In TN-XXL SF mutations were introduced in both chromophores to increase protein folding. GCaMP (GC) 2 differs from GCaMP 1.6 in mutations that inhibit dimerization and increase brightness at $37^\circ C$.

(Yellow Cameleon-2 and -3). Their calcium sensor is wild-type calmodulin, which has 2 N-terminal and 2 C-terminal calcium binding sites (EF hands) of differing calcium affinity.

This causes a biphasic calcium binding curve. The amino acid substitution E104Q in the third complexation loop of *Xenopus* calmodulin removed the high affinity phase from Yellow Cameleon 2 resulting in variant -3 with a monophasic calcium response curve. Variant -4 with the mutation E31Q in the first calcium complexation loop shows a biphasic response curve with reduced calcium affinity (k_Ds of Cameleon -1: 11 μM & 70 nM, Yellow Cameleon 2: 700 μM & 83 nM, Yellow Cameleon 3: 4.4 μM [36]).

Early sensors showed deficits when applied in living organisms, especially in mammalian neurons: Fluorophores suffered from poor fluorescence properties, slow folding and chromophore maturation, sensitivity of the acceptor fluorophores to pH and chloride and fast photobleaching. pH sensitivity is a problem for neuronal calcium sensors because sustained neural activity is accompanied by cytosolic acidification, which can corrupt calcium associated fluorescence signals. This was addressed by the mutations V68L and Q69K, adjacent to the chromophore in EYFP (Yellow Cameleon 2.1 and 3.1 [75]). Citrine was derived from EYFP by the mutation Q69M. This led to lowered pKa (5.7), indifference to chloride, improved photostability and improved expression at 37°C. It was introduced e.g. in **Yellow Cameleon 3.3** [61], that will be analyzed in depth here. Citrine has excitation and emission peaks of 516 and 529 nm, respectively, a quantum yield of 0.76 and an extinction coefficient of 77,000 $molar^{-1}\ cm^{-1}$. A different mutation (F46L) in EYFP produced "Venus", with accelerated oxidation of the chromophore, which is thought to be the rate limiting step in the maturation at 37°C [49]. Further amino acid exchanges (F64L, M153T, V163A S175G) caused improved protein folding and tolerance to acidosis as well as chloride ions. Its excitation peaks at 515 nm and emission at 528 nm, its quantum yield is 0.57 and its extinction coefficient is 92,200 $molar^{-1}cm^{-1}$. Venus was included in Yellow Cameleons x.12 [62].

FRET Optimization in Ratiometric GECIs   FRET depends not only on the distance but also on the relative orientation of the two chromophores. The former is altered in constructs with circularly permuted fluorophores (see below) [76, 67, 66] and led to significant increase in maximum ratio changes. E.g. it was reported that the replacement of EYFP with cpVenus in Yellow Cameleon 3.60 increased the maximum fluorescence ratio change to 560 % as compared to previously 100 % in Yellow Cameleon 3.12 [62, 67] (both *in vitro*). **Yellow Cameleon 3.60 and 2.60** will be further examined here. The variant 2.60 differs from 3.60 by the amino acid exchange Q104E in calmodulin [36]. Significant research employing this series of GECIs has been published from *Cenorhabditis elegans* [77] but

there were no reports from mammals to my knowledge. This may be due to the employment of a vertebrate calmodulin from *Xenopus laevis* in all GECIs described before. The GECI's calmodulin and M13 might not only interact with each other but also with the abundant cellular interaction partners of calmodulin and the native calmodulin itself. Frog and mouse calmodulin are identical while fruit fly calmodulin differs in 2 and *Caenorhabditis elegans* calmodulin in 3 amino acid residues (Fig 1.9). Invertebrate calmodulin maybe evolutionary distinct enough to compromise interaction with these proteins.

DROSOPHILA 0 MADQLTEEQIAEFKEAFSLFDKDGDGTITTKELGTVMRSLGQNPTEAELQDMINEVDADGNGTIDFPEF

XENOPUS 0 MADQLTEEQIAEFKEAFSLFDKDGDGTITTKELGTVMRSLGQNPTEAELQDMINEVDADGNGTIDFPEF

MOUSE 0 MADQLTEEQIAEFKEAFSLFDKDGDGTITTKELGTVMRSLGQNPTEAELQDMINEVDADGNGTIDFPEF

LTMMARKMKDTDSEEEIREAFRVFDKDGNGFISAAELRHVMTNLGEKLTDEEVDEMIREADIDGDGQVNYEEFVTMMTAK 149
                                X   X
LTMMARKMKDTDSEEEIREAFRVFDKDGNGYISAAELRHVMTNLGEKLTDEEVDEMIREADIDGDGQVNYEEFVQMMTAK 149

LTMMARKMKDTDSEEEIREAFRVFDKDGNGYISAAELRHVMTNLGEKLTDEEVDEMIREADIDGDGQVNYEEFVQMMTAK 149

Figure 1.9: Calmodulin amino acid sequence from 3 species. Sequences compared are from *Drosophila melanogaster*, *Xenopus laevis* and *Mus musculus*. Differing residues are marked by X.

Recently, the putative interaction was tackled by two approaches. Palmer and colleagues reciprocally redesigned calmodulin and M13, such that interaction with wild-type proteins would become unlikely [78]. The interaction of calmodulin with M13 relies on salt bridges between acidic and basic amino acid residues. The authors interchanged these residues between M13 and calmodulin, which reduced the affinity for wild-type calmodulin by four orders of magnitude. In a second, more radical approach they first exchanged small but crucial amino acids in M13 by larger amino acids, and then computationally redesigned a calmodulin derivate that would fit to this new M13. In **D3cpv** this involved the exchange I14F in M13 and the mutations F19L, V31Q, M36L, L39 in calmodulin. Other mutations led to variants D2cpv and D4cpv with different k_Ds . The calcium responses of these sensors were unaltered by the presence of excess wild-type calmodulin [71]. D3cpv will be examined in detail here.

The second strategy to eliminate calmodulin interactions is to eliminate calmodulin altogether by replacing it with a different calcium binding protein: Troponin C is the calcium sensor in skeletal and cardiac muscles [79]. Together with troponin I and troponin T it interacts with myosin upon calcium triggered release of tropomyosin to induce muscle contraction. Wild-type troponin does not occur in neurons. In a first step, it was found that

troponin C alone without a target or interaction peptide suffices to confer FRET changes when fused between CFP and Citrine in a sensor named **TN-L15** [72]. Meanwhile, it has been shown that the response properties of TN-L15 are maintained when it is expressed in neurons of transgenic mice [80]. In a newer variant of this sensor type, named **TN-XL**, the maximum fluorescence change has been increased by replacing Citrine with a circular permutation (see 1.2.2) of Citrine (cp174). Two of troponin C's calcium binding sites are sensitive to magnesium. This has been addressed by amino acid replacements in troponin's C-terminal EF hands III and IV (N108D, D110N and N144D, D146N), which also led to decreased calcium affinity [66]. A yet newer variant named **TN-XXL** was generated by a duplication of the altered C-terminal EF hands III and IV to replace the N- terminal portion of the protein with the more low-affinity EF hands I and II. Alterations were N108D and D110N to reduce magnesium sensitivity as in TN-XL and I130T for increased calcium affinity. The polypeptide comprising amino acids 94 to 162 was then doubled and fused between CFP and Citrine cp174. The resulting sensor shows a calcium affinity, equal to that of TN-L15 and a maximum fluorescence change of 500 % (Marco Mank, unpublished data). All three troponin-based GECIs will be analyzed here.

Single Chromophore GECIs   All single chromophore GECIs today employ calmodulin as calcium sensor protein. Insertion of calmodulin between the YFP amino acid residues 145 and 146 led to Camgaroo-1 [76]. Protein maturation was improved in Camgaroo-2 by the mutation Q69M [61]. Camgaroos found application in isolated fly brains injected with acetylcholine [81].

GCaMPs and Pericams rely on circular permutations of GFP and YFP respectively: N- and C-terminal portions had been divided around position 145, then refused at the original termini with short linkers, and the new termini were connected via linkers to calmodulin and M13, respectively. Three types of Pericam have been generated by diverse mutations adjacent to the chromophore. Upon calcium binding flash Pericam becomes fluorescent, inverse Pericam loses fluorescence and ratiometric Pericam shows an altered excitation spectrum [82]. Ratiometric Pericam has been applied in myocytes [83]. Although ratiometric excitation is difficult to realize with laser scanning microscopy, a suitable system has been developed [84].

GCaMP is constructed as above described, and was further developed to **GCaMP 1.6** by mutations in cpEGFP (V163A and S175G), which supposedly facilitate chromophore formation, yielding a brighter variant with increased calcium affinity [85, 73]. Both types

found frequent application in the central nervous system of transgenic flies e.g. [86, 87, 88, 39] and in mice an application in smooth muscle was reported [89]. In GCaMP 2 [74] protein folding at $37°C$ is enhanced, so that successful application in cerebellar granule cells of transgenic mice was reported [90, 91]. D180Y and V93I are mutations that together with a c-terminal His-Tag increase brightness at $37°C$ 200-fold. The fluorescence change from 0 to saturated calcium however remains 4-5 fold as in GCaMP 1.6. The latter will be analyzed here. I examined GCaMP 1.6 because it proved superior to all other single fluorophore GECIs in a previous study [39]. I also generated flies expressing GCaMP 2, however these flies showed insufficient expression levels throughout.

GECI Problems & Solutions   GECIs generally showed reduced maximum fluorescence changes when expressed in living animals [92, 93, 94], failed to report calcium changes when targeted to cellular compartments in neurons, showed altered calcium affinity [38, 39] and were not successfully applied in mammalian brains [37, 80]. Only recently the sensor TN-L15 was reported to maintain its signaling properties in mammalian brains, when induced activity was measured *in vivo* [95]. However, no responses to endogenous activity have been shown. The reported changes in response properties when transfered from *in vitro* to *in vivo* situations have been essentially unpredictable, but it is generally assumed that a major source of perturbations are interactions with wild-type proteins at least for calmodulin-based calcium indicators. E.g. it has been shown that a large fraction of GECIs is not freely diffusible when expressed in mammalian neurons because of binding to native cellular proteins [37]. Thus the major approaches to circumvent these problems were to decrease likely interactions with wild-type proteins as far as predictable, as described above.

I conducted a thorough comparison of the *in vivo* response properties of 8 different calcium indicators (see Table 1.2) to allow for the rational choice of the best suited GECIs for optical imaging of neural activity in the fly's optic lobes. Of course, the conditions of test experiments should ideally be as reproducible as possible and as similar to the ultimate application as possible. Thus, I applied the neuromuscular junction preparation of transgenic, larval *Drosophila* as an *in vivo* test system for GECIs. In addition, these measurements were then complemented by response characterizations of GECIs in cuvettes. In a series of such experiments it will be shown that the most promising GECI for *in vivo* application in neuronal cytoplasm is TN-XXL. Also I will present preliminary experiments that demonstrate the first recordings of directional selective motion responses recorded with this GECI in LPTCs of adult flies.

1.3 Fly Larvae as GECI Testbed - the Neuromuscular Junction

As stated before, cuvette measurements do not allow conclusions about *in vivo* performance of GECIs. On the other hand *in vivo* preparation of adult flies for calcium imaging is laborious and difficult. Thus, I turned to a robust, simpler and reproducible system: the neuromuscular junction of fruit fly larvae [93]. As a testbed for GECIs this preparation was established in 2005 [39]. It is a well described and accessible system, that allows stable experiments (up to hours).
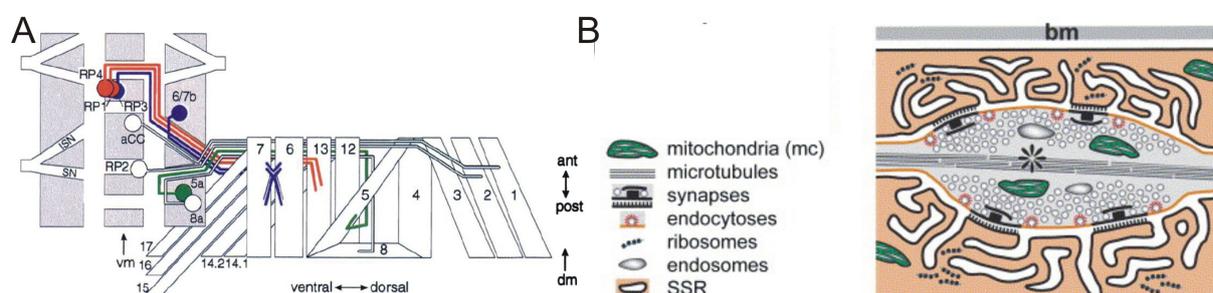
Figure 1.10: Schematics of muscle innervation in the fly larva. (A) Connectivity from motoneurons to muscles. Several principal muscle fibers are shown for a single abdominal hemisegment, extending from the ventral midline (vm) to the dorsal midline (dm). Anterior (ant) is to the top. The cns is shown to the left, shaded in gray with the neuropil and major nerve tracts (segmental and intersegmental nerves, SN and ISN) in outline. Motoneurons projecting to the muscle fibers 7 and 6, 13 and 5 are shown in blue, red and green, respectively. Other neurons are shown in outline. (B) Details of a bouton (*, nerve terminal; beige, muscle). At the late larval stage, the nerve terminal is detached from the basement membrane (bm) and folded into the interior of the muscle. The muscle membrane forms infoldings (SSR, subsynaptic reticulum). The terminal is characterized by high density of vesicles. Ribosomes are enriched at postsynaptic sites. (A) from [96], (B) from [97].

The anatomy, physiology and development of the glutamatergic neuromuscular junction in *Drosophila* late embryos and larvae have been extensively studied (see Fig 1.10) [98, 99, 100, 101]. In the ventral nerve chord, 30 motoneurons per hemisegment are known that innervate 30 muscles per hemisegment in a stereotyped pattern [102, 103] (see Fig 1.10 A). The glutamatergic motoneurons form boutons of type Ib or Is. More than one axon innervate one muscle fiber. Each axon forms a specific type of boutons, and one such axon can innervate more than 1 muscle. Differentiation of postsynaptic specializations like
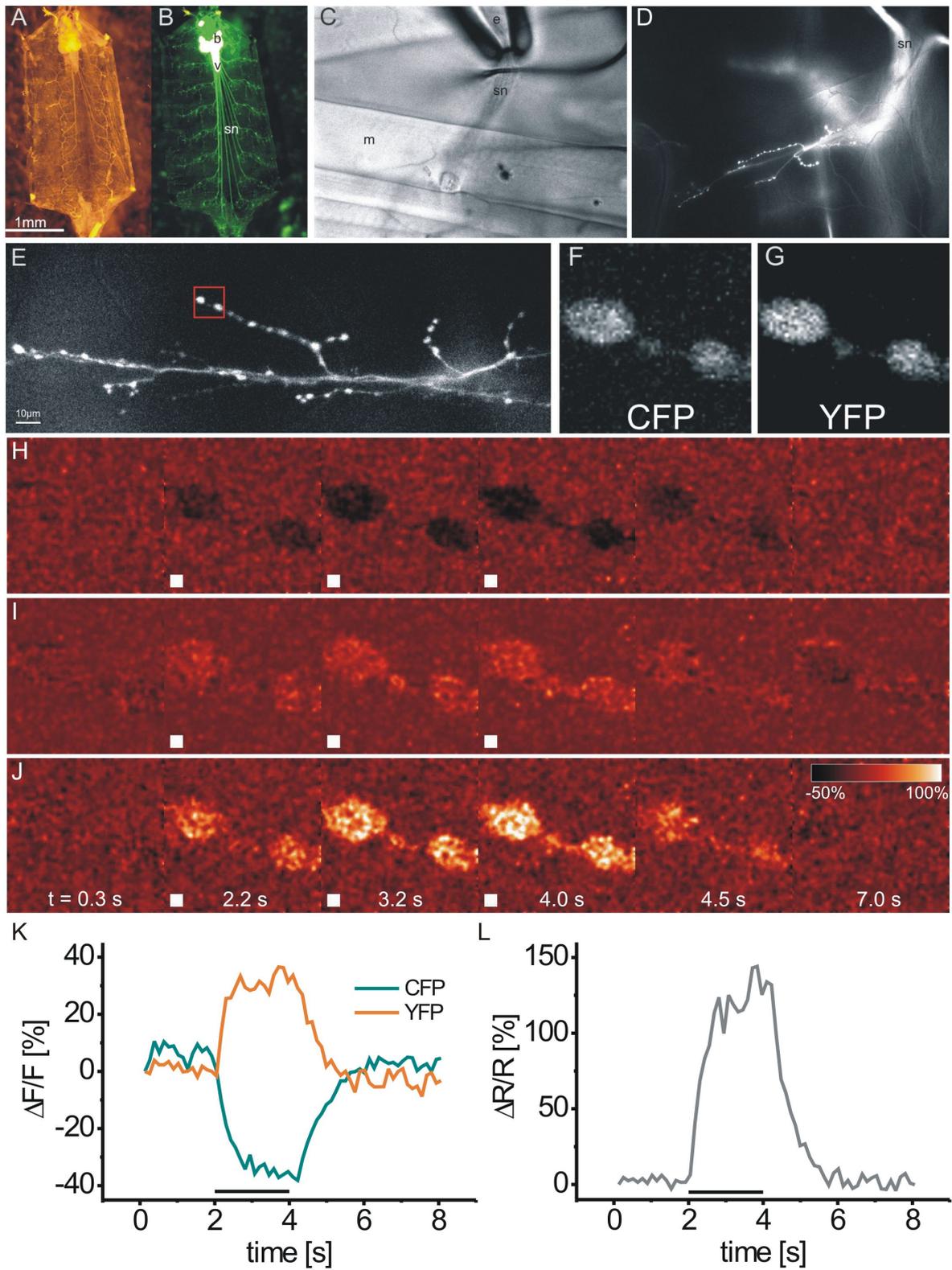
receptor localization is initiated by motoneuron activity.

I focus on boutons of the motoneuron 6/7, which innervates longitudinal muscles 6 &
7 via the segmental nerve branch SNb/SNd with boutons of type 1b (see Fig 1.10 A).
Action potentials arriving at presynaptic boutons (see Fig 1.10 B) elicit calcium influx
through voltage gated calcium channels. The calcium signal is detected by a protein
complex known as SNARE, that binds calcium and initiates vesicle fusion with the plasma
membrane. 4-5 calcium ions are needed to trigger vesicle release [104]. At functional
neuromuscular junctions action potential frequencies of up to 100 Hz have been described
[105]. L-glutamate is the excitatory neurotransmitter at the neuromuscular junction of
arthropods [106] incl. fruit flies [107], yet several motoneurons coexpress one of a number
of neuropeptides [102]. At the neuromuscular junction of fly larvae boutons comprise a

Figure 1.11: Neuromuscular junction preparation and experiment with a transgenic an-
imal expressing Yellow Cameleon 3.60. (A) Bright field microscopy of a
larval preparation. (B) Same preparation under fluorescence excitation.
Green/white structures are neurons (b - brain lobes). From the ventral nerve
cord (v) segmental nerves (sn) innervate each hemisegment. For experiments
sn are cut and b and v are removed. (C) Nerve ends are then placed into
suction electrode (e). The nerve disappears between muscle fibers (m). (D)
Neuromuscular junction with nerve bundle (sn) under fluorescence excitation.
For recordings it is switched to 2 photon microscopy: (E) Maximum intensity
projection of an image stack recorded with 2-photon microscopy, showing a
Yellow Cameleon 3.60 expressing neuromuscular junction at muscle 6/7. For
experiments movies of 2-5 boutons are taken, while the nerve is stimulated at
diverse action potential frequencies via the suction electrode. (F-G) Raw ex-
ample frames from CFP- and YFP-channel, recorded at boutons outlined by
the red box in (E), during an experiment. Action potential induced calcium
influx leads fluorescence responses. (H & I) Fractional fluorescence change in
false color coded images as recorded from the CFP channel (H) and from the
YFP channel (I). Fractional ratio change is shown in (J). Images are taken
during an 8 s recording period. Boutons were stimulated at 160 Hz action
potential frequency from t = 2-4 s. Frames during stimulation are marked
by white squares. In each line 6 frames are shown. Color scale and time are
indicated in (J). (K) Fractional fluorescence changes recorded in CFP and
YFP channels from boutons expressing Yellow Cameleon 3.60, when stimu-
lated with 160 Hz action potential frequency for 2 s. (L) Ratiometric analysis
of the data plotted in (K). Black bar indicates stimulus period. Note that the
peak in (K) is higher than in the image series shown in (J) because of back-
ground subtraction.

relatively large volume (2-70 μm^3) [103] compared to boutons at a central mammalian synapse (e.g. boutons at mammalian olfactory cortical synapses 0.2-0.4 μm^3 [108], mouse CA1 boutons $\approx$0.09 μm^3 [109], dendritic spine $\approx$0.01-1 μm^3 [109, 110]). Postsynaptically, calcium permeable glutamate receptors open upon glutamate binding.

The experimental procedure that is used to acquire *in vivo* response characteristics of GECIs at the neuromuscular junction is outlined in Fig 1.11. GECI expression can be directed to motoneurons (see 1.5.1) that synapse on body wall muscles [93]. Fillet preparations (see Fig 1.11 A & B) are made in the artificial hemolymphe like solution HL6.1 (see 2.5), nerves are severed, the brain is removed and nerve ends are placed in a suction electrode (see Fig 1.11 C), which allows to elicit action potentials. These travel down motoneurons to the presynaptic boutons at neuromuscular junctions (see Fig 1.11 D-G), where each action potential causes calcium influx. Ratiometric GECIs respond to calcium increases with fluorescence decrease in the CFP channel (Fig 1.11 H & K) and fluorescence increase in the YFP channel (Fig 1.11 I & K). YFP/CFP ratio changes are shown in (Fig 1.11 J & L).

GECIs are freely diffusible in the cytosol of presynaptic boutons and thus report volume averaged concentration changes. The presence of GECIs introduces an additional buffer, that slows down the apparent time course of fluctuations. Correction for this measurement artifact is not trivial [111] (see 4.2). To extract key features of GECI performance it is therefore desirable to measure calcium levels at a steady-state as done here. This is possible because the cytosolic calcium in boutons accumulates asymptotically at action potential frequencies of 5 Hz and above [112]. The accumulation is due to the time courses of ion flows related to individual action potentials which is in turn shaped by the cellular machinerie that controls cytosolic concentrations, such as transporters, pumps, receptors and buffers (see 4.2). Calcium is expelled from boutons mainly by a calcium-proton exchange pump [113]. At steady-state, calcium extrusion is in equilibrium with influx and the calcium-proton exchange pump acidifies the cytosol. Thus, volume averaged residual calcium concentrations can be measured independent of GECI concentrations. The concentration of calcium is a linear function of action potential frequency over a wide range of frequencies as will be shown. In experiments, the bath application of L-glutamate to the fillet preparation, at concentrations above 7 mM saturates postsynaptic L-glutamate receptors and effectively blocks muscle contractions. This allowed stimulation of nerves with voltage pulses of frequencies up to 160 Hz, while imaging of presynaptic boutons revealed calcium influx [39].

From the GECI responses to various stimulus frequencies the following GECI characteristics will be derived: amplitudes and signal-to-noise ratios at steady-state, calcium affinity (k_D), response kinetics (time-constant τ for the on- and offset of responses) and hill coefficients. The characteristics will be given in terms of absolute calcium concentrations after the concentrations corresponding to each stimulus are determined.

1.4 2-Photon Microscopy

In laser scanning microscopy a laser is raster-scanned across a sample plane. The resulting image is an intensity matrix sampled by photomultipliers over time. In 2-photon microscopy [114] the laser is focused in a focal plane, and 2-photon excitation occurs exclusively in the focus point. This offers one principal advantage over wide field light microscopy: selective excitation at the sampling-site only. Thus, sampled photons cannot be contaminated by out-of-focus fluorescence, even if detector pathways are fully open (in contrast to confocal microscopy). 2-photon microscopy relies on fluorescence excitation of a fluorophore by multiple photons essentially simultaneously ($10^{-16}s$). 2-photon excitation probability is extremely low, and is only made possible by a laser that is focused spatially and pulsed at 80 MHz frequency with 100 fs pulse duration. This allows to keep average light intensity low, but increases 2-photon excitation probability in a small volume at a certain point in time to a reasonable degree, such that in a fictive but reasonable 2-photon microscope as described by Zipfel and colleagues in [115], 100 photons per voxel per second will be emitted. Pulsing increases the excitation probability by 5 orders of magnitude. In other words without pulsing, far less than 1 photon per pixel per second would be emitted [115]. For common GECIs with cyan to green single-photon excitation peaks, this requires an infrared laser. 2-photon excitation maxima of fluorophores can be roughly estimated by doubling the maximum single-photon excitation wavelength. However deviations occur because "initial single-photon excited states are 2-photon forbidden" [115]. In a ratiometric GECI for 2-photon imaging, the excitation spectra of both chromophores should show as little spectral overlap as possible, because direct excitation of the acceptor chromophore reduces the apparent maximum ratio change. Imaging depth in mammalian brain tissue has been reported up to 800 μm.

Summarizing, the main advantages of 2-photon over conventional wide field microscopy include lower scattering in tissue due to the longer wavelengths used, essentially no scattered-excitation due to the confined 2-photon excitation probability along the Z-axis, both re-
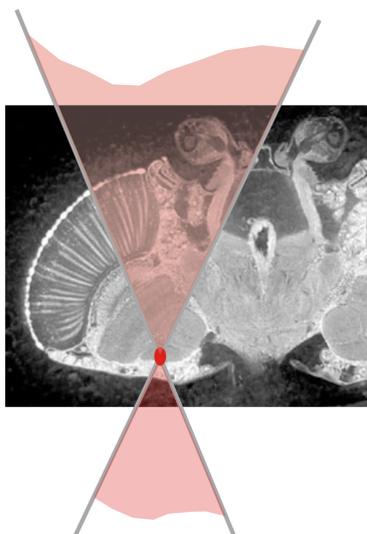
Figure 1.12: Schematic of 2-photon excitation in the flies visual system. The far red laser beam (transparent red) is focused to the lobula plate where LPTCs reside. 2-photon excitation only occurs in the focus (red oval). Outside the focal plane excitation probability is close to zero, including the region of photoreceptors.

ducing photo-damage and allowing superior background subtraction [116].

Imaging with GECIs at the neuromuscular junction does in principle not require 2-photon excitation. GECIs are targeted to neurons, which are highlighted in the background of muscle tissue exhibiting very low background fluorescence. Also, nervous structures are close to the surface of the preparation and do not require deep tissue penetration. However, 2-photon microscopy will be used for experiments in the visual system and is thus also used at the neuromuscular junction to keep experimental conditions comparable. For the examination of the visual system of the fly 2-photon excitation is without alternative, as the excitation light must be invisible for the animal. However, available GECIs are excited in the blue to yellow spectrum of light, which is visible to flies which see light in the range from far UV (Rhodopsin 3 absorption: 330 nm) to yellow-orange (Rhodopsin 5 absorption: 515 nm). Cyan (for ratiometric GECIs) and green excitation (for GCaMP or OGB-1) can be provided by invisible 2-photon excitation (> 800 nm). As the laser is focused in the visual ganglia, rhodopsins in the photoreceptors are not excited (see 1.12). A third wavelength of light is introduced in such a setup by the presentation of visual stimuli to the fly. Obviously, this light must be visible to the fly but prevented from invading the sampled signal. This was accomplished by temporal separation of optical data acquisition and visual stimulus presentation (Dierk F. Reiff, unpublished data, see 3.3).

1.5 Expression Systems for Transgenes in Fruit Flies

For the analysis of neural circuits forward genetic methods can be very useful. In *Drosophila* transgene expression systems have been established in the past 25 years and since then developed considerably [117, 118, 119]. These systems e.g. allow the functional dissection of a neural network by loss of function and gain of function experiments. Loss of function can be reversibly induced in classes of cells by transgene mediated blockade of neural activity. The use of such proteins to block neural activity in parallel to GECI-based imaging requires two separate systems for the expression of both transgenes in different sets of cells. Besides the classical Gal4-UAS system, I started here a second approach based on a bacterial transcription system called LexA. Next, I identified possibly interesting enhancer regions in the genome, cloned the respective genomic sequences and generated fly lines for GECI expression in visual interneurons under LexA control.

1.5.1 UAS-Gal4

Gene expression in cells and organisms is spatially and temporally well controlled. E.g., the segmentation gene *fushi trarazu* in *Drosophila* is expressed at low levels early during embryogenesis, is then upregulated and expression becomes spatially more and more refined until the pattern shows seven characteristic stripes around the longitudinal axis of the embryo, reflecting the even numbered parasegments 2-14 [120]. Gene expression is controlled by regulatory, non-coding DNA sequences, that are recognized by transcription factors. One type of regulatory elements is called promoter. These act on short range. An eukaryotic promoter consists of DNA motifs for RNA polymerases 50-75 bp upstream of a gene. A second class of regulatory elements are termed 'enhancers'. They act on far distances by diverse and partly unidentified mechanisms [121]. Enhancers are recognized by transcription factors and interact with the promoters of specific genes to increase the rate of transcription. Their distance from their specific promoter may be several, and even tens of kilo bases and they may reside upstream or downstream or even in exons of a gene. How enhancers exert their effect on promoters is poorly understood, but there is some evidence for the contribution of chromosomal loop structures that bring enhancer and promoter into physical contact or close proximity. This again may be subject to regulation by diverse elements and mechanisms. E.g. In the case of *fushi tarazu* the interaction between different promoters and enhancers or silencers is blocked by boundaries or insulators [120].

In yeast a directional class of enhancers is called upstream activating sequence (UAS).

The transcription factor Gal4 consists of a DNA binding domain, which binds to UAS and a transactivation sequence, which activates transcription of specific downstream genes. This expression system has been isolated, modified and transfered to transgenic flies to allow expression of any gene fused to the UAS sequence [118].

Enhancer-Trap

For transgene expression in flies the bipartite Gal4-UAS system is used because it allows exploitation of manifold combinations of different Gal4- and UAS-flies, and provides amplification of transgene expression: A transgene like the cDNA for a GECI is cloned into a fly transfection vector, downstream of five UAS sequence repeats. A fly strain carrying this transgene is called the effector line and will not express the respective GECI, because it lacks the yeast transcription factor Gal4. A second fly strain is transfected with the cDNA for Gal4; this line is called the driver line. The Gal4 sequence is preceded by a weak promoter. This fusion can be randomly inserted into the genome to pick up the expression pattern of any enhancer in the genomic surround (thus enhancer-trap). The flies cellular machinery is blind for the UAS sequence and the DNA binding protein Gal4 is blind for the flies enhancer sequences. Thus, flies carrying either transgene are phenotypically wild-type - if the insertion site is not critical to some gene's function.

When flies carrying the UAS-GECI transgene and flies carrying the Gal4 transgene are crossed, their offspring will express the GECI protein in the expression pattern of the enhancer controlling Gal4 expression. So-called libraries of driver- and effector-lines are established worldwide and can be combined for the expression of many different transgenes in many different cells. This random approach is called enhancer-trap. It requires post-transfectional screens for expression patterns of interest.

Promoter Fusions

A non-random approach to a specific expression pattern requires knowledge about a corresponding genomic enhancer. Often it is desirable to mimic the expression of a native gene with a transgene. Therefore several kb of non-coding DNA, mostly from the upstream regions of the native gene are cloned and fused to Gal4. The hope is that this sequence contains regulatory elements that activate expression in the desired pattern. This construct is inserted into the genome, in the ideal case bringing its own enhancer with it, that will eventually lead to the desired expression pattern. This expression pattern, however, is hardly predictable for two reasons: First the new insertion may behave like a new

enhancer-trap. Second the genomic region fused to Gal4 may contain regulatory elements that do not produce the desired expression pattern. In the majority of cases, far distance regulatory elements show no recognized sequence characteristics and have to be sought by best guesses. Nevertheless enhancers (and other long distance regulatory elements, [121]) are often picked up in 2-10 *kb* upstream of a gene. E.g. 2.6 kb of genomic DNA immediately upstream of the olfactory receptor gene Or83b were amplified and fused to Gal4. The Gal4 expression pattern in transgenic flies carrying this construct mimics Or83b expression in wild-type flies [88]. In the case of e.g. the *fushi tarazu gene* however, regulation is much more complex [120] (see 4.4).

The independent expression of two transgenes in one animal requires two separate expression systems. Gal4-UAS independent expression can be achieved by direct fusion of a transgene to a presumed enhancer sequence. This system, however, lacks the amplification step provided by Gal4-UAS and often leads to insufficient transgene expression levels.

Gal80

The yeast protein Gal80 binds to the Gal4-activating domain (GAD) of Gal4, inhibiting its function. This can be used to control and refine transgene expression [122]. A temperature sensitive variant of Gal80 loses Gal4 affinity at high temperatures. This can be used as a 'temperature-switch' for Gal4, allowing temporally controlled transgene expression [123].

1.5.2 LexA-pLOT

A second expression system, here named LexA-pLOT, has been isolated from bacteria and relies on the same logic as Gal4-UAS [124, 125]. In pLOT the bacterial operator (prokaryotic promoter) LexAop replaces UAS. The LexA protein, fused to a transcription activation domain, replaces Gal4. LexA is a bacterial DNA binding protein. It can be fused to, e.g. VP16 (the viral transcription factor VP16 acidic activation domain) or GAD (from Gal4) to function as a transcriptional activator. The GAD fusion form is susceptible to Gal80 inhibition like Gal4 [125]. The LexA-pLOT system can be applied in parallel to the Gal4-UAS system in the same animal to produce expression of two transgenes in different subsets of cells [125]. This is desired for neural network analysis by the parallel use of GECIs for calcium imaging in LPTCs and transgenes that inhibit neural activity in presynaptic partner cells.

1.6 Transgenes for the Inhibition of Neural Activity

In *Drosophila* a variety of transgenes are used for interference with neural activity at various levels: these proteins either induce cell death or silence chemical synapses or clamp the membrane potential.

The genes 'reaper' and 'head involution defective' induce apoptosis. The protein 'ricinA' is a protein synthesis inhibitor that effectively kills cells. 'Tetanus toxin light chain' silences chemical synapses by cleaving a protein necessary for vesicle fusion. These proteins were compared for effectively blocking information processing in a behavioral study [126]. Tetanus toxin light chain proved most effective in these experiments.

The protein 'dynamin' is necessary for vesicle reuptake. A temperature sensitive, dominant negative form of dynamin called 'shibire ts' [127] silences chemical synapses and has been used to map an olfactory memory trace to kenyon cells of mushroom bodies [128]. A major advantage of 'shibire ts' is the stringent temporal control (within minutes) it offers. A disadvantage is that its effect is restricted to chemical synapses. 'shibire ts' leaves electrical transmission unaffected.

The modified potassium channel 'kir' is constitutively open and renders neurons less excitable [129] by shunting input currents. Another potassium channel known as 'shaker' has been modified (and termed 'EKO channel') to act as a shunt for excitability of neurons [130]. The two latter silence neuronal transmission via both chemical and electrical synapses. All of these proteins can be expressed under control of Gal4-UAS and used for the functional analysis of neural circuits. In combination with the temperature sensitive form of Gal80 some temporal expression control could be gained which is desirable to exclude developmental effects [123].

1.7 Project Outline: Manipulation & Observation of a Neural Circuit

In this doctoral thesis, I tested and developed genetic tools for parallel calcium imaging and silencing of distinct sets of cells to allow for a future genetic dissection of the flies' neural circuits for visual motion detection.

I A growing variety of GECIs are available. As explained above (see 1.2.2) their response properties when expressed in visual interneurons cannot be predicted from their *in*

vitro characteristics. For a quantitative comparison of GECI performance, the intracellular calcium concentration at the neuromuscular junction at various levels of activity was determined using synthetic calcium indicators. Therefore a novel protocol for 2-photon guided dye injection with sharp microelectrodes was established.

II 8 different GECIs were then expressed at the larval neuromuscular junction to characterize their response properties *in vivo*. I demonstrate systematic differences between GECIs properties *in vivo* and *in vitro*, and show that a new generation of GECIs maintains aspects of the improved properties *in vivo*. The results also demonstrate, that each GECIs *in vivo* properties like k_D and response kinetics determine its applicability in a specific biological system for specific questions, and may serve as a researchers guide for the rational GECI choice. Together with this knowledge, the new GECIs will allow more versatile and more detailed neurophysiological analysis in the future.

III The quantitative comparison guided the choice of the most promising GECIs for expression in LPTCs. Thus, the first optical recordings of directional selective motion responses from fruit fly LPTCs were obtained, using the new troponin-based GECI TN-XXL. Recordings were made from axonal and dendritic compartments of VS cells. The measurements were sensitive enough to detect intracellular calcium accumulations during preferred direction motion but could not detect the expected reduction in calcium concentration during null direction motion.

IV A couple of enhancer-trap fly strains are available which show Gal4 expression in LPTCs or medullary neurons. I mapped the Gal4 insertion sites for several of them. Then putative corresponding genomic enhancer regions from one medullary and two LPTC enhancer-trap strains were cloned. These were fused to the LexA cDNA to generate transgenic flies. The LexA expression pattern in these strains should mimic the Gal4 pattern in the respective enhancer-trap strains. In parallel I generated flies that express promising GECIs under the control of LexAop. With these two types of fly strains, GECI expression can be driven by the LexA-pLOT system.

Thus Gal4-UAS can then be used in parallel to silence presynaptic partners of LPTCs, by expression of e.g. shibire ts. This will allow to analyze the processing of motion information in the fly's visual system.

2 Materials & Methods

2.1 Flies

2.1.1 Flycare

Flyfood   Flies were raised on standard corn meal medium supplemented with dry yeast. (All recipes are listed in 2.5). Soy flour, corn flour and dry yeast were mixed in one liter of cold water. Agar was soaked before adding another liter of cold water. Three liters were heated to 98 $°C$ and the agar was added. After one hour of heating, malcine, treacle and the flour mash were mixed with the boiling water. The solution was then filled up to five liters and cooled down to 65 $°C$. Propionic acid was added. The food was filled into plastic vials.

Breeding   Fly stocks were kept at 18 $°C$ and transfered to fresh vials every 14 days. Experimental flies and crosses were kept at 25 $°C$ and were flipped every week. All flies were kept at 70 % relative humidity at a 12 hour light/dark cycle. Generation time (from egg to adult) takes approximately seven days at 29 $°C$, nine days at 25 $°C$, eleven days at 22 $°C$, or 19 days at 18 $°C$ (source: Bloomington stock center). In our incubators this was somewhat slowed down to 11 days at 25 $°C$. For crosses 10 female and 5 male flies were collected.

2.1.2 Genetics

Fly Strains   All fly strains used in this study are listed below, together with the source and original publication (see Table 2.1).

Fly strain	source
wt Bayreuth w$^-$	provided by C. Lehner, University of Bayreuth, Germany
elav^{C155}-Gal4	provided by C.S.Goodman, University of California at Berkeley, Berkeley, USA [131]
DB331-Gal4	provided by R. Stocker, University of Fribourg, Switzerland
3A-Gal4	provided by M. Heisenberg, University of Wuerzburg, Germany [35]
1187-Gal4	provided by M. Heisenberg, University of Wuerzburg, Germany [132]
NP1132-Gal4	provided by K. Ito, National Institute for Basic Biology Myodaiji, Okazaki, Japan [133]
NP2056-Gal4	provided by K. Ito, National Institute for Basic Biology Myodaiji, Okazaki, Japan [133]
UAS-mDsRed	provided by G. Tavosanis, MPI of Neurobiology, Martinsried, Germany
UAS-YellowCameleon 3.3	generated by A. Ihring & D.F. Reiff, MPI of Neurobiology, Martinsried, Germany [39]
UAS-YellowCameleon 3.6	generated by T. Hendel & W. Essbauer, MPI of Neurobiology, Martinsried, Germany (Hendel et al, in press)
UAS-YellowCameleon 2.6	generated by D.F. Reiff & W. Essbauer, MPI of Neurobiology, Martinsried, Germany (Hendel et al, in press)
UAS-D3cpv	generated by T. Hendel & W. Essbauer, MPI of Neurobiology, Martinsried, Germany (Hendel et al, in press)
UAS-GC1.6	generated by A. Ihring & D.F. Reiff, MPI of Neurobiology, Martinsried, Germany [39]

UAS-TN-L15	generated by A. Ihring & D.F. Reiff, MPI of Neurobiology, Martinsried, Germany [39]
UAS-TN-XL	generated by T. Hendel & W. Essbauer, MPI of Neurobiology, Martinsried, Germany (Hendel et al, in press)
UAS-TN-XXL	generated by T. Hendel & W. Essbauer, MPI of Neurobiology, Martinsried, Germany (Mank et al, in press)
LexAop-YC3.60	generated by T. Hendel & W. Essbauer, MPI of Neurobiology, Martinsried, Germany
LexAop-TN-XXL-SF	generated by T. Hendel & W. Essbauer, MPI of Neurobiology, Martinsried, Germany
OR83b-LexA-VP16::SV40	provided by Tzumin Lee, La Jolla, USA [125]

Table 2.1: Name and source for all used fly strains.

2.1.3 Transfection & Stock Breeding

Injection Mix DNA was cleaned by spin dialysis before injection. Small columns were prepared by cutting the lid of a plastic tube A and poking a hole in the bottom with a thin needle. Tube A was filled with 25 μl glass beads (300 μm diameter)and 250 μl Sepharose CL6B. Then tube A was inserted in another tube B and both were centrifuged at 3000 rpm for 3 min. After discarding tube B, tube A was inserted in a new tube C. DNA was incubated at 65 °C for 10 min and applied carefully onto the sepharose coated glass beads and centrifuged at 3000 rpm for another 3 min. Tube A was discarded. 6 μg of spin dialysed DNA from tube C and spin dialysed Δ2-3 (transposase, 2 μg) were diluted in 100 μg water. For precipitating the DNA mix 3 M Na-Acetat (10 % of total volume) was added to the solution and mixed. 2.5 x 100 % EtOH was added before incubation at -70 °C for 30 min and centrifuged at 15,000 rpm for 30 min. The supernatant was discarded and the sample was washed with 100 μl 70 % EtOH. After centrifuging at 15 000 rpm for 30 min, the supernatant was discarded again and the DNA was dried exposed to air. The DNA was diluted in 20 μl 1x injection buffer. 0.5 -1 μl of the sample was run on an agarose gel for analysis.

Germline Transfection For P element mediated germline transfection [117] of *Drosophila* embryos, 2 day old flies were allowed to lay eggs on grape agar plates for 20 to 30 min, then flies were transfered on a fresh plate. Eggs were collected, washed in PBT, washed in 50 % Klorix for 1.5 min to remove the chorion, rinsed in water and aligned smoothly with a paint brush side by side on an agar block. Aligned eggs were transferred onto a cover slip coated with glue, such that the posterior end faced the edge of the slip. The slip was then transferred to a drying chamber for 10-14 min. Eggs were fixed to a microscope table, where injections were done using an electrode holder, connected to a syringe via an oil filled (Voltalef 3S) rubber tube. Ultra thin glass electrodes (GB150F-10, Science Products, Hofheim, Germany) were prepared using a sutter puller (Flaming/Brown Micropipettepuller P-97, Sutter Instruments, Novato, CA, USA) and back filled with 1 μl of injection mix. A small air bubble separated the aquous injection mix from the oil. The electrode tip was gently pushed against the side of the cover slip to break the tip. Then each egg was injected with a small volume of injection mix to its posterior end, where the polar cells form which set up the germline. Importantly, injections need to be performed in the syncytial stage of embryos. Cell membranes develop after the 13th nuclear division, at room temperature approximately 1 h after egg laying. Polar cells are the first cells to form

in the developing embryo. Eggs were then coated with oil (Voltalef 10S) and transferred to a humidified agar plate for embryos to hatch on.

Breeding Stocks Hatched embryos were collected during the next 2 days and transferred to fresh fly vials. Freshly hatched adults were collected and individually crossed to freshly hatched w$^-$ wild type BT (originally collected in Bayreuth, Germany) flies. Successful transfection is indicated by red eyed progeny. These again were collected right after hatching and crossed individually to balancer flies (rl/Sm6Tm6), recognizable by the marker phenotypes "curly wings" and "tubby larva". Progeny was collected for red eyes and presence of the balancers, yielding stable lines if insertions hit 2nd or 3rd chromosome. Flies with X chromosomal instertions were backcrossed to yield homozygous stable lines.

2.2 Physiology & Optical Imaging

2.2.1 Neuromuscular Junction Preparation

The neuromuscular junction experiments with GECI expressing animals were done as described in [39]. The larval preparation was done according to Macleod et al. [112]. Unless stated otherwise, artificial hemolymphe HL6.1 (see 2.5) with 7 mM L-glutamate and 1.5 mM calcium at pH 7.2 was used for superfusion of preparations and filling of electrodes. L-Glutamate effectively blocks postsynaptic muscle contractions at concentrations ≥ 5 mM without influencing presynaptic calcium dynamics [134]. Late third-instar larvae were pinned to the bottom of a recording chamber with sylgard lining and cut open along the dorsal midline using buckled scissors (Frohnhäuser, Unterhaching, Germany) (Fig 1.11 A). Fat body, gut and big trachea were removed. Segmental nerves were severed and the brain and ventral nerve cord were removed. Larval neuromuscular junctions were recorded at muscle 6/7 in abdominal segments 2, 3 or 4 (Fig 1.10). Presynaptic boutons were stimulated by placing the cut end of a segmental nerve into a glass suction electrode (GB100F-10, Science Products, Hofheim, Germany) (Fig 1.11 B). Action potentials were induced by applying voltage pulses to the nerve (Iso-Stim 01-D, NPI Electronics, Tamm, Germany). Pulses (5.5 V, 0.3 ms) were applied at frequencies of 0, 10, 20, 40, 80 and 160 Hz, respectively. The sequence of stimulus frequencies was altered pseudorandomly. Recording time was 8 s (12 s for YC2.60, due to slow decay time-constant of the calcium response) and the stimulus period was 2 s starting after 2 s recording time. The interval between individual recordings was 1 min at least. Experiments were controlled by custom software

written by Jürgen Haag in Delphi (Borland, Scotts Valley, CA), using an analog-to-digital converter (DAS-1602/12; Computerboards, Middleboro, MA). Action potentials induced accumulating calcium influx that reached steady-state during the stimulus period for all GECIs except Yellow Cameleon 2.60. The steady-state calcium concentration is a linear function of stimulus intensity, as will be shown (see 3.1.2), and causes fluorescence changes in GECIs, that were monitored by 2-photon microscopy. Time-constants for the rise and decay of fluorescence signals were determined by fitting single exponential functions. For these values 40 Hz responses were analyzed. Stimulation at lower frequencies did not elicit detectable fluorescence signals in all GECIs and stronger stimuli led to saturation in most GECIs which influences time-constants of the responses (see Fig 3.13).

2.2.2 2-Photon Microscopy

Individual boutons were imaged using a custom-built 2-photon microscope [135] (design kindly provided by Winfried Denk), which allowed for wide-field or 2-photon imaging through the same objective (63 x / 0.90 n.a. for GECIs, 40 x / 0.80 n.a. for OGB-1 and Magnesium Green, water immersion, IR Achroplan; Zeiss, Jena, Germany). Wide-field illumination used a 150 W mercury arc lamp (USH 102 D; Ushio Inc.; Tokyo, Japan Power Supply: Model 1600, LampHousing: Arc Model 770 WT; both Opti-Quip, Highland Mills, NY), with optical filters (for YFP/CFP 450/50 excitation, 480 LP dichroic and 510/50 emission; for mDsRed 565/30 excitation, 585 LP dichroic, and 620/60 emission; all optical filters and dichroic mirrors by AHF, Tuebingen, Germany). The epifluorescence condenser was coupled to the microscope head containing tube lens, mirrors, and step motors to move the objective in three dimensions while the optical path was kept nearly constant (steering: Sutter MP285, Sutter, Novato, USA). Emitted light was projected onto the chip (1,040 x 1,392 pixels) of a CCD camera (Cool Snap HQ and MetaView software; Visitron Systems, Puchheim, Germany). Switch from wide-field to 2-photon microscopy involved moving of two mirrors. 2-photon fluorescence was excited by a mode-locked Ti:Sapphire laser ($<$ 100 fs, 80 MHz, 700-1000 nm; pumped by a 10 W Millenia laser; Tsunami; Spectraphysics, Darmstadt, Germany). Laser intensity was held constant at 6-15 mW for GECIs and at 45 mW for OGB-1 and Magnesium Green to minimize photo-bleaching and allow sufficient SNR [136]. Ratiometric GECIs were excited at 830 nm, GC1.6 at 920-930 nm, OGB-1 and Magnesium Green at 950 nm. An emission filter (700 SP) was inserted in front of a cassette of two photomultiplier tubes allowing simultaneous recording of different wavelengths of light. The photomultiplier tubes were equipped with bandpass

dichroic mirrors (485/40 for CFP, 535/30 for YFP, 510/50 for GCaMP 1.6, OGB-1 & Magnesium Green and 620/60 for mDsRED). Image acquisition was controlled by custom software (CfNT, written by R. Stepnoski, Bell Labs and M. Müller, Max-Planck-Institute for Medical Research, Heidelberg). Calcium signals were recorded at 64 x 64 pixel resolution at 8 Hz framerate or at 1 x 64 pixel line-scans at 500 Hz, respectively. Experiments were controlled by custom software (written in Delphi, Borland, Scotts Valley, CA, by J. Haag, Max-Planck-Institute of Neurobiology, Martinsried) using an analog-to-digital converter (DAS-1602/12; Computerboards, Middleboro, MA). All data were analyzed using custom software written in IDL (RSI, Boulder, CO, USA) by A. Borst.
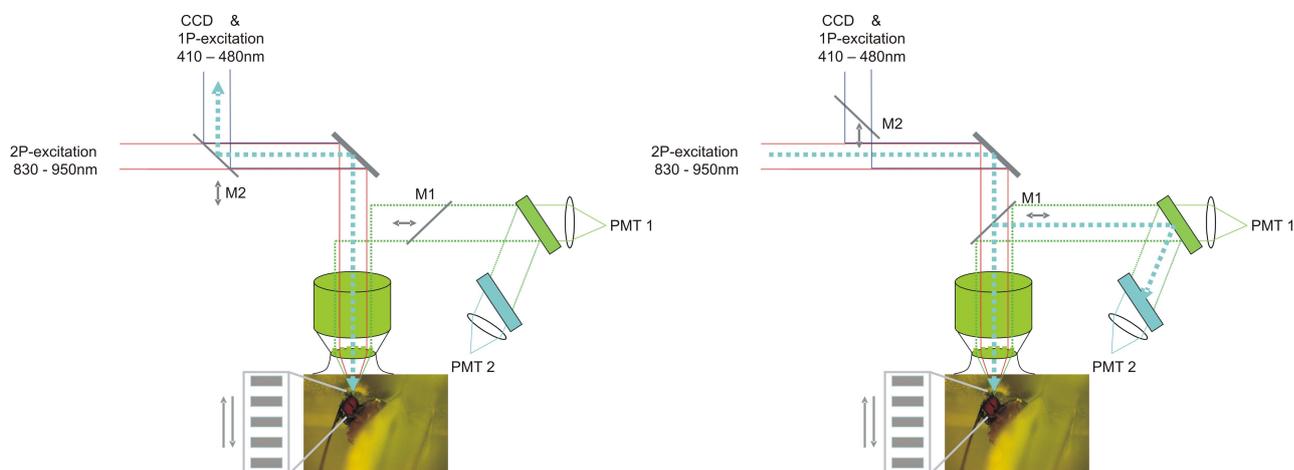
Figure 2.1: Simplified schematic of the optical paths in the 2-photon microscope. 2-P excitation source to the left, 1-photon excitation & CCD camera to the top, specimen & objective (green) below, photomultiplier tubes (PMTs) for photon detection during 2-photon microscopy to the right. Left panel: Depicted position of the mirrors M1 and M2 guides light from an arc lamp through the objective to the specimen. Emitted photons from the specimen that hit the objective are guided back along the same path and are sampled by the chip of a CCD camera. Right panel: Movement of M1 and M2 along the arrows guides 2-photon excitation to the specimen and emitted photons to the photomultiplier tubes, which are equipped with bandpass filters e.g. for CFP or YFP detection (green and cyan blocks). As indicated at the bottom of the panels, the setup can be equipped with a visual stimulus device for the presentation of movin gratings during *in vivo* imaging. (Sketch kindly provided by DF Reiff.)

2.2.3 Data Analysis

Aquired movies were analyzed using a custom software written in IDL (by Alexander Borst). Regions of interest were defined and fluorescence intensity in that region was averaged in each frame. A region of no interest was analyzed and used to subtract background fluorescence from each frame. Evaluation of these traces and signal processing was done in Matlab R2006b (MathWorks, Munich, Germany) software and Origin7.5 (Additive, Friedrichsdorf, Germany).

Single chromophore indicators: For background subtraction, a homogeneous region neighboring individual boutons was selected and its intensity was subtracted from the intensity of the bouton. For line scans a time-averaged mean intensity aside each bouton was subtracted as background. Bleaching kinetics are complex because they depend on the calcium binding state of indicators, i.e. different bleaching rates apply during stimulated and non stimulated periods. This is most obvious in responses to 160 Hz stimuli from GCaMP 1.6. 3.10. Here, bleaching during the stimulus period is pronounced. This could not be fully corrected, as can be seen from the decay of fractional fluorescence change during the steady-state period of stimulation. Bleach correction of individual bouton intensity traces was done by deleting the stimulation period before fitting a single exponential function to each trace and subtracting the resulting function from the original fluorescence trace. Where fits did not reach a quality threshold a linear fit was calculated and subtracted. From the resulting corrected trace for each bouton, the fractional fluorescence change (ΔF/F) was calculated by subtracting the average intensity measured before stimulus onset (average of 9 control frames = F_{cntrl}) from the fluorescence in each image F_t of a series and subsequently dividing the difference by F_{cntrl}.

For double-chromophore indicators, the ratio of fluorescence values from both channels was calculated after background subtraction and bleach correction form individual channels. The resulting trace was processed as described above to yield relative changes in the fluorescence ratio (ΔR/R) (for the respective Matlab scripts see Appendix).

Amplitudes and signal-to-noise ratios were then calculated for each bouton based on the mean ΔR/R or ΔF/F from 5 frames around peak amplitude and the corresponding standard deviation of the mean. Presented values for each GECI represent mean signal-to-noise ratio of all boutons measured at one stimulus protocol. Line scans were treated like movies for both single- and double-chromophore indicators. The average of the first 240 lines was used as F_{cntrl}. Ten frames were averaged for amplitudes and signal-to-noise ratios.

2.3 Quantitative Calcium Measurements with Synthetic Indicators

To quantify the calcium concentrations in boutons at rest and at steady-state during stimulation, I loaded motoneurons with synthetic dyes of well described response characteristics.

2.3.1 Dye Application by Anterograde Loading of Nerve Fibres

I first applied a method of dye application that relies on axonal transport of dextran conjugated dyes [112]. Therefore blunt suction electrodes were pulled and the opening melted to a diameter of $\approx 20~\mu m$, just wide enough to fit an intersegmental nerve. The electrode served for both stimulation and dye application. An ultrathin capillary (Microfil Custom CMF90U8cmL; World precision instruments, Sarasota, FL, USA) was inserted into the electrode till the tip of the capillary at most $\approx 50~\mu m$ away from the opening of the electrode. Through the capillary dye solution could be injected into the tip of the electrode after the nerve was sucked in. This was necessary because bath solution was sucked into the electrode tip together with the nerve. The capillary was connected to a pipette. By dye release from the capillary the dye concentration inside the electrode tip was increased. Then dextrane coupled dye diffused into the severed nerve endings and was actively transported down the axon along with the microtubular axonal transport [112]. Working speed was essential in this procedure because membranes of severed nerve ends reseal within 5 min after cutting and then do not take up dye.
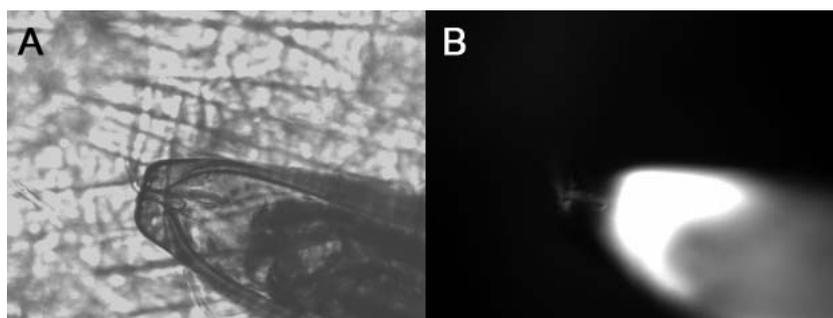
Figure 2.2: (A) Larval preparation with blunt suction electrode under wide field microscopy. A capillary for dye injection is visible as shadow inside the electrode (outer diameter is 90 μm and serves as scale bar, inner diameter is $\approx 15~\mu m$). A segmental nerve is sucked into the tip opening of 15 μm diameter. (B) The same preparation under fluorescent light shows fluorescent dye solution and faint staining in the descending nerve.

These experiments were done using wide field microscopy (Axiovert 35M; Zeiss, Ober-kochen, Germany), a CCD camera (Cool Snap HQ; Visitron Systems, Puchheim, Germany), and 1-photon fluorescence excitation. Light of 470 nm wavelength was generated using a monochromator (Polychrome IV; TILL Photonics, Martinsried, Germany). A 40x water immersion objective was used for wide-field epifluorescence detection. Images were acquired at 10 Hz framerate and 3x3 binning of the CCD chip. Dextrane-OGB-1 was imaged by excitation at 470 nm using a 480 nm longpass filter and a 535/50 nm bandpass filter for emission detection.

2.3.2 2-Photon Guided Dye Injection

Sharp quartz electrodes (with filament, length = 10 cm, outer diameter 1.0 mm, inner diameter 0.6 mm; Science Products, Hofheim, Germany, R 100$M\Omega$) were made on a laser puller (Sutter Instruments, P-2000, Novato, USA) and backfilled with OGB-1 or Magnesium Green solutions respectively (10 mM dye, in 0.5 $MKCl$ and 2 $MKAc$). Photomultipliers of the 2-photon microscope were equipped with one red (620/60 nm) and one green bandpass filter (535/50 nm) (AHF, Tuebingen, Germany). The red channel visualized the neuroanatomy of larval neuromuscular junctions expressing mDsRed and the green channel showed the filled electrode tip. Excitation was adjusted to 980 nm for dye injection and to 950 nm for recordings to allow improved visualization of mDsRed or of OGB-1 and Magnesium Green respectively. Pressure was applied to the electrode to provide a minimal efflux from the tip and to avoid calcium diffusion into it. For this a syringe was connected to the channel of the electrode holder via a plastic tube of 1 mm inner diameter. Injections were done directly into boutons (Fig 3.2). The injection electrode was steered with electronic manipulator units (Luigs & Neumann Feinmechanik, Ratingen, Germany). Membrane potentials between -20 and -55 mV were measured. Motoneurons displaying lower membrane potentials did not show calcium responses after dye injection. Dye concentration in cells is unknown, but does not influence response amplitudes in steady-state calcium measurements, because $\Delta F/F$ normalized for dye concentrations. So data from different experiments were pooled and averaged. Time-constants of fluorescence signals are affected by dye concentrations, so the presented time-constants represent an average over different concentrations in an applicable range.

2.3.3 Calcium Measurement without Wavelength Ratioing

I used a method that allows intracellular calcium measurements without wavelength ratioing as described by Maravall et al. [137]. This method relies on three measures: (i) the k_D for the applied indicator must be determined. Ideally this should be done *in situ*. However this is not always possible. (ii) *In situ* measurements of $R_f = F_{max}/F_{min}$ are necessary. F_{max} is the fluorescence intensity of the indicator when every indicator molecule is bound to calcium and F_{min} is the fluorescence intensity when no calcium is bound to the indicator. (iii) In the system under observation a linear relation of the concentration change $\Delta[Ca^{2+}]$ and the stimulus intensity must be given.

$[Ca^{2+}]_0$ (concentration at rest) is then provided by:

$$\frac{[Ca^{2+}]_0}{k_D} = \frac{(1 - R_f^{-1})}{\Delta f_{max}},\tag{2.1}$$

with $\Delta f_{max} = maximum\,fractional\,fluorescence\,change\,\Delta F/F$.

$\Delta[Ca^{2+}]$ at a given steady-state response is calculated as:

$$\frac{\Delta[Ca^{2+}]}{k_D} = \frac{F_{max}}{F_0}(1 - R_f^{-1})\frac{\Delta f}{(\Delta f_{max} - \Delta f)\Delta f_{max}}.\tag{2.2}$$

See [137] for a mathematical justification of the equations.

As dye diffusion could contribute to changes in resting fluorescence F_0 I monitored fluorescence changes after injection (Fig 2.3). I found that after 12-13 min, dye concentrations equilibrated throughout the entire neuromuscular junction. All experiments were done 20 min post injection.

(i) The k_D of OGB-1 was determined in a cuvette as 240 nM, in good accordance with values in the literature. No efforts have been reported to estimate an *in vivo* k_D for OGB-1 to my knowledge. I tried to adjust intracellular calcium concentrations to discrete values by perforating membranes using ionomycin. Ionomycin forms calciumpores inside membranes. This happens not only in neurons but also in muscles where it leads to fast calcium induced contractions, which made fluorescence measurements impossible and quickly destroyed the preparations. Blocking contractions with cytochalasin-D was effective but also altered the preparations morphology, probably by full relaxation of actin-myosin contacts.

(ii) F_{max} for OGB-1 is given by 160 Hz stimulation at neuromuscular junctions. Saturation of OGB-1 under these conditions was confirmed by the lack of further fluorescence increase at extracellular pH 8.8. The main calcium clearance mechanism in boutons of
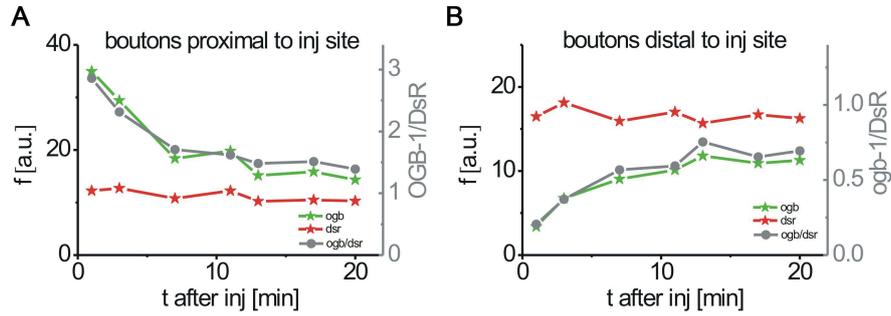
Figure 2.3: Fluorescence intensity is plotted as a function of time after injection. Images were taken at boutons neighbouring the injection site (A) and at boutons in a different side branch of the neuromuscular junction (B). Red traces show mDsRed fluorescence. Intensity in the red channel does not change over time in either group of boutons. Green traces show OBG-1 fluorescence. Diffusion leads to intensity decrease in boutons nearby the injection site, and to fluorescence increase in boutons distal from injection site. Grey traces indicate the ratio of red and green channel fluorescence. Both green and grey traces reach plateau in proximal and distal boutons after 12 and 13 min, respectively.

the larval neuromuscular junction is a calcium-proton exchanger [113]. Thus the amount of extracellular protons available can limit calcium clearance, i.e. increase of extracellular pH slows down calcium clearance and leads to higher steady-state accumulation of calcium after prolonged stimulation [113].

F_{min} was determined by bath applying BAPTA-AM (Molecular Probes) in HL6.1 (See 2.5). Hydrophilic compounds estered with an AM-group (acetoxymethyl) acquire lipophilic properties that allow crossing of cell membranes. Esterases in the cytosol cleave the ester-bonds, trapping the hydrophilic compound in the cytosol. Using transgenic animals expressing Yellow Cameleon 2.60 I determined effective concentrations and exposure times for BAPTA-AM application. Yellow Cameleon 2.60 was used because its calcium affinity was described *in vitro* as 40 nM. If that were true *in vivo* it should allow the detection of reduced calcium concentrations from resting values (around 50 nM according to [138, 134]). After a preparation was exposed to HL6.1 at zero calcium, 1 mM EGTA and 130 μM BAPTA-AM for 30 min, nerve stimulation induced no calcium responses after readministering calcium and washout of EGTA/BAPTA-AM. Washout after 15 min led to incomplete intracellular calcium buffering and Yellow Cameleon 2.60 showed calcium responses upon stimulation. Size and kinetics of these responses were reduced compared to normal responses from this GECI, likely by calcium buffering of BAPTA-AM. The intra-

cellular BAPTA concentrations reached after 30 min of exposure abolished the responses completely: no fluorescence responses to stimuli at any stimulus frequency were noticable, indicating that all remaining calcium was bound to BAPTA, and F_{min} could be recorded after a preparation injected with OGB-1 had been exposed to 130 μM BAPTA-AM for 30 min in HL6.1 at zero calcium and 1 mM EGTA.

(iii) Linearity of the stimulus-response curve at the neuromuscular junction was determined by calcium-response measurements with the low affinity indicators Fluo4FF (k_D = 10 μM) and Magnesium Green (k_D = 6 μM) respectively. For any calcium sensor, the fluorescence intensity is a linear function of the calcium concentration up to values of approximately half of the respective k_D [137].

2.3.4 GECI Performance in Neurons of Living Animals and in the Cuvette

Cuvette measurements

Protein expression and purification   Protein preparation and spectroscopy in cuvettes were done by Marco Mank. Procedures are briefly described here. For spectroscopic determination of calcium binding curves, GECI cDNAs were subcloned into the pRSETB vector (Invitrogen), which is optimized for protein expression using the T7 expression system and carries a histidin tag (6xhis), upstream of the multiple cloning site. Protein expression was achieved using the E.coli strain BL-21 (Invitrogen). Protein expression was induced to an OD 600 of 0.6 to 0.8 with 0.5 mM IPTG ($Isopropyl-\beta-D-Thiogalactosid$) for 2-3 hours at 37 $°C$. His-tagged protein was bound to a Ni-NTA-sepharose column by shaking for 2 h at 4 $°C$. The column was washed with 10 ml of protein wash buffer (containing 10 mM imidazol) and the protein was eluted by competitively displacing it with a high concentration of imidazol (150 mM). Yellow Cameleon 3.60 was amplified from pUAST by PCR using primers with attached EcoRI restriction sites (7&8 see 2.5). The product was then ligated into the EcoRI site of pRSETb. All other GECIs tested in cuvettes were already available in pRSETb.

Spectroscopy   Freshly purified protein was used to determine the k_D-values. For titration a prewarmed (room temperature) titration kit (Calcium Calibration Buffer Kit with Magnesium #1, C3721; Invitrogen) was applied. Two stock solutions were prepared: Zero calcium (mix 1 ml of zero calcium buffer with 1 volume of protein solution; $\approx 0.2 - 1 \mu M$

protein, directly into the cuvette; Hellma Precision Cells Quartz Suprasil, type 101-QS, 10 mm path), and high calcium (mix 5.4 ml of 39.8 $\mu\mu M$ free calcium buffer with 5.4 volumes of protein solution). Subsequently, the zero calcium stock was inserted into the fluorescence spectrophotometer (Cary Eclipse fluorometer, Varian) and a baseline spectrum was measured. Excitation wavelength for a CFP/YFP-FRET pair was 432 nm. Emission was determined in the range of 450 to 600 nm (all bandwidths 5 nm). Excitation wavelength for GCaMP 1.6 was 470 nm. Emission was determined in the range of 470 to 600 nm (all bandwidths 5 nm). Excitation wavelength for OGB-1 was 475 nm (bandwidth 10 nm). Emission was determined in the range of 490 to 600 nm (bandwidths 5 nm). Adjustment of free calcium was achieved by reciprocal dilution to the desired concentrations: A certain volume of zero calcium buffer was replaced with the same volume of calcium stock. 0, 0.065, 0.100, 0.225, 0.350, 0.600, 0.850, 1.35, 1.73, 2.85, 4.87, 7.37, 14.9, 29.9 and 39.8 μM free calcium was used as reference points to determine the k_D-value for GECIs (for OGB-1 concentrations were 0, 0.017, 0.038, 0.065, 0.1, 0.15, 0.225, 0.351, 0.602, 1.35, 39.8 μM free calcium). Calculation of the volumes that had to be replaced was along the manufacturers manual (http://probes.invitrogen.com/media/pis/mp03008.pdf).

Comparative Data Analysis

After spectroscopic measurements, $\Delta R/R$ at distinct calcium concentrations was calculated as:

$$\Delta R/R = \frac{R_x - R_{rest}}{R_{rest}} \tag{2.3}$$

with R_x = Ratio of YFP/CFP intensities at $[Ca^{2+}]$ = x and R_{rest} as resting calcium concentration. (Similarly for $\Delta F/F$ for GC1.6 and OGB-1).

To make cuvette measurements at the spectrophotometer comparable to *in vivo* data acquired at the 2-photon microscope, two corrections were made.

(i) Usually ratiochanges in spectroscopy are calculated relative to zero calcium. I calculated $\Delta R/R$, with R_{rest} at the lowest calcium concentration used (R_{rest} = 0.065 μM). In cuvette meaurements, D3cpv shows a steep slope of the titration curve close to zero calcium. Thus the assumed resting calcium level is a more critical value here than for most other GECIs. R_x for a hypothetical calcium level of 35 nM was interpolated for the titration of D3cpv and this value was used as R_{rest}. The same was applied to OGB-1.

(ii) I mimicked bandpass filters by integrating the emission intensities from 465 to 505 nm for CFP and from 520 to 550 nm for YFP. A titration curve of a purified GECI protein

was measured at the 2-photon microscope in aqueous solution as described for cuvette measurements and found that this bandpass correction leads to a maximum difference in ΔR/R under both imaging conditions of only 3.7 %. Applying this procedure, data from spectroscopy and from 2-photon microscopy can be compared, and detected differences are probably due to the GECIs environments *in vivo* and *in vitro* rather than the imaging methodology.

Extraction of the k_D-values was done by sigmoidal fits to the dose response curves (delta ΔR/R, normalized to 39.8 μM $[Ca^{2+}]$, versus logarithmic $[Ca^{2+}]$). The same method was applied to determine *in vivo* k_Ds.

2.4 Cloning

2.4.1 General DNA Methods

DNA concentration Double-stranded DNA has an absorption maximum at 260 nm. By measuring the absorption of DNA in water in a 1 cm quartz cuvette, the concentration of DNA samples can be calculated as:

$$[DNA](\mu g/ml) = OD_{260} * 50 * dilution factor. \tag{2.4}$$

PCR Primer-annealing temperatures varied in different reactions and were chosen according to the predicted primer melting temperature which correlates to length and GC content of the primers annealing regions.

PCR reaction mix:
50-60 ng plasmid DNA as reaction template
1 μl dNTP solution (12.5 mM)
2 μl primer A (50 μM)
2 μl primer B (50 μM)
5 μl polymerase buffer (10 x, provided by manufacturer)
38 μl H2O
1 μl (2 U) Vent polymerase.

Reaction cycles:
5 min heating to 95 °C

30 amplification cycles:

30 s 95 °C: melting of double-stranded DNA

30 s annealing of primers; temperatures varying from 52-62 °C

2 min 72 °C: DNA synthesis

After cycle completion: 3 min 72 °C; reaction termination by cooling to 4°C

Restriction Site Cleavage of DNA   DNA restriction digests were used to generate a vector or insert fragments necessary for DNA cloning. Insert and vector were cut with either one or two restriction enzymes at a time. For analytical purposes 0.5 - 1 μg DNA or about 10 μg DNA for larger preparations were cut with 1 U restriction enzymes per μg DNA. Buffers were used according to the manufacturers protocols. To avoid unspecific cutting, the volume of each reaction was raised to a minimum of 10 x the volume of restriction enzyme used. Incubation times were at least 2 hours at 37°C. The efficiency of the restriction was controlled by running a test sample on an agarose gel.

Ligation of "Sticky" DNA Fragments   In DNA ligations, the ratio of insert to vector should be at least 3:1; DNA concentrations were determined by spectrometric measurements. The ligation reaction mix was incubated overnight at 16°C or at room temperature for 2 h.

Ligation mixture:

60 ng vector DNA

180 ng insert DNA

1 μl ligase buffer (10 x)

1 μl (400 U) T4 DNA Ligase

10 μl with H_2O

Ligation of Blunt-End DNA Fragments   Incubation of a blunt-end ligation reaction in the presence of an excess amount of an appropriate restriction enzyme can dramatically increase the yield of recombinant plasmids. The role of the restriction enzyme is to cleave circular and linear concatemers at restriction sites that are re-formed when linear, because blunt-ended plasmid molecules may ligate to themselves. In almost all cases, ligation of the PCR product to the plasmid destroys the restriction site. The constant reclamation

of vector molecules drives the equilibrium of the ligation reaction strongly in favor of the chimeric plasmid containing the PCR product.

Ligation mixture:
1 μl intact plasmid (50 $ng/\mu l$)
0.05-0.5 $pmol$ PCR product (gel-purified)
2 μl 10x Universal KGB buffer
2 μl dNTP mixture (2.0-2.5 mM each)
1 mM ATP
2 μl restriction enzyme
1 U T4 DNA polymerase
3 U T4 DNA ligase
adjust volume to 20 μl with H_2O

The mixture was incubated for 4 h at 22 °C, then for 10 min at 65 °C to inactivate the enzymes. The restriction enzyme (2 U) was added and incubated for another 30 min. This step reduced the ratio of intact plasmid in the reaction mixture. E. coli were transformed as usual using 0.5 μl of the reaction mixture. The transformed cultures were spread out on plates containing IPTG and X-gal. Typically, 10-80 % of white colonies contain recombinant plasmids. The length of the inserts in the plasmids were checked by restriction digests and positives were confirmed by PCR. (from: Molecular Cloning, 3rd edition, Sambrook and Russell eds., CSHL Press, 2001.)

Chemotransformation of Competent E. Coli   Chemically competent E. coli cells, kept in 50 μl aliquots in 1.5 ml Eppendorf cups at -80 °C were thawed on ice, mixed with the desired DNA plasmid and incubated on ice for about 20 min. A heat shock was applied to the cells by transferring them into a 42 °C water bath for 1 min, and afterwards they were again incubated on ice for about 2 min. The cells were then diluted in 150 μl LB medium, shaken in a 37 °C incubator for 45 min and plated onto LB agarose plates containing the appropriate antibiotic for selection.

Plasmid Isolation from E. Coli   For minipreps 3 ml LB/Amp-Medium (100 $\mu g/ml$ ampicillin) was inoculated with a single colony and incubated overnight at 37 °C under constant agitation. Cultures were transferred into 2 ml Eppendorf tubes and cells were centrifuged (14000 g, 1 min, at room temperature). Plasmids were isolated from bacterial cells using

anion exchange columns (Qiagen) following manufacturers protocols. For midipreps a single colony was inoculated in 3 ml LB/Amp-Medium and shaken for 3 h at 37 °C before this preculture was poured into 200 ml LB/Amp-Medium and incubated overnight at 37 °C under constant agitation. Plasmids were extracted following the manufacturers protocol.

Gel Electrophoresis The efficiency of restrictions was evaluated by running samples on 1 % agarose gels. Therefore agarose was diluted in TAE buffer. After pouring the solution in a gel chamber, Ethidiumbromide was added. After the gel solidified the samples were applied individually.

2.4.2 Site Directed Mutagenesis

The original vector pRSETb is used due its 3 kb size. The mutagenic primer pair (9&10, see 2.5) contains the DNA sequence with a mutated base located in the middle with about 10-15 bases of the original DNA sequence on both sides. The length of the primer was chosen so that a melting temperature (Tm) of about 74 °C is achieved (based on the formula: $Tm = (2°C) * (A + T) + (4°C)(G + C)$). The primers should have a minimum GC content of 40 % and should terminate 3' with G or C. Primer extension time was set to 2 min per 1000 base pairs, leading to a total extension time of 5 min for the 3 kb long pRSETb.

2.4.3 P element Mapping by iPCR

For the identification and cloning of putative enhancer elements for transgene expression in LPTCs, randomly inserted P elements (pGaWB) producing Gal4 expression patterns including LPTCs were mapped by inverse PCR (iPCR). Genomic DNA of an enhancer-trap line was purified following a standard protocol (www.fruitfly.org/ about/ methods/ inverse.pcr.html). The genomic DNA is digested using restriction enzymes that cut close to the ends of pGaWB insertions and statistically every 256 bp in a random genome sequence (4 bp recognition site, like Sau3A, HinPI or MspI). The size of the resulting genomic DNA-fragments is on average 256 bp + about 100 bp plasmid DNA. Ligation in a large volume leads to circularisation of fragments. PCR with forward and reverse primers complementary to the plasmid part amplifies only circular fragments that contain plasmid DNA (Primers 1-6, see 2.5). Sequencing of these products gives plasmid sequence and flanking genomic sequence. Genome BLAST of the genomic part then reveals genomic positions of

pGaWB insertions. This can be done for 3' and 5' ends of inserted P elements.

Genomic DNA   30 anesthetized flies were collected in an Eppendorf tube and frozen at -80 °C. Flies were grinded in 200 μl DNA extraction buffer A, 200 μl buffer A were added and grinding was continued until only cuticles remained. The suspension was incubated at 65 °C for 30 min. 800 μl LiCl/KAc solution were added and incubated on ice for at least 10 min. Then the mix was spinned for 15 min at RT and 1 ml of the supernatant was transferred into a new tube, avoiding floating crud. 600 μl isopropanol were added, mixed, and again spinned for 15 min at room temperature. The supernatant was aspirated away. The cup briefly centrifuged and the supernatant aspirated again, washed with 70 % ethanol and dried. Then the DNA was resuspended in 150 μl TE and stored at -20 °C.

Restriction Digest

HinPI (3' end):
40 μl genomic DNA
5 μl NEB buffer 2
4 μl HinPI
1 μl H_2O

Sau 3A (5' end):
40 μl genomic DNA
8 μl Sau 3A buffer
8 μl Sau 3A
1 μl BSA
23 μl H_2O

3h at 37 °C
heat inactivation 1h at 65 °C

Selfligation

40 μl digested DNA

40 μl 10x T4 buffer

4 μl T4-Ligase (400.000 U/ml)

316 μl H_2O

over night at 4 $^{\circ}C$

iPCR-5'end

PCR-program:

1) 94 $^{\circ}C$ - 4 min

2) 94 $^{\circ}C$ - 30 s

3) 68.7 $^{\circ}C$ - 2 min

4) 72 $^{\circ}C$ - 3 min

5) back to 2), 30 cycles

6) 72 $^{\circ}C$ - 7 min

7) 4 $^{\circ}C$

PCR-mix:

5 μl DNA

5 μl 10X-Buffer

1 μl dNTPs

1 μl Primer 1, (see 2.5)

1 μl Primer 2, (see 2.5)

1 μl Taq-Polymerase

36 μl H_2O

(dNTPs stock: 12,5 mM, = 250 μM, Primerstock: 50 μM, = 1 μM)

iPCR-3'end

PCR-program:

1) 94 $^{\circ}C$ - 4 min

2) 94 °C - 30 s
3) 63.4 °C - 2 min
4) 72 °C - 3 min
5) back to 2), 30 cycles
6) 72 °C - 7 min
7) 4 °C

PCR-mix:
5 μl DNA
5 μl 10X-Buffer
1 μl dNTPs
1 μl Primer 3, (see 2.5)
1 μl Primer 4, (see 2.5)
1 μl Taq-Polymerase
36 μl H_2O

(dNTPs stock: 12,5 mM, $= 250$ μM, Primerstock: 50 μM, $= 1$ μM)

Nested PCR:
PCR-program & mix as before
Primers 5&6, (see 2.5)

2.4.4 Enhancer Cloning

Enhancer fragments were cloned by PCR. As PCRs on genomic DNA tended to result in multiple products or no products at all, the reactions were performed on BAC clone DNA. BAC clones were identified after genomic regions of interest were mapped by iPCR. PCR on BAC-clone DNA was performed as described. PCR primers were designed according to standard protocols and extended by KpnI restriction sites (successfull primers: 30-33, see 2.5). Resulting PCR products were subcloned in pBluescript (pBSK II-). Where nessecary, fragments were polished for blunt ligation, pBSK II- was digested with EcoRV resulting in blunt ends and ligation procedure was performed as described. Putative enhancer fragments were excised from pBSK II- by KpnI digestion and inserts were purified.

2.4.5 The Driver Construct: Enhancer-LexA Fusion

A pCasper4 vector, carrying a LexA::VP16 construct, fused to an SV40 polyadenylation signal sequence (see: 2.4) under the control of the OR83b genomic enhancer was provided by Tzumin Lee (University of Massachusetts, USA) [125]. The OR83b enhancer normally drives expression of the gene OR83b in larval and adult olfactory receptor neurons. Sequencing (primers 15-29, see 2.5) revealed KpnI restriction sites 5' and 3' of the OR83b enhancer. The 5' KpnI site is not included in the original publication. The enhancer fragment could thus be excised by KpnI digest and the remaining vector treated with Calf Intestinal Alkaline Phosphatase (CIP), to minimize self-ligation by removing the 5'-phosphate from both termini of the linear vector. I then inserted genomic enhancer sequences extracted from pBSK II- as described above.
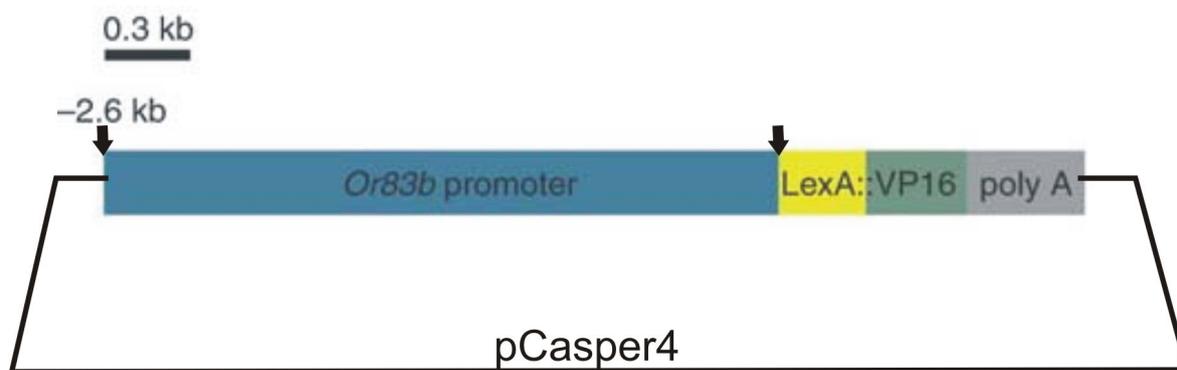
Figure 2.4: LexA::VP16 expression cassette in the vector pCasper4. It consists of the genomic enhancer region for OR83b, LexA fused to VP16 and the PolyA sequence from SV40. The 2.6 kb OR83b fragment can be excised by KpnI digest (arrows) and replaced by putative enhancer fragments for expression in interneurons of the visual system (modified from [125].

2.4.6 The Effector Construct: TN-XXL and Yellow Cameleon 3.60 in pLOT

I obtained the construct shown in Fig 2.5 without rCD2::GFP insertion from Tzumin Lee (University of Massachusetts, USA) [125]. This construct is based on pUAST with the major change that the UAS sites are replaced by the LexA binding site (LexAop). cDNA for Yellow Cameleon 3.60 was excised from pUAST by NotI digest and inserted into the NotI restriction site of pLOT.

The SF (super folder) version of TN-XXL contains additional mutations (ECFP: S30R Y39N A206K, Citrine: S30R Y39N F64L V163A S175G A206K) that are supposed to enhance protein maturation at 37 $^{\circ}C$, but that do not alter the signalling properties of TN-XXL (Marco Mank, unpublished data). cDNA for TN-XXL-SF was obtained in pcDNA3 from Marco Mank, in a BamHI and EcoRI fragment including a kozak sequence with 5' NotI site and TN-XXL cDNA. Kozak and TN-XXL were excised by NotI digest and inserted into the NotI site of pLOT. Orientation of the insertion was checked by sequence analysis (primers 13&14, see 2.5). Transgenic flies were generated as described and expression was tested by crossing transformed flies to flies expressing LexA under OR83b control.
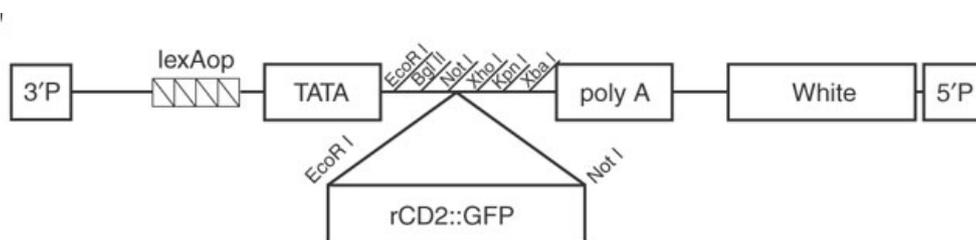
Figure 2.5: pLOT vector with rCD2::GFP insertion in the mcs. The vector is based on pUAST and contains the bacterial operator LexAop instead of UAS sites, a TATA box, multicloning site, poly adenylation sequence and a mini-white marker gene (From Lai & Lee 2006).

2.4.7 GECIs in pUAST

TN-XXL cDNA for TN-XXL was excised from pcDNA3 as described above and inserted into the NotI site of pUAST. Orientation of the insertion was checked by sequence analysis (primers 13&14, see 2.5).

Yellow Cameleon 3.60 cDNA for Yellow Cameleon 3.60 was obtained in pcDNA3, excised by NotI digest and ligated into the NotI site of pUAST. Orientation of the insertion was checked by sequence analysis (primers 13&14, see 2.5).

Yellow Cameleon 2.60 Yellow Cameleon 2.60 was generated from Yellow Cameleon 3.60 by site directed mutagenesis in pRSETb (Wolfgang Essbauer and Dierk F. Reiff). Yellow Cameleon 3.60 was flanked by NotI sites in pcDNA3 and was excised it with HindIII and XhoI, inserted in pRSETb and performed site directed mutagenesis, using primers 9&10

(see 2.5). From pRSETb the NotI/NotI fragment was excised and inserted into the NotI site of pUAST.

D3cpv D3cpv was obtained from Maz Hasan and Roger Y. Tsien in pcDNA3. D3cpv was inserted in pcDNA3 between the BamHI and EcoRI sites. A His repeat with a 5' NotI site was inserted between HindIII and BamHI. I excised a NotI fragment and inserted it into the NotI site of pUAST. Orientation of the insertion was checked by sequence analysis (primers 13&14, see 2.5).

GCaMP 2 A BglII/NotI fragment containing GCaMP 2 preceeded by His repeats was isolated from pN1 (provided by Junichi Nakai) and inserted between the BglII/NotI sites of pUAST.

2.5 Recipes, Solutions, Materials

Flyfood

5 l H_2O
28 g agar
110 g treacle
400 g malcine
400 g corn flower
50 g soy flower
90 g dry yeast
31.5 ml nipagin

Egglaying Medium

Grapeagar dishes were prepared for flies to lay eggs on. 200 ml red grape juice (Rio D'Oro, Aldi) were warmed up in the microwave for 2 minutes and mixed with 3 g Select Agar. After reheating, the solution was poured into petri dishes. Fresh plates were prepared on the day of injection. After clearing all eggs from a plate it was reused.

HL6.1 after Macleod et al., 2003

15,0 mM $MgCl_2$

24,8 mM KCl

23,7 mM $NaCl$

10,0 mM $NaHCO_3$

13,8 mM Isethionic acid (Na^+)

5,0 mM BES

80,0 mM Trehalose x $2H_2O$

5,7 mM L-Alanine

2,0 mM L-Arginine HCl

14,5 mM Glycine

11,0 mM L-Histidine

1,7 mM L-Methionine

13,0 mM L-Proline

2,3 mM L-Serine

2,5 mM L-Threonine

1,4 mM L-Tyrosine

1,0 mM L-Valine

adjust to pH 7.2 for experiments add 1.5 mM $CaCl_2$ and L-Glutamate 7 mM

KGB Buffer

1 M KCl

250 mM Tris-acetate (pH 7.6)

100 mM magnesium acetate tetrahydrate

5 mM ß-mercaptoethanol

0.1 mg/ml bovine serum albumin

10x restriction endonuclease buffer was stored in aliquots at -20°C.

DNA Extraction Buffer A

100 mM Tris-HCl, pH 7.5

100 mM EDTA

100 mM $NaCl$

0.5 % SDS

LiCl/KAc Solution

1 part 5 M KAc stock
2.5 parts 6 M $LiCl$ stock

Injection Buffer pH 6.8 10x

0.2 ml 0.5 M $NaPi$
5 ml 1 M KCl
94.8 ml H_2O
sterile filtration of 1x solutions

TAE Buffer 50x

(Tris-Acetate-EDTA)
242 g Tris base
57.1 ml glacial acetic acid
100 ml 0.5 M EDTA
add ddH_2O to 1 l and adjust pH to 8.5.

Tris-Cl pH 7.5

121.1 g Tris in 800 ml H_2O
65 ml concentrated HCl
add ddH_2O to 1l
autoclave

TE Buffer 1x

(Tris EDTA)
10 mM Tris-Cl (pH 7.5)
1 mM EDTA (pH 8)
autoclave

Sepharose CL6B

wash sepharose (2x) in 3x volume TE

discard TE supernatant and mix sepharose (2part) in TE (1part)

autoclave

PBT 10x

1 l PBS 10x

5 ml 100 % Triton X-100

Materials and Suppliers

Consumables

Material	Supplier
Tubes	Eppendorf, Hamburg (Germany)
PCR Tubes	Eppendorf, Hamburg (Germany)
Falcon 50ml & 15 ml tube	Becton Dickinson, Franklin Lakes (USA)
QIAquick Mini & Midiprep Kit	Qiagen, Hilden (Germany)
QIAquick Gel Extraction Kit	Qiagen, Hilden (Germany)
QIAquick PCR Purification Kit	Qiagen, Hilden (Germany)
Glass pipettes GB150F-10	Science Products GmbH, Hofheim (Germany)
Glass pipette GB100F-10	Science Products GmbH, Hofheim (Germany)

Table 2.2: Table of Consumables and Suppliers.

Chemicals

Material	Supplier
Adenosine Triphosphate (ATP)	Sigma, St. Louis (USA)
Agar	Sigma, St. Louis (USA)
Ammonium Acetate	Merck, Darmstadt (Germany)
Ampicillin Sodium Salt	Roth, Karlsruhe (Germany)
BAPTA-AM	Invitrogen, Karlsruhe (Germany)
BES	Roth, Karlsruhe (Germany)
Bovine Serum Albumin (BSA)	New England Biolabs, Beverly (USA)
Calcium Chloride dihydrate	Sigma, St. Louis (USA)
Cytochalasin D	Tocris, Bristol (UK)
Deoxyribonuclease	Sigma, St. Louis (USA)
DMSO (Dimethylsulfoxide)	Sigma, St. Louis (USA)
D-Trehalose Dihydrate	Sigma, St. Louis (USA)
EGTA (Ethylene-glycol-bis (beta-amino-ethylether-tetra-acetic acid))	Sigma, St. Louis (USA)
Fluo-4FF, pentapotassium salt	Invitrogen, Karlsruhe (Germany)
Glucose (D-(+)-Glucose anhydrous, min 99%)	Sigma, St. Louis (USA)
Glycine	Merck, Darmstadt (Germany)
HEPES free acid	Sigma, St. Louis (USA)
Ionomycin calcium salt	Sigma, St. Louis (USA)
L-Glutamic Acid	Tocris, Bristol (UK)
Magnesium Chloride, Hexahydrate	Merck, Darmstadt (Germany)
Magnesium Green, pentapotassium salt	Invitrogen, Karlsruhe (Germany)
Oregon Green 488 BAPTA-1, hexapotassium salt	Invitrogen, Karlsruhe (Germany)
Pfu Polymerase	Stratagene, La Jolla (USA)
Poly-L-lysine Hydrobromide	Sigma, St. Louis (USA)
Potassium Chloride	Merck, Darmstadt (Germany)
Ribonuclease A	Sigma, St. Louis (USA)
Saccharose	Merck, Darmstadt (Germany)
Sepharose CL6B	Sigma, St. Louis (USA)
Sodium Bicarbonate	Sigma, St. Louis (USA)
Sodium Chloride	Sigma, St. Louis (USA)
Sodium Phosphate Monobasic, Anhydrous	Sigma, St. Louis (USA)
Streptomycin-Penicillin solution	Sigma, St. Louis (USA)
Taq Polymerase	Fermentas, Leon-Rot, (Germany)
T4-Ligase	New England Biolabs, Beverly (USA)
Triton	Sigma, St. Louis (USA)
Trizma Base	Sigma, St. Louis (USA)
Voltalef 10S oil	Lehmann & Voss & Co., Hamburg (Germany)
Voltalef 3S oil	Lehmann & Voss & Co., Hamburg (Germany)
Yeast extract	Sigma St. Louis (USA)

Table 2.3: Table of Chemicals and Reagents and Suppliers.

Consumables

Enzyme	Recogntion Site	Supplier
BamHI	GGATCC	New England Biolabs GmbH, Frankfurt (Germany)
EcoRI	GAATTC	New England Biolabs GmbH, Frankfurt (Germany)
EcoRV	GAT.ATC (blunt)	New England Biolabs GmbH, Frankfurt (Germany)
Hind III	AAGCTT	New England Biolabs GmbH, Frankfurt (Germany)
HinP1	GCGC	New England Biolabs GmbH, Frankfurt (Germany)
KpnI	GGTACC	New England Biolabs GmbH, Frankfurt (Germany)
NotI	GCGGCCGC	New England Biolabs GmbH, Frankfurt (Germany)
Sau3A	GATC	New England Biolabs GmbH, Frankfurt (Germany)
SpHI	GCATGC	New England Biolabs GmbH, Frankfurt (Germany)
XbaI	TCTAGA	New England Biolabs GmbH, Frankfurt (Germany)

Table 2.4: Table of Restriction Endonucleases.

Plasmids

Plasmid	Supplier
pcDNA3 (5,4 kb)	Invitrogen, Carlsbad (USA)
pCasper4	Drosophila Genomics Resource Center, Indiana (USA)
pCasper4-OR83b-LexA::VP16::SV40 (12kb)	Tzumin Lee, University of Massachusets
pLOT (9 kb)	Tzumin Lee, University of Massachusets
pMT (3,5 kb)	Invitrogen, Carlsbad (USA)
pRSETb (3,3 kb)	Invitrogen, Carlsbad (USA)
pTGal (11 kb)	Drosophila Genomics Resource Center, Indiana (USA)
pUAST (9,5 kb)	Drosophila Genomics Resource Center, Indiana (USA)

Table 2.5: Table of Plasmids.

Primers

	Name	Sequence
1	PGaw2	CAGATAGATTGGCTTCAGTGGAGACTG
2	PGaw3	CGCATGCTTGTTCGATAGAAGAC
3	Pry4	CAATCATATCGCTGTCTCACTCA
4	Plw3-2	TAACCCTTAGCATGTCCGTGGGGTTTG
5	Plw3-3	CAAAGCTCTAGCTAGAGGATC
6	Spep1	GACACTCAGAATACTATTC
7	yc3.6puast_fw	GGGAATTCGTTAACAGGTCTTGCATGG
8	yc3.6puast_rv	GGAATTCCGAGGCACCCGCGAGCGCTTAC
9	Q104E_forw	GGCTACATCAGCGCTGCTGAATTACGTCACGTCAT GACAAACC
10	Q104E_rev	GGTTTGTCATGACGTGACGTAATTCAGCAGCGCTG ATGTAGCC
11	Seq_CaMfor	AAGGATGGGGACGGCACC
12	Seq_CaMrev	CTTCCAGCGCCTCTTCCC
13	puast_rev new	CTCTGTAGGTAGTTTGTCCAA
14	puast_forw new	CAATCTGCAGTAAAGTGCAAG
15	pCas4_mcs_rev	TTTTAAATCTACATTCTCC
16	pCas4_for2	GTTGATTAACCCTTAGC
17	pCas4_for3	CATAATATTAATTAGACG
18	pCas4_rev2	GAGACGGCGATATTTCTG
19	pCas4_rev3	GTTCAATGATATCCAGTGC
20	SV40_3'rev	GATTCTAATTGTTTGTG
21	SV40_5'rev	GAATGCAATTGTTGTTG
22	VP16_3'rev	CAATTCCAAGGGCATC
23	VP16_5'rev	CGCCGTCTAAGTGGAGC
24	LexA_3'rev	CAGGCGCTTAACGGTAAC
25	LexA_5'rev	CAGCCGCGTTTGGGGAAC
26	VP16_for1	GCGCTAGACGATTTCG
27	SV40_for1	CACTGCATTCTAGTTG
28	SV40_for2	GACTAGAGATCATAATC
29	SV40_rev	GATTATGATCTCTAGTC
30	2056_fw_Kpn	AAACGGGGTACCCCCTGCAAGATAAATGGGCAAA CTTGAT
31	2056_rv_Kpn	AAACGGGGTACCCCCACTTCACATTAGCCCATCC
32	1187_fw_kpn	ACATCGGGGTACCATCACCCGCATCCTCCGAATC
33	1187_rev_kpn	ACATCGGGGTACCCGCTAATAGACCCTCGTCAAGC

Table 2.6: List of all used primers.

3 Results

The properties of calcium indicator proteins *in vivo* cannot be predicted from *in vitro* analysis. It has been shown that their fluorescence changes in response to calcium changes were markedly reduced or absent when expressed in neurons of living animals [38, 39, 37]. Moreover, initial attempts to optically record motion responses in LPTCs of adult flies using GECIs failed in our laboratory. Thus, I set out to characterize the *in vivo* response properties of one unpublished and a variety of recently developed calcium indicators in a suitable *in vivo* test system, the larval neuromuscular junction. There, electrical stimulation of GECI expressing motoneurons leads to stimulus induced calcium influx at presynaptic boutons (see 1.3). In the cytosol of boutons calcium accumulates dependent on the stimulus intensity and elicits fluorescence responses in GECIs which can be recorded. This allowed a qualitative comparison of GECI response properties *in vivo* under reproducible conditions as frequency and number of action potentials can be precisely controled [39]. However, to allow for a quantitative comparison of different GECIs in neurons *in vivo* and their response characteristics *in vivo* vs. *in vitro*, I determined the absolute calcium concentrations in presynaptic boutons of the neuromuscular junction at rest and at various levels of induced neural activity. This was done using synthetic calcium sensors. Although the neuromuscular junction is in principle well accessible with 1-photon excitation fluorescence imaging [93, 112], 2-photon microscopy was used throughout, except stated otherwise. As these experiments should ultimately allow for the rational choice of the most suitable GECIs for optophysiological characterizations of LPTC response properties, which requires 2-photon microscopy, I kept imaging conditions in both types of experiments as similar as possible. On the basis of this analysis I chose two GECIs for *in vivo* imaging of LPTCs of adult, transgenic flies during visual motion stimulation. Using one of these GECIs it was possible to optically record directional selective motion responses in visual interneurons of living fruit flies.

3.1 Quantitative Calcium Measurements with Synthetic Indicators

Standard methods of intracellular calcium quantification make use of ratiometric excitation of the dye fura-2 [47]. However, ratiometric excitation is not possible at our 2-photon microscope. I thus used a method described by Maravall and colleagues [137] to estimate resting calcium and steady-state calcium concentrations in presynaptic boutons at different stimulus frequencies using the synthetic calcium sensor OGB-1. For this method ratiometric excitation is not necessary, and fewer parameters need to be determined in each experiment (see 2.3).

3.1.1 Dye Loading into Presynaptic Boutons

Anterograde Dye Loading by Dextrane Coupled Transport

The major disadvantage of synthetic dyes over transgenic dyes is the difficulty of loading them into cells of known identity. I first applied a method for dye loading under wide field microscopy [112]. The dye is loaded via the suction electrode that houses the severed nerve
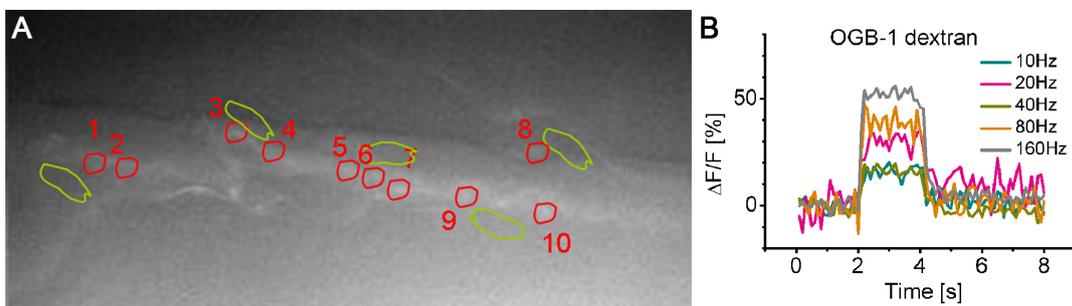
Figure 3.1: Imaging calcium activity in presynaptic boutons of neuromuscular junctions filled with dextrane conjugated OGB-1. (A) Raw image, taken after anterograde dye loading during 160 Hz stimulation at t = 3 s. Fluorescence intensity from boutons barely exceeds background fluorescence. Red circles and numbers indicate evaluated "regions of interest" where boutons were identified. Green circles indicate "regions of no interest", that were evaluated for background subtraction from traces of nearby boutons. (B) Average fractional fluorescence changes are ploted over time. Each trace represents the averaged responses of 9 boutons. Action potentials of various frequencies were elicited between t = 2-4 s. Note, that peaks of the fluorescence responses were not proportional to stimulus intensity.

end (Fig 2.2). The nerve takes up dye by diffusion. Dextrane is transported anterogradely along microtubules by the fast axonal transport machinery. Loading of dextrane conjugated OGB-1 was achieved as described (2.3.1). Then, fluorescence responses were recorded at presynaptic boutons in response to action potentials, induced at frequencies of 10-160 Hz. Loading efficiency was poor. Approximately 5 min after the nerves were cut, axonal membranes resealed. I was not able to increase working speed enough to allow sufficient dye loading. This resulted in very limited dye loading so that some boutons could only be identified during stimulation (see Fig 3.1 A). Low fluorescence intensity at the low dye concentrations occasionally yielded fluorescence recordings as shown in Fig 3.1. This was the only set of experiments in which 1-photon excitation and CCD-camera imaging were applied for measurements. In all further experiments 1-photon excitation and CCD camera imaging were used for initial approach of electrodes, and recordings were then done using 2-photon microscopy. Next, an alternative method of dye application was developed based on 2-photon microscopy and iontophoretic dye injection to reliably achieve sufficient dye loading.

2-Photon Guided Dye Injection

Synthetic calcium dyes were directly injected into genetically labeled neuromuscular junctions (see Fig 3.2). Therefore, flies carrying the mDsRed transgene under UAS control were
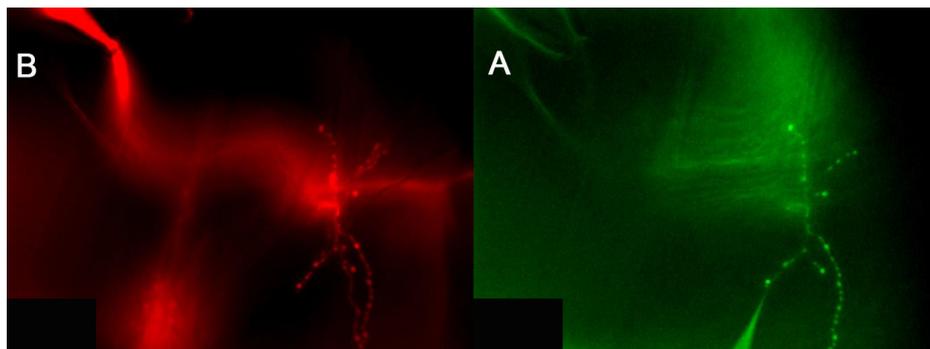

Figure 3.2: CCD-camera images of a genetically red labeled neuromuscular junction, loaded with a green, synthetic calcium dye. Pictures were taken with two different spectral filter sets. (A) Filter set for DsRed visualized the neuromuscular junction and the segmental nerve inside the suction electrode (upper left) that was used for electrical stimulation. (B) A spectral filter set for green fluorescence visualized the neuromuscular junction and the injection electrode (bottom) after dye injection.

crossed to flies carrying the $elav^{c155}$ Gal4 insertion. $elav^{c155}$ is the name of a panneuronal driver line and progeny of the crosses expressed mDsRed in all neurons. For sufficient staining intensity flies were bred homozygous for both the Gal4 and the UAS insertion.

Initial approach of the injection electrode to the neuromuscular junction was done under 1-photon fluorescence excitation using a mercury arc lamp and CCD-camera imaging with red and green filter sets sequentially (Fig 3.2). Then, I switched to 2-photon microscopy,
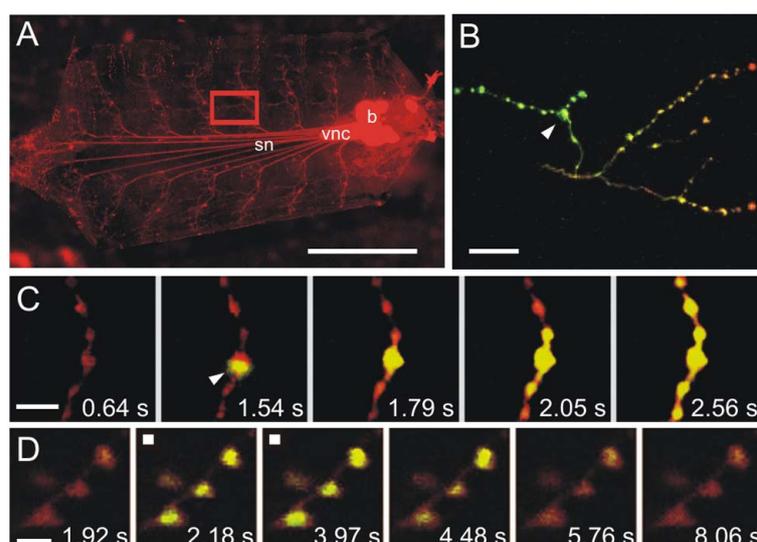

Figure 3.3: Injection and recording synthetic calcium sensors in genetically labeled neurons. (A) Wide field fluorescence image of a fillet preparation of a transgenic *Drosophila* larva expressing mDsRed in all neurons (red). Neuromuscular junctions on muscle 6/7 (red box and B) were electrically stimulated and imaged. Corresponding somata reside in the ventral nerve cord (vnc); axons innervate muscles via segmental nerves (sn); for experiments sn were cut, brain (b) and vnc were removed and loose nerve ends were placed in a suction electrode for electrical stimulation. (B) Overlay of red and green channels of a 2-photon microscopy image taken at a neuromuscular junction expressing mDsRed and filled with OGB-1. 1 *min* after injection, the strongest green staining is seen nearby the injection site (white arrowhead). (C) Dye diffusion along motoneuron terminal during injection. Injection site marked by arrowhead. Images were taken at the times indicated. Injection started at t = 1.54 *s*. (D) Calcium response at OGB-1 filled boutons. Action potential trains induce accumulating calcium influx, leading to fluorescence changes at presynaptic boutons. Imaging resolution was 64x64 pixels, frame rate 8 *Hz*, 64 frames recorded, frames shown are 15, 17, 31, 35, 45 & 64, voltage pulses were applied from t = 2 *s*-4*s* (frames 16-31). scale bars: (A) 1 *mm*, (B) 20 *μm*, (C) 10 *μm*, (D) 5 *μm*. Genotype: $elav^{c155} - Gal4; UAS - mDsRed$.

which allowed monitoring of red and green fluorescent molecules in parallel (Fig 3.3). mDsRed, expressed in larval motoneurons, and green calcium indicators in the quartz electrode can both be visualized by 2-photon excitation at wavelengths of 950-980 nm. Emitted photons of different wavelengths were then filtered by optical band-pass mirrors (see 2.1). This allowed guidance of the green electrode tip to red boutons.

Synthetic, green calcium indicators were injected into genetically red labeled boutons (Fig 3.2 & Fig 3.3 A&B) of 2-5 μM diameter, or into axonal branches of ≈ 1 μM diameter. Iontophoresis caused progressive dye loading into motoneuron axons (Fig 3.3 C). After a few seconds, the electrode was withdrawn. Dye diffusion reached a plateau after 13 min (see Fig 2.3). After 20 min calcium measurements were started. Fig 3.3 D shows selected false color coded fractional fluorescence change images of calcium responses in four boutons. The axon was stimulated with a train of action potentials at 160 Hz over 2 s starting after 2 s of recording. Stimulus frames are marked by white squares. The decay of the fluorescence responses is slower than the rise. ≈ 2 s after the offset of the stimulus, baseline fluorescence is reached again. Amplitude of the fluorescence response is a function of stimulus frequency. Similar experiments were performed using calcium dyes of different affinities to allow quantification of calcium concentrations: Fluo-4FF (Fig 3.4), Magnesium Green (Fig 3.5), and OGB-1 (Fig 3.6).

3.1.2 Stimulus-Response Relation at the Neuromuscular Junction

The method I applied for calcium quantifications first requires a description of the relationship of stimulus intensity and calcium concentration changes in presynaptic boutons of the neuromuscular junction. This relation should be linear over the whole stimulus regime. For the logic of the method for calcium quantification refer to 2.3.3. Calcium indicators report increases in concentrations with linear fluorescence changes up to calcium concentrations of about half the indicators k_D. Expected cytosolic calcium concentrations at presynaptic boutons do not exceed several μM ([134]). High-affinity dyes like OGB-1 ($k_D = 240$ nM) can thus not be used to assess the stimulus response relation in motoneuron terminals, because high calcium affinity of the indicator leads to its saturation at moderate stimulus regimes. Indicator saturation may mask the true relation of calcium influx and action potential frequency, intrinsic to the biological system. Low-affinity calcium reporter, like Fluo4-FF and Magnesium Green, with k_Ds in the range of 10 μM should report calcium concentration changes at the neuromuscular junction with linear fluorescence increases.

Fluo4FF
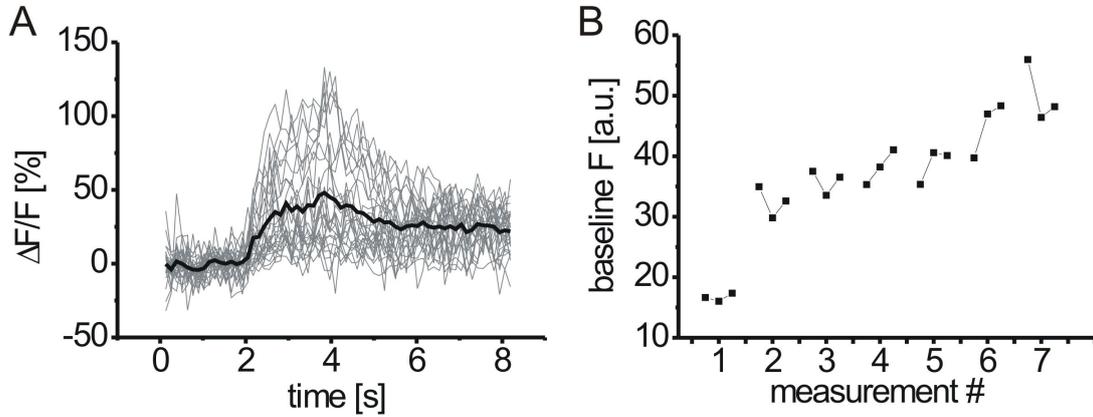
Figure 3.4: Fluorescence intensity of Fluo-4FF increases over trials. (A) $\Delta F/F$ is plotted as a function of time. Fluorescence changes recorded from boutons in response to different stimulus frequencies are plotted in the same graph (gray traces). The black trace represents the average of all traces. Note that the traces do not return to baseline despite Fluo4-FFs high k_D value. (B) Average raw baseline fluorescence is plotted as a function of measurement number. Every point corresponds to one bouton. Connected points represent boutons imaged in the same experiment. Fluorescence intensities from the first ten frames of a movie, i.e. before stimulus-onset, were averaged for each bouton. Note that raw baseline fluorescence increases over consecutive measurements.

Fluorescence responses from Fluo-4FF ($k_D = 10~\mu M$) showed incomplete decrease to baseline after stimulus offset (see Fig 3.4 A) and an increase in baseline fluorescence intensity over recordings (see Fig 3.4 B). As this was unlikely due to calcium binding, I assume that binding of heavy metal ions contributed significantly to the fluorescence responses. Heavy metal ions can in principle be complexed by the efficient chelator TPEN. However, to avoid changes in the composition of the bath solution, I decided to use Magnesium Green as low-affinity calcium indicator with lower heavy metal sensitivity.

Magnesium Green

Neuromuscular junctions were injected with Magnesium Green as described. Motoneurons were then stimulated via a suction electrode and action potential induced calcium influx at boutons led to fluorescence signals from the calcium sensor. Fluorescence responses exhibited fast kinetics and fluorescence traces returned to baseline immediately after stimulus
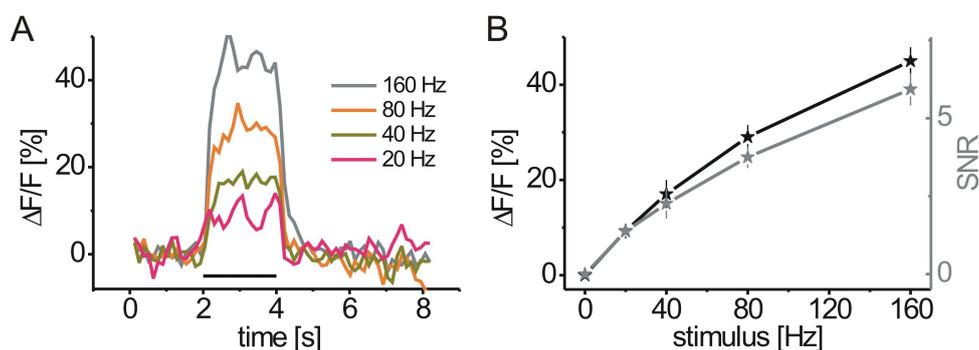
Figure 3.5: Fluorescence responses at presynaptic boutons measured with Magnesium Green. (A) Fractional fluorescence changes are plotted as a function of time. Black bar indicates the stimulus period. Responses show steep on- and offset at beginning and end of the stimulus period. (B) Amplitudes (black) and signal-to-noise ratios (gray) are plotted as a function of stimulus frequency. Amplitudes increase with stimulus frequency. Error bars represent s.e.m. $29 < n < 33$.

offset (Fig 3.5 A). Response amplitudes increased almost linearly with stimulus frequency (at 20, 40, 80, 160 Hz) (Fig 3.5 B). Both findings reflect Magnesium Green's low calcium affinity. The slightly sublinear stimulus-response curve (Fig 3.5 B) can be explained by beginning saturation of the indicator as the calcium concentration approaches half the k_D (k_D of Magnesium Green $= 6$ μM in $vitro$). This assumption is supported by the intracellular calcium concentration at 160 Hz, that was determined as 1.8 μM, as will be shown in 3.1.3. Thus, calcium influx at presynaptic boutons of the neuromuscular junction is a linear function of action potential frequency over the whole range of applied stimuli (up to 160 Hz).

3.1.3 Calcium Quantification with OGB-1

Next, boutons were injected with the high affinity calcium sensor OGB-1 and fractional fluorescence changes were measured in response to stimulus frequencies of 10, 20, 40, 80 and 160 Hz. Responses exhibited slower on- and off-kinetics (Fig 3.6 A) than found with Magnesium Green. The stimulus-response curve exhibits beginning saturation at stimulus frequencies above 20 Hz (Fig 3.6 B). As Magnesium Green exhibited linear response increases, this saturation must be attributed to saturation of OGB-1 and reflects its high calcium affinity. Note that steady-state response amplitudes reach a plateau at maximum stimulation reflecting complete indicator saturation.
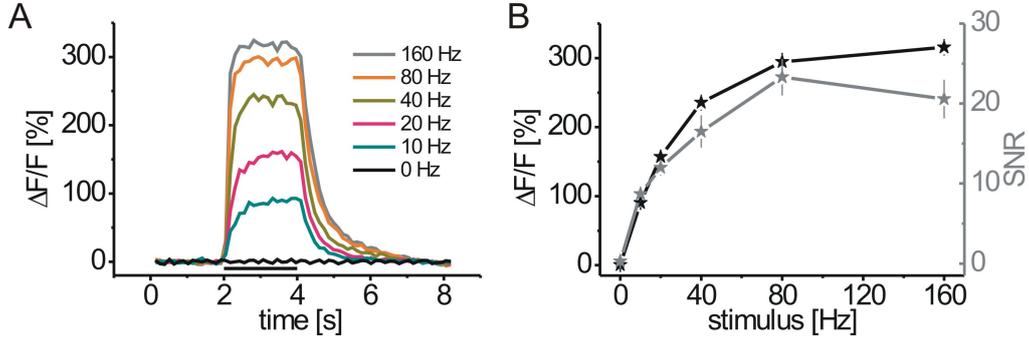
Figure 3.6: Fluorescence responses at presynaptic boutons measured with OGB-1. (A) Fractional fluorescence changes from presynaptic boutons are plotted as a function of time for stimulus frequencies between 0 and 160 Hz. Black bar indicates stimulus period. (B) Amplitudes (black) and signal-to-noise ratios (gray) are plotted as a function of stimulus frequency. OGB-1 response amplitudes reveal beginning saturation above 20 Hz and reach plateau at 160 Hz indicating saturation. Error bars represent s.e.m. $29 < n < 33$.

Conversion of the fluorescence responses into changes in calcium concentration requires to determine the maximum possible fluorescence change, R_f, and the calcium affinity, k_D, of an indicator, ideally *in situ*. R_f of an indicator is defined as fluorescence when fully saturated with calcium (F_{max}) over fluorescence when no calcium is bound (F_{min}). This needs to be determined *in situ* as R_f is influenced by the cellular environment. However, as the cellular environment is stable over experiments, it is sufficient to determine R_f once for all experiments.

F_{max}

OGB-1 was chosen despite its moderate maximum fluorescence change (≈ 14 *in vitro*), as it is visible at intracellular resting calcium concentrations inside motoneurons. Furthermore, OGB-1 can be saturated *in situ* at non-toxic calcium concentrations. OGB-1 is fully saturated with calcium at 160 Hz stimulation. This allowed simple determination of F_{max} for OBG-1 *in situ*: F_{max} is given by the asymptote of the stimulus-response curve in Fig 3.6 (B) (ΔF/F $= 318$ %). To test whether this value could still be increased, I increased the extracellular pH from 7.2 to 8.8 and repeated the 160 Hz stimulation (see Fig 3.7). As the main calcium clearing mechanism in the neuromuscular junction relies on a calcium-proton exchanger, reducing the amount of available protons reduces the calcium clearing rate and increases intracellular calcium accumulation. This effect was verified using the
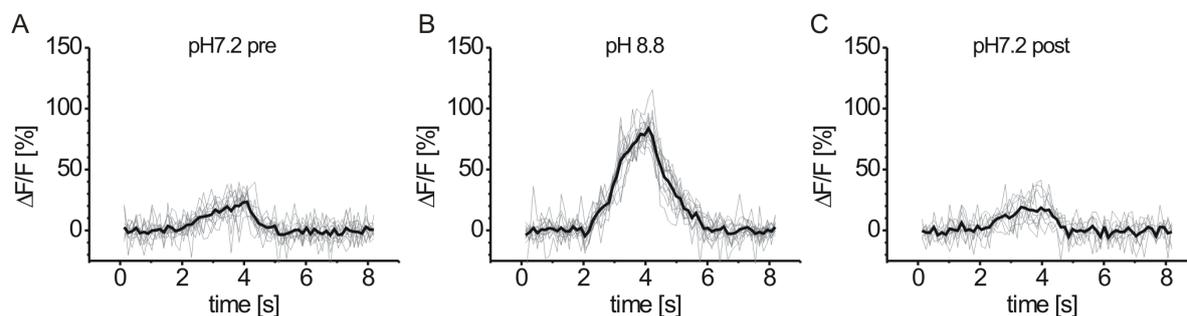
Figure 3.7: pH effect on calcium accumulation in presynaptic boutons. Fractional fluorescence changes at presynaptic boutons are plotted as a function of time. A neuromuscular junction expressing the GECI GCaMP 1.6 was stimulated at $40 Hz$ over $2\ s$ as described before. Grey traces represent individual boutons, averaged in the black traces in each graph. Experiments were done in HL6.1 first at pH 7.2 (A), then at pH 8.8 (B), and then repeated at pH 7.2 (C). When bath solutions were exchanged, preparations were washed with the new solution 3 times for $2\ min$. High extracellular pH increased fluorescence responses about 3-fold. (from 27% in (A) and 85% in (B) to 22% in (C)).

GECI GCaMP 1.6, summarized in Fig 3.7.

However, using OGB-1 the amplitudes of responses to 160 Hz stimulation did not increase at high pH (Fig 3.8, compare the two left bars). I concluded that all indicator molecules were bound to calcium at this action potential frequency and thus used the fluorescence intensity measured at 160 Hz stimulation at pH 7.2 as F_{max}.

F_{min}

F_{min} was determined by buffering calcium with excess concentrations of the high affinity calcium chelator BAPTA ($k_D \approx 40\ nM$). Intracellular accumulation of BAPTA was achieved by exposure to 130 μM BAPTA-AM for 30 min (see 2.3.3). Fluorescence intensity from OGB-1 at rest after exposure to BAPTA-AM was reduced compared to resting fluorescence before exposure (Fig 3.8, compare third and fourth bar). This value was thus used as F_{min}. pH change did not affect resting fluorescence (Fig 3.8, compare the two right most bars). For details refer to 2.3.

Conversion of Stimulus Frequency into Changes in Calcium Concentration

The maximum fluorescence change from OGB-1 was thus determined as $R_f = F_{max}/F_{min} = 7.1$. (Fig 3.8). The k_D for OGB-1 was determined in the cuvette as 240 nM. Using equation
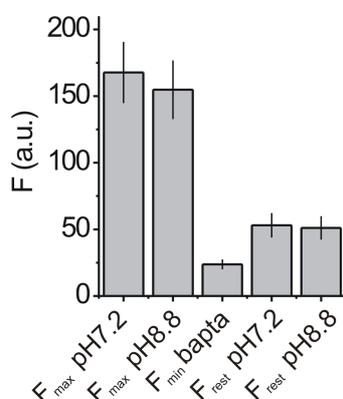
Figure 3.8: *In situ* determination of F_{min} and F_{max} for OGB-1 in presynaptic boutons. Raw fluorescence intensities are plotted. F_{max} was measured as the amplitude of the response to 160 Hz stimulation at pH 7.2 (1st bar) and did not increase at pH 8.8 (2nd bar). F_{min} was measured after exposure to BAPTA-AM (3rd bar). Exposure reduced resting fluorescence to about 50 % of the normal resting fluorescence (4th bar). Extracellular pH had no influence on the resting fluorescence (5th bar). Error bars indicate s.d.
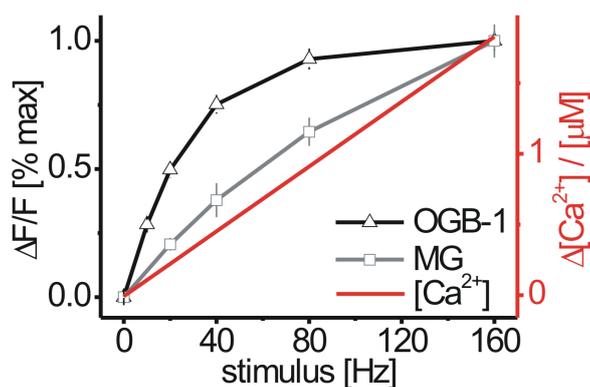

Figure 3.9: Normalized fractional fluorescence changes for OGB-1 (black) and Magnesium Green (gray) are plotted as a function of stimulus frequency. Calcium concentration (red) is plotted as a function of stimulus frequency along the right y-axis and represents an extrapolated linear fit to calculated calcium levels at 0, 10 and 20 Hz stimulation. Error bars indicate s.e.m.

2.1 I determined the resting calcium concentration as $[Ca^{2+}]_{iRest} = 31\ nM$. Equation 2.2 resulted in changes in calcium concentrations of $\Delta[Ca^{2+}]_{10Hz} = 92\ nM$ and $\Delta[Ca^{2+}]_{20Hz} = 229\ nM$. The change in calcium concentration was shown to be a linear function of action potential frequency at the applied stimulus regimes. Extrapolating a linear fit to the three calculated points, resulted in estimates of intracellular calcium at steady-state for each of the applied stimulus frequencies (Fig 3.9). Thus the stimuli applied in the presented experiments elicit calcium concentration changes between 0.1 and 1.8 μM superimposed on the resting calcium concentration of 31 nM(0.11 μM at 10 Hz, 0.22 μM at 20 Hz, 0.45 μM at 40 Hz, 0.91 μM at 80 Hz and 1.83 μM at 160 Hz).

3.2 GECIs at the Neuromuscular Junction

3.2.1 GECI Responses to Sustained Neural Activity

After the calibration of intracellular steady-state calcium concentrations in response to various action potential frequencies, I went on to quantify the *in vivo* fluorescence response properties of several different GECIs. Therefore flies were bred that expressed GECIs under UAS-control in all neurons using the panneuronal driver line $elav^{c155}$ Gal4. In some cases, GECI expression in F1 larvae was not strong enough, and so F1 flies were crossed for several generations to yield flies that were homozygous for either the Gal4 or the UAS insertion or both if necessary.

8 different GECIs were compared: Yellow Cameleon 3.3, 3.60, 2.60, D3cpv, TN-L15, TN-XL, TN-XXL and GCaMP 1.6. 2-photon image series of up to five boutons simultaneously were acquired at 8 Hz frame rate (64x64 pixels). The corresponding nerves were stimulated at frequencies of 0-160 Hz as described for OGB-1 (Fig 3.6). Fig 3.10 shows fractional fluorescence changes plotted as a function of time for all tested GECIs (left column). Then, GECI responses were evaluated for amplitude and signal-to-noise ratios at steady-state (right column), and the results were plotted as a function of stimulus frequency and changes in intracellular calcium concentration.

Yellow Cameleon 3.3 (Fig 3.10 (A)) responded with a signal-to-noise ratio > 2 to stimulus intensities of 20 Hz and above. Linear increase in stimulus intensity led to a linear increase in ΔR/R up to 40 Hz and beginning saturation at higher frequencies. A maximum ΔR/R of $66.6 \pm 0.9\ \%$ was observed. The half maximum ΔR/R was reached at $\approx 38\ Hz$, reflecting a k_D of 0.47 μM *in vivo*. Rise and decay of the 40 Hz response displayed time-constants of 1.41 s and 1.05 s, respectively (Fig 3.12). Samples sizes: $48 < n < 63$.

Yellow Cameleon 3.60 (Fig 3.10 B) showed major improvements compared to Yellow Cameleon 3.3: 5-fold higher fluorescence changes at 10 Hz stimulation were observed, with the highest signal-to-noise ratio (> 3) in this study at this frequency. Responses increased linearly up to 40 Hz. Higher stimulus intensities led to sublinear increases in the signal amplitude with a maximum change of 135.8 ± 4.4 % ΔR/R. The half maximum ΔR/R relates to ≈ 30 Hz or a k_D of 0.36 μM. Time-constants of the 40 Hz response were 0.82 s for the rise and 0.73 s for the decay (Fig 3.12). Sample sizes: $33 < n < 71$.

Yellow Cameleon 2.60 (Fig 3.10 C) detected 10 Hz stimulation with signal-to-noise ratio > 2. ΔR/R increased linearly up to 40 Hz. At 80 Hz and 160 Hz amplitudes increased sublinearly with a maximum change of 193.8 ± 9.7 % ΔR/R. Responses of comparable size had previously not been reported for any other GECI *in vivo*. Half maximum ΔR/R relates to ≈ 32 Hz or a k_D of 0.40 μM. Fits to 80 Hz responses showed time-constants of 0.88 s for the rise and 3.9 s for the decay (Fig 3.12). 40 Hz responses could not be fit to single exponentials. The time-constant for the rise may be underestimated, as Yellow Cameleon 2.60 reaches saturation at 80 Hz stimulation, which leads to apparent speed up of the kinetics. The response amplitudes may be underestimated because plateaus are not reached after 2 s stimulation, due to slow kinetics. Sample sizes: $29 < n < 30$.

D3cpv (Fig 3.10 D) is a reengineered Yellow Cameleon, unperturbed by wild type calmodulin *in vitro*. Response amplitudes to 10 Hz stimulation were comparable to Yellow Cameleon 3.60 and 2.60 (signal-to-noise ratio > 2). Signal amplitudes increased sublinearly with stimulus frequency and reached a maximum of 89.7 ± 3.9 %. The half maximum fluorescence change was reached at ≈ 41 Hz reflecting a k_D of 0.49 μM. Rise and decay of 40 Hz responses were fit to single exponentials with time-constants of 0.36 s for the rise and 1.83 s for the decay (Fig 3.12). Sample size: $48 < n < 56$.

TN-L15 (Fig 3.10 E) employs the same chromophores as Yellow Cameleon 3.3. Signal-to-noise ratio exceeded 2 at 20 Hz. A roughly linear increase up to 40 Hz was observed. 160 Hz stimulation evoked a maximum ΔR/R of 59.5 ± 2.3 %. The half maximum fluorescence change relates to ≈ 30 Hz or 0.36 μM cytosolic calcium. 40 Hz responses were described by an exponential function with time-constants of 0.81 s for the rise and 1.49 s for the decay (Fig 3.12). Sample size: $27 < n < 30$.

Using TN-XL (Fig 3.10 F), no detectable responses were recorded at 10 and 20 Hz. Only at 40 Hz and above did fluorescence change amplitudes exceed signal-to-noise ratio of 2. 160 Hz evoked a maximum fractional fluorescence change of 105.9 ± 2.7 % ΔR/R. The stimulus-response relationship was supralinear up to 40 Hz and sublinear at frequencies
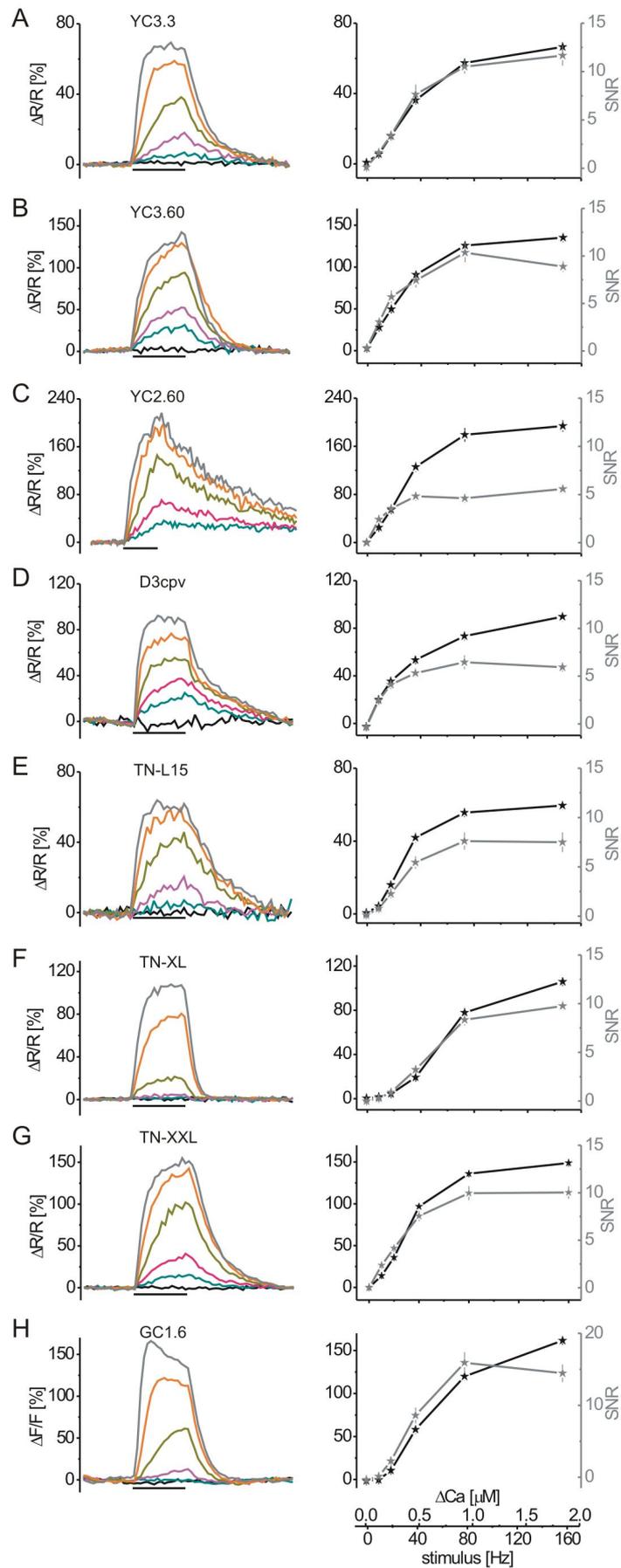
above 40 Hz. The half maximum fluorescence change was reached at ≈ 65 Hz ($k_D = 0.77$ μM). TN-XL responses showed time-constants of 0.59 s for the rise and the fastest decay time-constant of all GECIs with 0.20 s (Fig 3.12). Sample sizes $48 < n < 87$.

Signals reported by TN-XXL (Fig 3.10 (G)), mimicked those from Yellow Cameleon 3.60 in some respects. Responses at 10 Hz reached signal to noise ratio above 2. Responses showed linear to slightly supralinear increase at stimulus frequencies up to 40 Hz. Above 40 Hz TN-XXL showed beginning saturation with a maximum fluorescence change of 148.8 $\pm$ 2.4% ΔR/R, reflecting a k_D of 0.39 μM . Time-constants of the 40 Hz responses were determined as 1.04 for the rise and 0.88 for the decay (Fig 3.12). Sample sizes $52 < n < 60$.

The single chromophore indicator GCaMP1.6 (Fig 3.10 (H)) showed responses that exceeded a signal-to-noise ratio of 2 at 20 Hz action potential frequency. Signal amplitudes increased supralinearly with stimulus intensity up to 40 Hz and sublinearly above. 160 Hz induced responses of 161.6 $\pm$ 13.1 % ΔF/F with the highest signal-to-noise ratio observed in this study (signal-to-noise ratio 160 Hz = 14.4 $\pm$ 1.2). The half maximum fluorescence change was reached at ≈ 54 Hz ($k_D = 0.64$ μM). Time-constants of 40 Hz responses were 1.38 s for the rise and 0.45 s for the decay (Fig 3.12). Sample sizes $42 < n < 52$. GCaMP 2 was not analyzed here. I do not expect improved performance at the temperatures I apply. The optimization of the probe for use at 37°C may also be the cause for very low expression levels that were observed throughout with GCaMP 2 at temperatures of 20-25°C.

These results are summarized in Fig 3.11 and in Tables (see Table 3.1 & 4.1). Desired properties of a GECI for the use in the cytosol of neurons in the central nervous system, specifically in LPTCs are (i) high sensitivity to small changes in calcium concentration from low baseline at rest, (ii) a wide linear response regime and (iii) fast response kinetics.

Figure 3.10: GECI responses to sustained neural activity *in vivo*. Responses recorded from boutons expressing either of 8 different GECIs: (A) Yellow Cameleon 3.3, (B) Yellow Cameleon 3.60, (C) Yellow Cameleon 2.60, (D) D3cpv, (E) TN-L15, (F) TN-XL, (G) TN-XXL and (H) GCaMP 1.6. Signals were recorded from presynaptic boutons at 8 Hz frame rate for 8 s (12 s for Yellow Cameleon 2.60, note different timescale). Left column: for each GECI, fractional fluorescence change (ΔR/R and ΔF/F for GCaMP 1.6 respectively) is plotted as a function of time (stimulus bar under each graph represents 2 s). Right column: for each GECI fluorescence change amplitudes (black) and corresponding signal-to-noise ratios (SNR) (gray) are plotted as a function of stimulus frequency and change in calcium concentration in boutons. Sample sizes are given in the text. Error bars represent s.e.m.
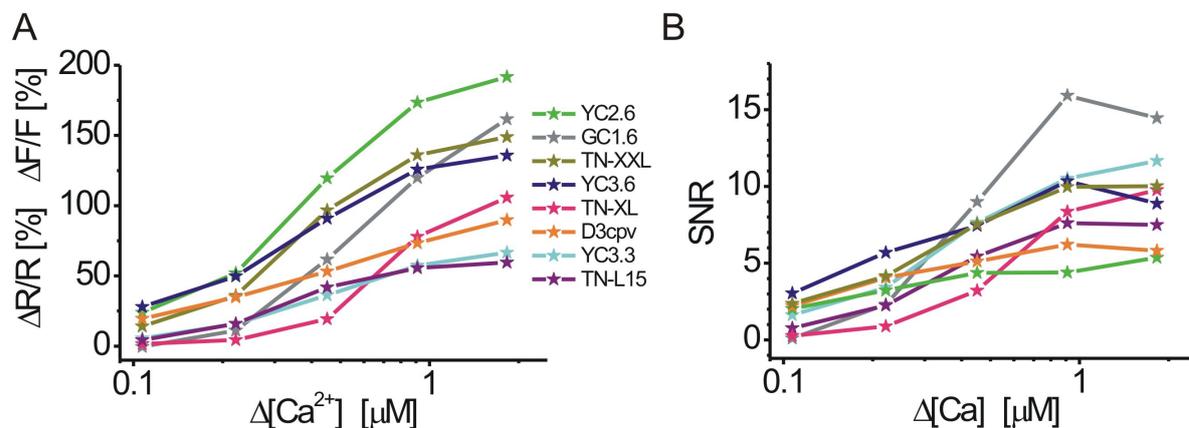
Figure 3.11: Fluorescence changes and signal-to-noise ratios for all GECIs. Summary of data from Fig 3.10. (A) Response amplitudes are plotted as a function of change in intracellular calcium concentration. A calcium concentration increase of 0.11 μM is reported by Yellow Cameleon 3.60 and 2.60, D3cpv and TN-XXL. Highest maximum fluorescence changes are exhibited by Yellow Cameleon 3.60 and 2.60, GCaMP 1.6 and TN-XXL. (B) Signal-to-noise ratios of the fluorescence responses are plotted as a function of change in intracellular calcium concentration. A calcium concentration increase of 0.11 μM is detected with signal-to-noise ratio above 2 with Yellow Cameleon 3.60 and 2.60, D3cpv and TN-XXL. Highest maximum signal-to-noise ratios are exhibited by GCaMP 1.6. Note logarithmic axes.

(i) 10 Hz stimuli revealed the GECIs with highest sensitivity to small changes in calcium ($\approx 0.1\ \mu M$) from low baseline concentrations ($\approx 0.03\ \mu M$). The ratiometric indicators Yellow Cameleon 3.60 and 2.60, D3cpv and TN-XXL reported such changes with signal-to-noise ratios above 2. Responses from GCaMP 1.6 and TN-XL exceeded signal-to-noise ratios of 2 only at 20 Hz ($\approx 0.2\ \mu M$) or 40 Hz ($\approx 0.5\ \mu M$) stimulation, respectively.

(ii) Of the 4 GECIs with signal-to-noise above 2 in fluorescence responses to 10 Hz stimuli, D3cpv displayed the lowest saturation threshold, i.e. changes in calcium concentrations related to stimulus frequencies above 20 Hz ($\approx 0.2\ \mu M$) were reported with sublinear increases in response amplitudes. Yellow Cameleon 2.60, 3.60 and TN-XXL, show beginning saturation at calcium influx related to stimulus intensities above 40 Hz ($\approx 0.5\ \mu M$). TN-XL and GCaMP 1.6 responses displayed the highest saturation threshold of all GECIs: responses increased markedly sublinear with stimulus intensity only stimulus intensities of 80 Hz and above ($\approx 0.9\ \mu M$).

(iii) Of all GECIs Yellow Cameleon 2.60 showed by far the slowest kinetics of the response
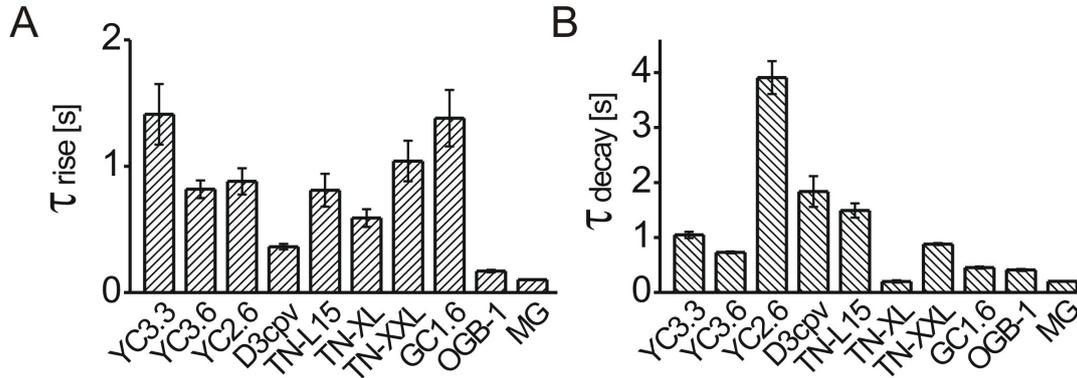
Figure 3.12: Response kinetics. Time-constants for the rise (A) and for the decay (B) of
responses from calcium indicators to 40 Hz stimulation are plotted (80 Hz
for Yellow Cameleon 2.60). Time-constants were determined by fitting single
exponential functions to the onset (A) and the offset (B) of the respective
fluorescence response curves to 40 Hz stimulation shown in Fig 3.10 in the
left column. Time-constants of the rise are fastest for OGB-1 and Magnesium
Green. Decay time-constants are fastest in TN-XL and Magnesium Green.
Error bars indicate s.d.

decay ($\tau = 3.91\ s$). TN-XL displayed time-constants for the signal decay ($\tau = 0.20\ s$),
that were faster than for the synthetic calcium sensor OGB-1 ($\tau = 0.41\ s$).

Time-constants for the rise and decay of fluorescence signals were determined by fitting
single exponential functions to the rise and decay phase of the responses. 40 Hz responses
were analyzed. Stimulation at lower frequencies did not elicit detectable fluorescence signals
in all GECIs and stronger stimuli decreased time-constants of the response onset due to
saturation in many GECIs (see Fig 3.13 (A)). D3cpv and Yellow Cameleon 3.3 also show
decreased time-constants of the response decay at 80 Hz stimulation (see Fig 3.13 (B)).

Summary Yellow Cameleon 3.60, D3cpv and TN-XXL show high sensitivty to small
concentration changes and display moderate response kinetics (time-constants in the range
of 1 s for on- and offset of responses to 40 Hz stimulation). This is considerably slower
than TN-XL, but the latter showed no responses to small calcium changes at all. GCaMP
1.6 shows the highest maximum signal-to-noise ratio for any of the recorded responses from
GECIs. However, GCaMP 1.6 was not responsive to small calcium changes.

Based on these findings Yellow Cameleon 3.60, D3cpv and TN-XXL were identified as the
most promising GECIs for applications in the visual system of fruit flies. For preliminary
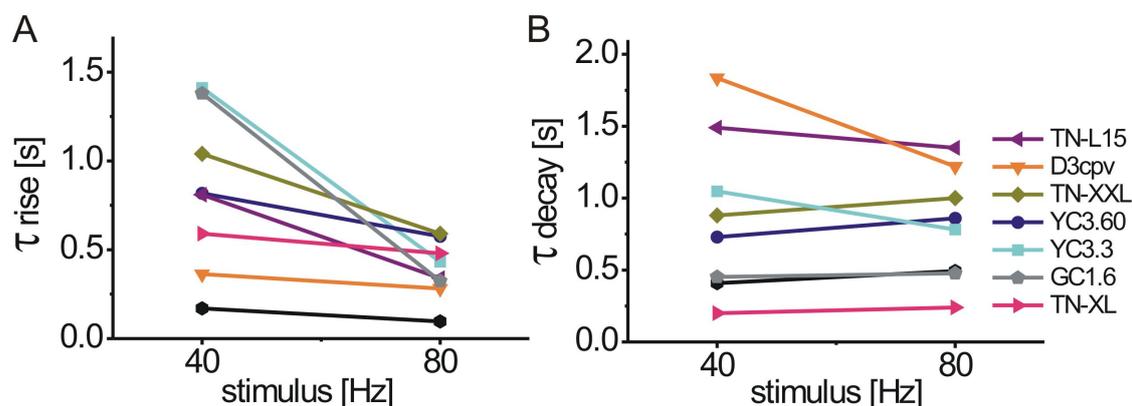
Figure 3.13: Time-constants of the rise (A) and decay (B) of fluorescence changes in re-
sponse to 40 and 80 Hz stimulation are compared. As a general tendency, the
time-constants of the response onsets decreased at higher stimulus intensity
(markedly for TN-L15, Yellow Cameleon 3.3, GCaMP 1.6 and TN-XXL). The
time-constants of the response offset decreased at higher stimulus intensity
only for Yellow Cameleon 3.3 and D3cpv.

imaging experiments in LPTCs of adult flies I used Yellow Cameleon 3.60 and TN-XXL
(see 3.3).

To demonstrate and quantify effects of the cellular environment on the characteristics of
the calcium responses of GECIs, I sought to complement the *in vivo* analysis with calcium
titrations of purified GECI proteins in cuvettes. Such data are in principle available in the
literature for each GECI in this study. However, slight differences in buffer compositions
(such as magnesium ion concentration) strongly influence titration results, and so literature
data are not necessarily comparable. Thus, calcium responses in cuvettes were measured
in vitro for most GECIs and OGB-1 under identical conditions.

3.2.2 GECI Responses in the Cuvette and in Living Neurons

Calcium responses of purified GECI proteins were measured in the cuvette, in collaboration
with Marco Mank in the laboratory of Oliver Griesbeck. Protein purification and spec-
troscopy of purified proteins was done by Marco Mank. I did comparative data analysis.

Data acquisition differs between the spectrometer and the 2-photon setup in several re-
spects. First, data acquisition in 2-photon microscopy used bandpass filters of 40 and 30
nm spectral width (485/40 for CFP, 535/30 for YFP, 510/50 for GFP). Using the spec-
troscope, emitted photons were sampled over the spectrum in bands of 5 nm. Integrating

the such acquired data spectrally over 40 and 30 nm or 50 nm before the calculation of ratio changes, results in a reduction of the fractional ratio changes. Thus, the bandpass filters used for fluorescence detection in 2-photon microscopy were mimicked by integrating spectroscopic data over 40 and 30 nm for CFP and YFP respectively, or 50 nm for GCaMP 1.6 and OGB-1, before fractional fluorescence changes were calculated, to allow a fair comparison of data acquired with both techniques.

Second, the reference point for the calculation of fractional ratio changes differs. In spectroscopic calcium titrations, the applied concentrations ranged from 0 calcium to 39.5 μM. However, the cytosolic calcium concentration at rest has been determined as 31 nM in presynaptic boutons. Calculation of fractional ratio changes from spectroscopy were thus done relative to the lowest calcium concentrations used (65 nM). Single chromophore indicators GCaMP 1.6 and OGB-1 were analyzed accordingly. For D3cpv and OGB-1 the cuvette titrations show steep linear onsets at the lowest calcium concentrations applied (see Fig 3.14). The deviation of the mimicked resting calcium (65 nM) from the real, determined resting calcium (31 nM) will thus have strong influences of calculated fractional fluorescence changes for these two indicators. Thus, I interpolated a fluorescence ratio for a "virtual" calcium concentration of 31 nM and used this as reference for the calculation of fractional fluorescence changes. This interpolation was only done for D3cpv and OGB-1 as for all other GECIs the difference between fluorescence at 0 and 65 nM was negligable (see Fig 3.14).

Together, both corrections allow direct comparison of the data acquired under 2-photon microscopy and spectrophotometric measurement with 1-photon excitation (see 2.3.4). The effectivity of these corrections was verified by measuring a calcium titration curve of TN-XXL protein in solution at the 2-photon microscope (see 2.3.4).

Yellow Cameleon 3.60 showed similar stimulus response properties *in vitro* and *in vivo* at low calcium concentration changes, however, above 0.5 μM (stimulus frequency > 40 Hz) fractional ratio changes *in vivo* were smaller than *in vitro* (Fig 3.14 (A)). For TN-L15 (B), D3cpv (C), TN-XL (D) and TN-XXL (F) I also found good accordance of *in vivo* and cuvette measurements for calcium concentrations < 0.5 μM. In contrast to Yellow Cameleon 3.60 however, I found that fractional ratio changes were smaller in the cuvette than *in vivo* at concentrations > 0.5 μM. For GCaMP 1.6 (E), *in vivo* signals were bigger than *in vitro* at high concentration changes (above 1 μM) and smaller at low concentration changes (below 1 μM). Calcium response curves from OGB-1, recorded in the cuvette and *in vivo* (G) are similar over the full range of concentrations.
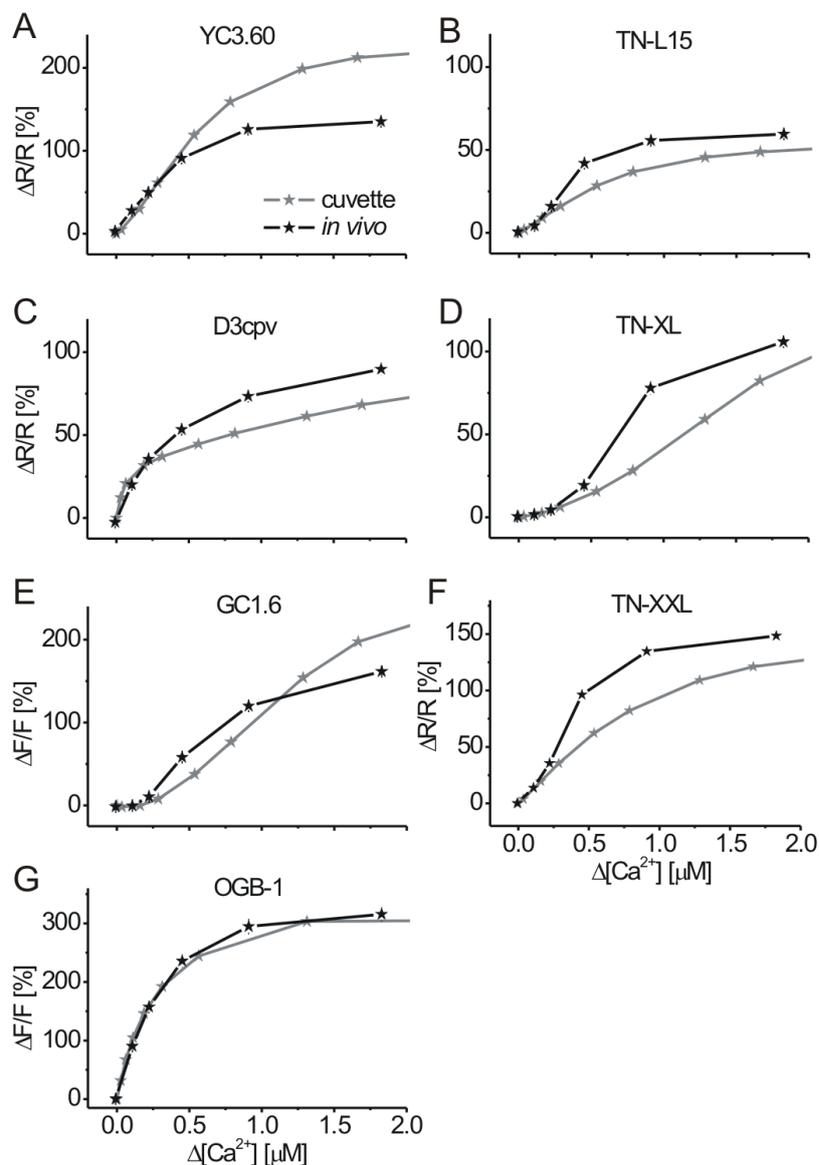
Figure 3.14: *In vivo* vs. *in vitro* comparison of calcium evoked fluorescence changes of calcium indicators. Fractional fluorescence changes are plotted as a function of change in calcium concentration. *In vivo* responses (black) are directly compared to *in vitro* data from cuvette measurements (gray). GECIs measured in both conditions are (A) Yellow Cameleon 3.60, (B) TN-L15, (C) D3cpv, (D) TN-XL, (E) GCaMP 1.6, (F) TN-XXL. For comparison (G) OGB-1 is plotted.

Summarizing, GECIs with wild-type calmodulin (Yellow Cameleon 3.60 & GCaMP 1.6) show decreased fluorescence responses *in vivo*. All other GECIs (troponin-based GECIs
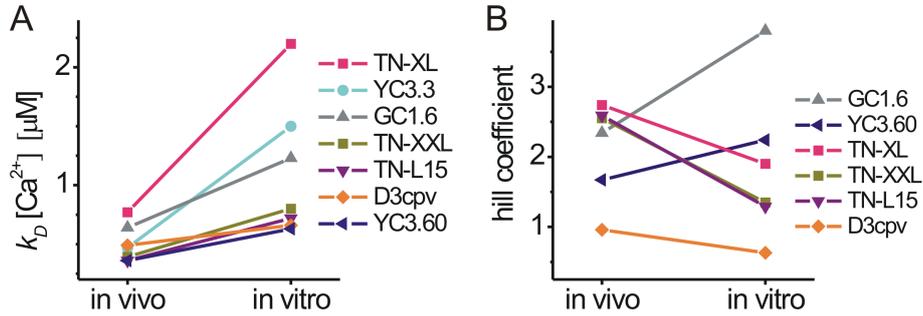
Figure 3.15: k_Ds and hill coefficients of GECIs as determined *in vivo* and *in vitro* in cuvettes. (A) k_D values of GECIs are lower *in vivo* than *in vitro*. (Yellow Cameleon 3.3 *in vitro* k_D from [61]). (B) Hill coefficients for calmodulin-based GECIs are decreased *in vivo* compared to *in vitro* (Yellow Cameleon 3.60 & 2.60 and GCaMP 1.6). Troponin-based GECIs show the opposite tendency: hill coefficients are increased in *in vivo* (TN-L15, TN-XL and TN-XXL). GCaMP 1.6 *in vitro* hill coefficient from [73].

and D3cpv) do not show this reduction. Their fluorescence change amplitudes even appeared increased *in vivo*. Thus, the differences in GECI fluorescence responses under both conditions are probably due to effects of the cellular environment, such as calmodulin interactions as demonstrated in [71], because only those GECIs show reduced in vivo responses for which calmodulin related interactions are expected.

k_D values were extracted from cuvette data and compared to values obtained from *in vitro* experiments (see Fig 3.15 A). In general, k_Ds appear decreased *in vivo*. This was not true for Yellow Cameleon 2.60, which was excluded from the figure. Cuvette measurements have not been done and the determined *in vivo* k_D is an overestimate as calcium signals did not reach steady-state during 2 s stimuli, thus the degree of saturation and thus the calcium affinity cannot be deduced from these data.

Hill coefficients change from *in vitro* to *in vivo* analysis as well (see Fig 3.15 B), but with a marked difference between calmodulin-based GECIs and all other GECIs tested: while Yellow Cameleons show reduced hill coefficients *in vivo*, troponin-based GECIs and D3cpv display increased hill coefficients *in vivo*. This is in line with the idea, that heterophilic interactions between Yellow Cameleons and native cellular calmodulin or calmodulin interaction partners perturb FRET response increases in a calium dependent way. For Yellow Cameleon 3.3 no *in vitro* hill coefficient is given in the literature.

3.2.3 Transient Calcium Events Reported by OGB-1 and GECIs

In the experiments shown so far, the most sensitive GECIs reveal about half the sensitivity of OGB-1 in terms of amplitude and signal-to-noise ratio of responses to calcium concentration changes at steady-state (at undefined but realistically applicable dye concentrations). I next asked, what temporal resolution could be achieved, and which minimal calcium events could still be detectable with the various GECIs and OGB-1.

To assess the minimal stimulus, sufficient to evoke a calcium induced fluorescence response from calcium indicators, I applied brief volleys of 10, 5, 2 and single action potentials (volleys separated by 500 ms, action potential frequency within volleys was 100 Hz) and recorded fluorescence changes from individual boutons with high temporal resolution (line scans at 500 Hz).

OGB-1 was the only indicator to report indiviual action potentials in these experiments (with fluorescence changes of 43.6 $\pm$ 2.5 % ΔF/F, see Fig 3.16). It also reliably reported volleys of 10, 5 and 2 action potentials (see Fig 3.17 B). GECIs also reported volleys of 10 action potentials, although with widely differing amplitudes and signal-to-noise ratio (Fig 3.17 (C)-(I)). All GECIs except Yellow Cameleon 3.3 showed detectable responses to volleys of 5 action potentials. None of the GECIs reliably reported 2 action potentials. Yellow Cameleon 3.60 showed fluorescence fluctuations time-locked to the stimuli, however, with a signal-to-noise ratio of 0.9. Similar data for TN-XXL are still to be acquired. Data are summarized in Tab 3.1.

The fluorescence recordings shown in Fig 3.10 display calcium accumulation during the stimulus period. The stimulus frequency is reflected in the amplitude of the responses. However, the individual action potentials within the stimulus cannot be reflected in the recorded traces, because the imaging frame rate was insufficient in these experiments (8
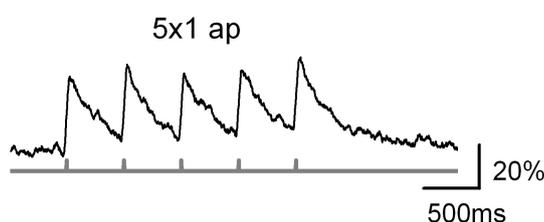
Figure 3.16: OGB-1 responses to single action potentials. Fractional fluorescence change recorded from a single bouton in line scan mode at 500 Hz scan rate. Raw data smoothed with a boxfilter of 40 ms width.
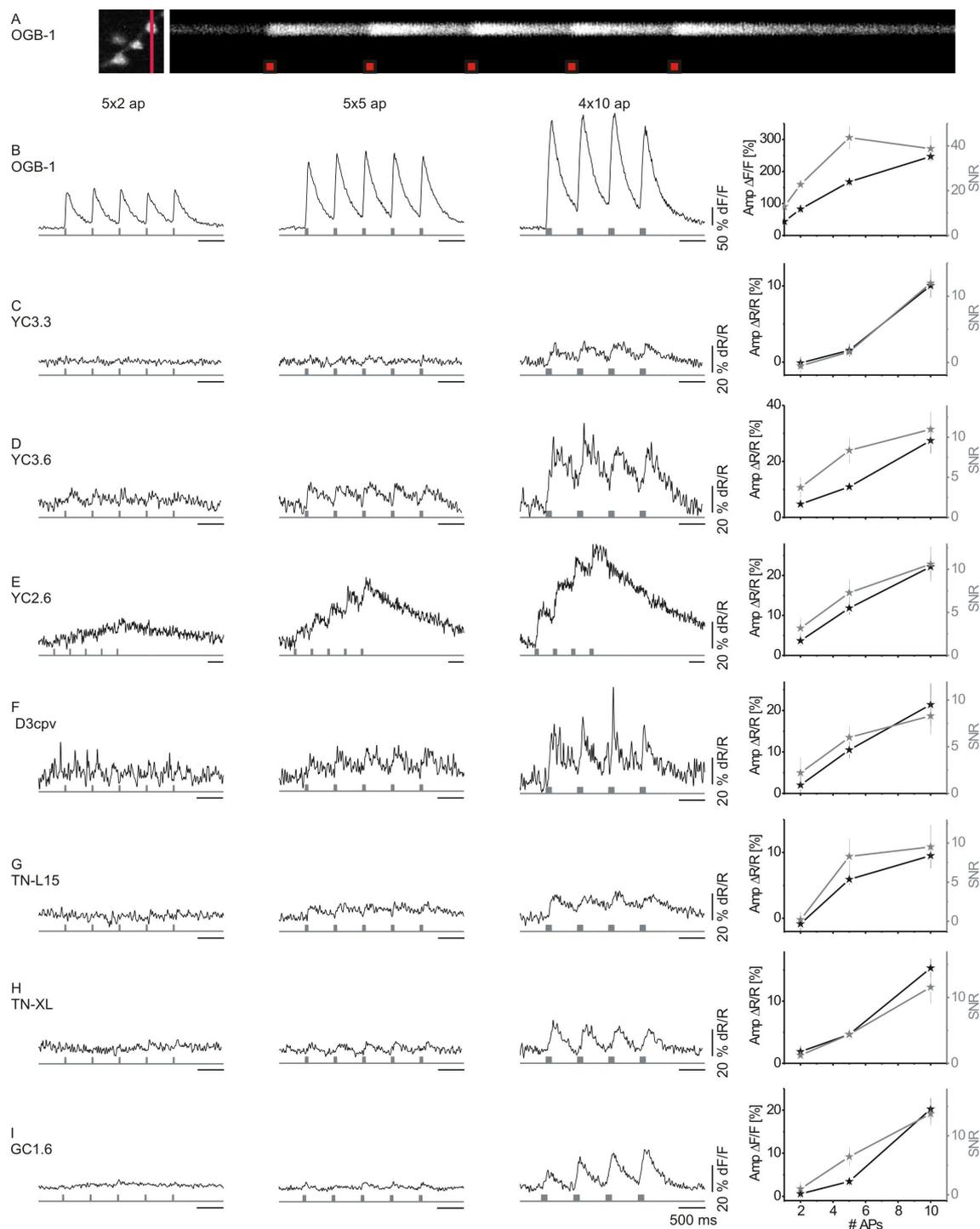
Figure 3.17: Fluorescence responses to transient activity. (A) Raw image of an OGB-1 filled bouton (left, line scan axis in red). Raw line scan data (500 Hz) plotted over time during stimulation with 5 volleys of 5 action potentials each (red squares). Space between two squares represents 500 ms. (B)-(I) Repeated action potential volleys (100 Hz) of 2 (first column), 5 (second column) or 10 action potentials (third column) were elicited. Volleys were spaced by 500 ms. OGB-1 (B) and GECI traces (C)-(I) represent the mean of 4 measurements from different boutons. Mean amplitudes and signal-to-noise ratios (SNR) of fluorescence responses are summarized in the right column (Data represent means ± s.e.m. of responses from 4 boutons).
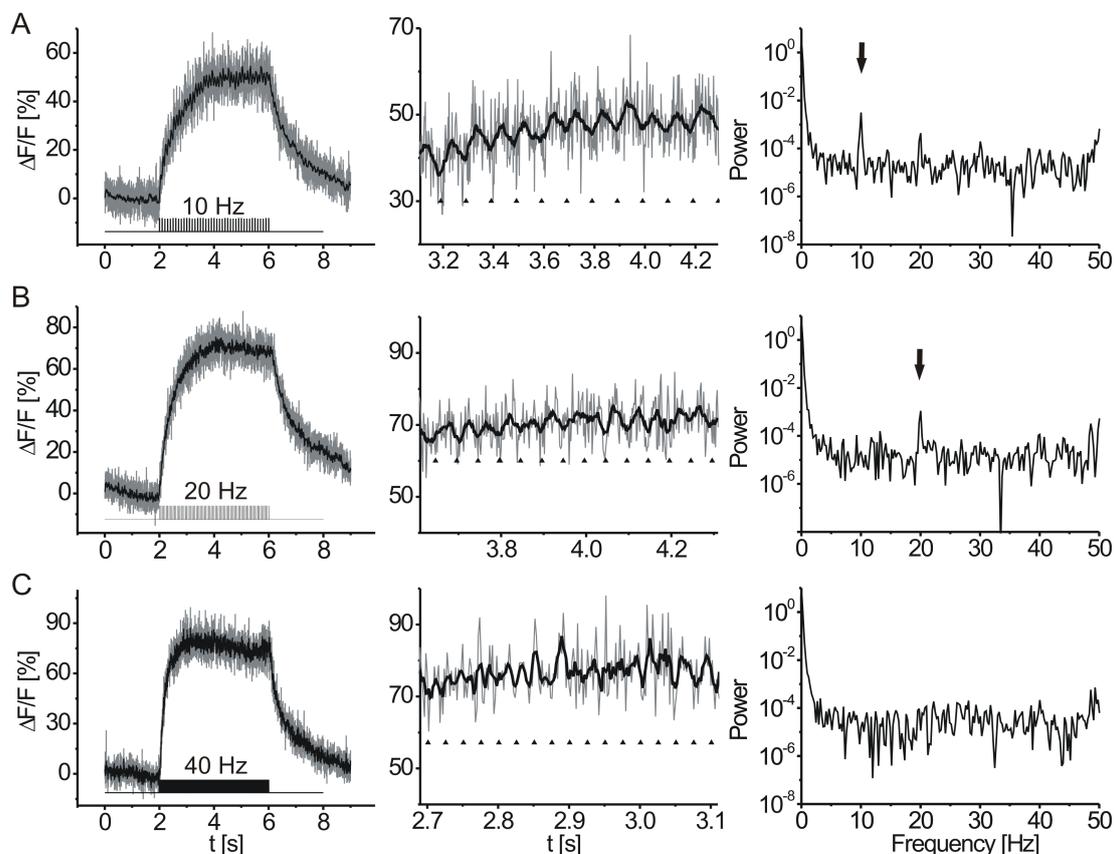
Figure 3.18: Fluorescence responses to fast calcium fluctuations recorded with OGB-1. Recordings were done in line scan mode at 500 Hz scan rate. Boutons were stimulated at (A) 10, (B) 20 and (C) 40 Hz action potential frequency. The left column shows fractional fluorescence changes, plotted as a function of time over 9 s. The middle column shows a blow up of the traces to the left (within stimulus period). Action potentials are marked by triangles under the fluorescence traces. The right column shows fast fourier transforms of the traces during the stimulus periods. Action potentials elicit fluctuating fluorescence responses at the respective frequencies as can be seen by the respective peaks in the power spectra (arrows) in (A) and (B). (C) 40 Hz stimulation does not lead to a corresponding peak in the power spectrum. (A)-(C): n=8, 7 &6 boutons. (A)&(B) Grey traces show average raw fractional fluorescence changes, in black this trace was filtered with a box filter of 40 ms width.

Hz).

I thus recorded fractional fluorescence changes from individual boutons expressing TN-XL in line scan mode at 500 Hz scan rate. TN-XL was chosen for these experiments because

it revealed the fastest decay time-constants of all tested GECIs in previous experiments. This should allow separation of closely timed calcium events. When action potentials were induced at 10, 20, 40 and 80 Hz over a 4 s period, power spectra of the recorded fluorescence traces did in no case reveal significant peaks corresponding to the stimulus frequency (data not shown). Power spectra of responses to 10 Hz stimulation recorded with Yellow Cameleon 3.60 did also not reflect the stimulus frequency. Similar measurements at OGB-1 filled boutons revealed stimulus related peaks for 10 and 20 Hz experiments but not above (Fig 3.18). This may be due to indicator saturation and insufficient response kinetics of OGB-1.

Excurs: Voltage Imaging While synthetic compounds for the imaging of membrane potential are frequently used [41], no satisfying genetic probes for voltage imaging have been developed to date. One promising approach combined transgenic membrane-tagged-GFP expression (CD8-GFP) with a synthetic compound that resides inside the membrane and quenches GFP emission dependent on the membrane potential [139]. The synthetic compound in this system is known as Dipicrylamin (Hexanitro-diphenylamin, DPA). The compound is highly lipophilic and inserts effectively into membranes. There, its negative charges determine its position closer to the inner or the outer leaflet, dependent on the membrane potential [140]. The highly conjugated pi-electron system of DPA, although not fluorescent itself, will there quench GFP fluorescence more or less effectively, dependent on proximity to GFP, bound to the inner leaflet of the plasmamembrane. So the change in membrane potential can be detected as change in GFP emission intensity. Disadvantages of the method are severe: it is not commercially available anymore because it is poisonous and because its synthesis produces highly explosive intermediates. It has formerly been used as potassium chelator. In a collaboration with organic chemists (Florian Büsch and Thomas Carel, LMU München), who synthesized DPA, I tested its applicability, with mCD8 expressing transgenic larvae. Administration of DPA immediately killed larval preparations, making calcium measurements impossible.

In the same group a new fluorescent compound had been synthesized (Eva-Maria Jahn and Thomas Carel, LMU München). Based on its structure, membrane insertion seemed likely. I hypothesized that it could function as FRET partner for membrane bound GFP and tested this. However, the compound turned out to cross cell membranes, and did not selectively reside inside membranes. It also showed fluorescence from the cytosol after washout. Thus all previous and all further analysis and explanations refer to calcium

imaging with GECIs.

stimulus	Δ calcium	YC3.3	YC3.60	YC2.60	D3cpv	TN-L15	TN-XL	TN-XXL	GCaMP1.6
10 Hz, 2 s amp	0.11 μM	5.6 ± 0.5	27.9 ± 2.9	25.1 ± 2.9	20.1 ± 2.2	4.3 ± 1.2	1.6 ± 0.5	14 ± 1.1	-0.4 ± 1.3
SNR		1.6 ± 0.2	3.0 ± 0.4	2.4 ± 0.4	2.4 ± 0.2	0.8 ± 0.2	0.3 ± 0.1	2.4 ± 0.2	0.1 ± 0.3
20 Hz, 2 s amp	0.22 μM	15.9 ± 0.4	49.7 ± 3.1	54.5 ± 5.3	35.4 ± 1.8	16.0 ± 2.0	4.5 ± 0.6	36 ± 1.8	11.2 ± 1.2
SNR		3.4 ± 0.2	5.7 ± 0.7	3.5 ± 0.3	4.1 ± 0.3	2.3 ± 0.3	0.9 ± 0.1	4.2 ± 0.2	2.3 ± 0.2
40 Hz, 2 s amp	0.45 μM	36.2 ± 0.9	90.9 ± 5.2	125.7 ± 8.1	53.4 ± 2.3	41.9 ± 2.7	19.3 ± 1.2	96.8 ± 4.4	61.7 ± 4.4
SNR		7.6 ± 1.0	7.4 ± 0.8	4.8 ± 0.4	5.3 ± 0.4	5.4 ± 0.6	3.2 ± 0.2	7.5 ± 0.5	8.6 ± 1.1
80 Hz, 2 s amp	0.91 μM	57.4 ± 1.0	125.9 ± 4.1	179.0±11.6	73.4 ± 3.0	55.7 ± 1.8	77.9 ± 3.9	136 ± 2.1	119.9 ± 4.8
SNR		10.5 ± 0.7	10.4 ± 1.0	4.6 ± 0.4	6.5 ± 0.7	7.6 ± 0.9	8.3 ± 0.6	10.0 ± 0.7	15.9 ± 1.5
160 Hz, 2 s amp	1.83 μM	66.6 ± 0.9	135.8 ± 4.4	193.9 ± 9.7	89.7 ± 3.9	59.5 ± 2.3	105.9 ± 2.7	148.8 ± 2.4	161.6 ± 13.1
SNR		11.7 ± 1.1	8.9 ± 0.6	5.6 ± 0.4	5.9 ± 0.3	7.5 ± 1.0	9.8 ± 0.5	10.0 ± 0.7	14.4 ± 1.2
2 ap, 100 Hz amp	-	-0.1 ± 0.8	4.7 ± 4.6	3.7 ± 1.3	2.0 ± 2.4	-0.9 ± 1.0	1.9 ± 1.0	-	0.6 ± 0.5
SNR	-	-0.6 ± 1.0	3.7 ± 1.3	3.2 ± 1.2	2.2 ± 1.6	0.2 ± 1.0	1.2 ± 0.7	-	1.0 ± 1.2
5 ap, 100 Hz amp	-	1.5 ± 0.9	10.9 ± 1.4	11.8 ± 1.6	10.5 ± 1.9	5.9 ± 0.9	4.7 ± 0.6	-	3.5 ± 0.4
SNR	-	1.6 ± 0.8	8.4 ± 1.6	7.3 ± 1.5	6.0 ± 1.2	8.3 ± 2.3	4.4 ± 0.8	-	6.4 ± 1.4
10 ap, 100 Hz amp	-	10.0 ± 1.5	27.4 ± 1.3	22.2 ± 2.5	21.4 ± 5.1	9.5 ± 1.1	15.3 ± 1.5	-	20.2 ± 2.6
SNR	-	12.0 ± 2.1	11.0 ± 2.2	10.6 ± 2.0	8.3 ± 2.0	9.5 ± 2.8	11.5 ± 2.5	-	13.7 ± 2.0

Table 3.1: Summary of GECI-fluorescence responses. Stimulus protocols are indicated in the column to the left. 'Δ calcium' gives respective changes in calcium concentration. In each cell the first line indicates the peak amplitude of the fluorescence changes ± s.e.m. in % ΔR/R (% ΔF/F for GCaMP 1.6 respectively). The second line indicates signal-to-noise ratios.

GECIs still lack sufficient sensitivity to report volume averaged calcium concentration changes related to individual action potentials at presynaptic boutons of neuromuscular junctions. At steady-state, however, small changes in calcium concentrations ($0.1 \ \mu M$) were reported with sufficient signal-to-noise ratios (> 2) by the GECIs Yellow Cameleon 2.60, 3.60, D3cpv and TN-XXL. When GECI characteristics *in vivo* and *in vitro* were compared, only those GECIs that employ wild-type calmodulin-M13 as calcium sensors showed a calcium dependent reduction of response amlitudes *in vivo*. In line with this finding, only these GECIs showed reduced hill coefficients *in vivo*.

3.3 Directional Selective Calcium Responses in Fruit Fly LPTCs

After the anaysis of GECI signaling properties *in vivo*, Yellow Cameleon 3.60, D3cpv and TN-XXL were identified as promising GECIs for *in vivo* application in LPTCs. I started out using Yellow Cameleon 3.60 and TN-XXL to record fluorescence signals from LPTCs while large field moving gratings were shown to living flies. These experiments were done together with Maximilian Joesch-Krotki and Bettina Schnell. GECIs were expressed in flies under UAS-control using the Gal4-Driver line DB331. The expression pattern of DB331 involves LPTCs but also comprises columnar neurons in neuropils other than the lobula plate, e.g. the medulla (see Fig 3.19).
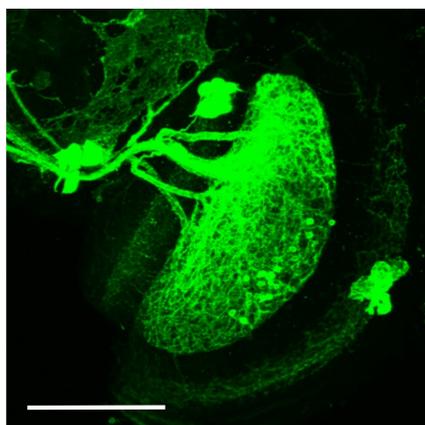
Figure 3.19: GFP fluorescence shows expression pattern of the Gal4 enhancer trap line DB331 (Genotype: DB331-Gal4/DB331-Gal4; UAS-mCD8-GFP/UAS-mCD8-GFP). Maximum intensity projection of a confocal image stack of the lobula plate. Strongest expression is seen in LPTCs (VS and HS cells) with dendritic arborizations in the lobula plate and axonal projections to the central brain. The expression pattern also comprises columnar elements in the medulla and central structures. Orientation: Lower right - lateral, upper/left - central, upper/right - dorsal. Scale bar 50 μm. Picture kindly provided by Shamprassad Raghu.

I used a preparation of adult flies for *in vivo* imaging under visual stimulation that was developed by Dierk F. Reiff and Maximilian Jösch-Krotki (unpublished). For experiments, an adult young female fly was anesthetized by cooling, its back was glued to a plastic holder and the legs were fixed using wax as glue. The wax was mixed with paraffin oil to decrease the melting temperature. The fly's head was bent down and glued to its thorax,

to expose the posterior head capsule under which the lobula plate lies. The posterior head capsule was opened unilaterally using fine capillaries as cuttery. Air sacks, major trachea and fat cells were removed. An aperture was placed upon the holder with the hole above the opening in the head, and ringer was applied to avoid drying of the fly. Then the holder was placed under the objective of the microscope, with the fly facing the stimulus arena.

The used visual stimulus device was developed by Dierk F. Reiff. The light source was an array of five ultra bright LEDs. These illuminated a mirror that was placed inside a rotating stripe-cylinder at an angle $45°$ to the longitudinal axis of the cylinder. This way, the mirror projected a grating through a lens onto a rectangular array of 25x50 light guide fibers. The opposite ends of these fibers were mounted in a half cylindrical array generating a semi-spherical screen as the fly's movie screen where the gratings were shown. Rotation of the cylinder around the mirror moved the grating projection perpendicular to the orientation of the stripes. The orientation was altered by rotating the entire cylinder housing in front of the planar array of light guides. For the initial experiments presented here I did not measure luminance nor contrast levels nor exact angular width of the stimulus. In all experiments shown, the contrast frequency was $\approx 1\ Hz$. The LEDs were flashed at a rate of $500\ Hz$, in phase with the movement of the fast scan-mirror of the 2-photon microscope. In each pulse, the light was on for $380\ \mu s$, precisely time locked to the reset-movement of the fast scan mirror. Photons sampled in the photomultipliers during this time were shed. Thus, the stimulus lights were on when no light was sampled. The pulse frequency of the LEDs exceeded the highest flicker frequency that leads to detectable modulations in ERG recordings from blowflies ($\approx 300\ Hz$) so that the stimulus light should appear as continuous to the fly. While photons emitted by GECIs were sampled in the photomultipliers, the light of the visual stimulus was shut off and the only photons that were sampled were those emitted by GECI expressing cells after 2-photon excitation.

3.3.1 DB331 - Yellow Cameleon 3.60

In a first experiment, a fly of the genotype DB331-Gal4 / DB331-Gal4; UAS-YC3.60 / UAS-YC3.60 was prepared as described. Double homozygous flies displayed high expression levels of Yellow Cameleon 3.60 (see Fig 3.20), which allowed imaging of LPTCs with good contrast even in dendritic branches of 3rd and 4th order and in axon terminals. Imaging at axon terminals is hindered by three obstacles: tissue scattering due to the depth at which the structures reside, cuticle structures, that cut off parts of the excitation light cone, reducing excitation energy and air filled trachea, that reflect and scatter the excitation
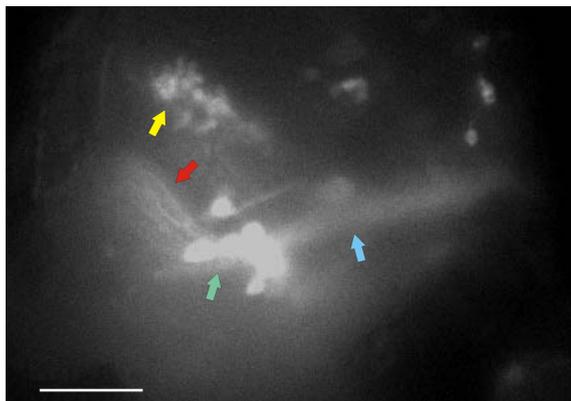
Figure 3.20: CCD camera image of a flybrain expressing Yellow Cameleon 3.60 predomi-
nantly in LPTCs. Left side of the head capsule is opened. Lateral is to the left
and central to the right. Preparation was done as described. Bright structure
contains the cluster of LPTC somata (green arrow). Left of these, the dorsal
branches of dendritic arborizations of VS cells are visible (red arrow). To
the right, their axons project to the central brain (blue arrow). In the upper
part another cluster of cells also shows fluorescence (yellow arrow). Genotype:
DB331-Gal4/DB331-Gal4; UAS-YC3.60/UAS-YC3.60. Scale bar 50 μm.

light. Removal of trachea, however, may cause functional damage to the neural circuits
under observation.

We found no calcium signals from LPTCs in two flies expressing Yellow Cameleon 3.60
under DB331-control, when presenting a large field moving grating to almost the entire
visual field of the ipsilateral eye. The fly was alive, as indicated by small pumping move-
ments of the flies inner organs. Our impression was, that despite all circumstances being
permissive, Yellow Cameleon 3.60 failed to report calcium fluctuations in dendritic and
axonal parts of different VS cells and one HS cell. However this conclusion is based on
experiments with 2 flies and therefore remains preliminary.

3.3.2 DB331 - TN-XXL

In a second set of experiments we used flies that expressed TN-XXL in LPTCs. When
we recorded fluorescence signals from VS cells of these flies, using 2-photon microscopy,
while large field visual motion was presented in front of the ipsilateral eyes of these flies,
we found reproducible, motion related fluorescence responses in axons and dendrites of VS
cells, indicative of directional selective calcium responses in VS cells (Fig 3.21 & Fig 3.22).

A fly of genotype DB331-Gal4/DB331-Gal4; UAS-TN-XXL/UAS-TN-XXL was pre-

pared as described and mounted with the opened side of the head capsule centered under the objective of the microscope. The stimulus screen was positioned to stimulate almost the entire receptive field of the eye on the opened side of the head. VS cells were identified under CCD camera imaging. Then we switched to 2-photon microscopy and zoomed in onto VS cell axons (see Fig 3.21 A-C). Fluorescence signals from VS cell axons were recorded close to their axon terminals in the central brain of the fly over 25 s in each experiment: The horizontal grating was presented for 3 s before the onset of preferred-direction motion (downward, 5 s). Then the grating was steady for 5 s before the onset of null-direction motion (upward, 5 s). After this the grating was presented steady for additional 7 s. Fluorescence changes, recorded at VS cell axons during visual stimulation showed an increase in $\Delta R/R$ with the onset of preferred-direction motion. $\Delta R/R$ increased to a plateau of an average average amplitude of 19.1 % $\Delta R/R$. The rise of this signal was fit by a single exponential function with a time-constant of 0.7 s. After the offset of preferred-direction motion$\Delta R/R$ decreased to baseline. The decay of the signal was fit by single exponen-
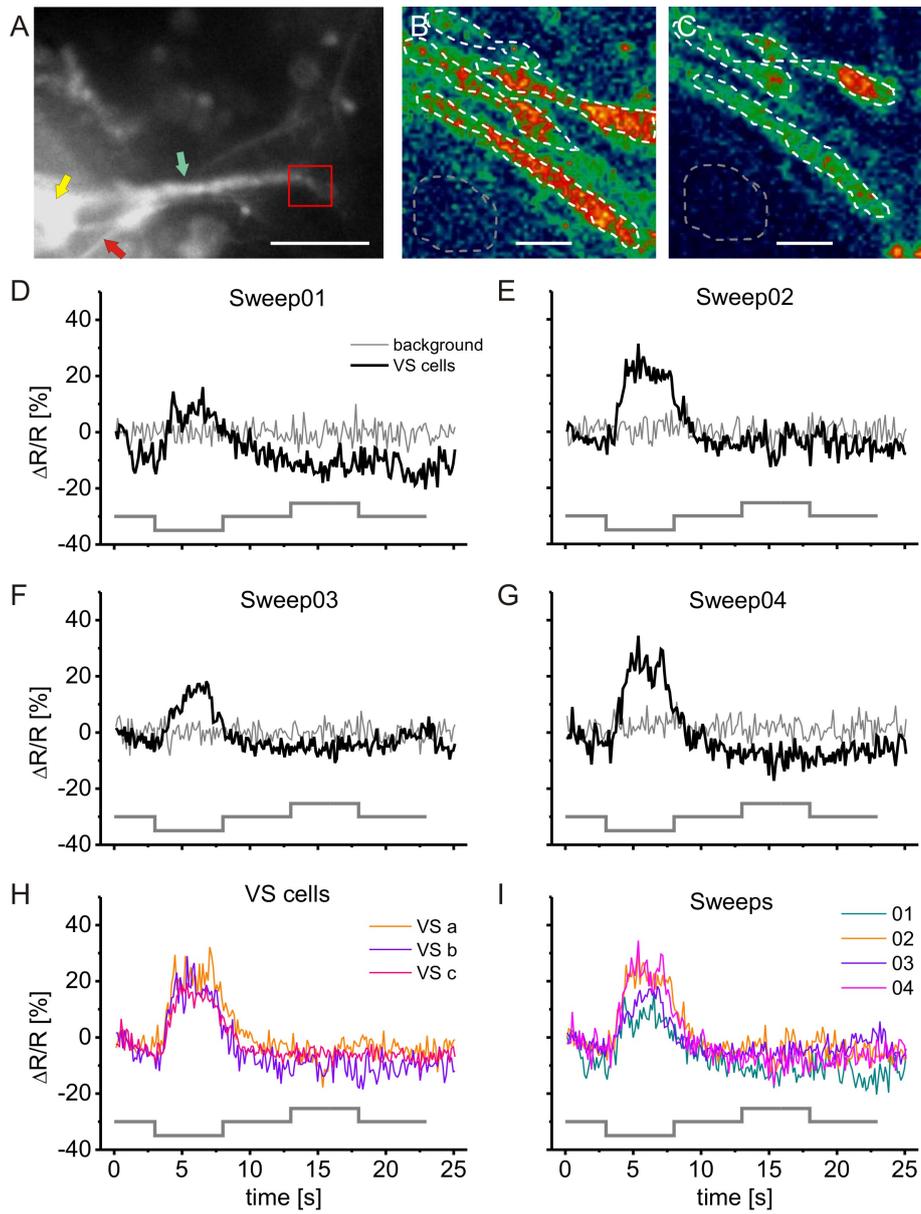
Figure 3.21: Directional selective calcium responses in VS cell axons. (A) CCD camera image of a flybrain expressing TN-XXL in LPTCs under control of DB331-Gal4. Bright structure are LPTC somata (yellow arrow). Axons of VS cells (green arrow) project to the central brain. Red arrow indicates HS cells. Optical recordings were done on axons of VS cells (red square) using 2-photon microscopy, while the fly was visually stimulated with a horizontal grating that moved first downward and then upward. (B)&(C) Raw fluorescence images from 2-photon microscopy recordings show axons of VS cells in false color code. Change in focus was due to motion of the fly. White dashed lines outline evaluated regions, gray dashed lines outline regions evaluated for subtraction of background fluorescence. Example frames are taken from two experiments shown in (D)&(E). (D)-(G) Average fractional fluorescence changes, recorded at VS cell axons are plotted as a function of time for 4 consecutive experiments (Sweeps 01-04). 3-4 VS cell axons were imaged in each sweep during visual motion stimulation (indicated by the grey square trace: -30 = no motion, <-30 = downward motion, >-30 = upward motion). In every experiment, fractional fluorescence changes recorded from VS cell axons reported increases in intracellular calcium during downward motion but not during upward motion. Background fluorescence did not exhibit motion related responses. (H) Fractional fluorescence changes for three VS cells (a-c) are averaged over 4 sweeps and plotted as a function of time for each cell. (I) Average fractional fluorescence changes from VS cells in each sweep (01-04) are plotted as a function of time. Scale bars: (A) 50 μm, (B)&(C) 5 μm.

tial function with a time-constant of 1.5 s. During null-direction motion no fluorescence changes were found (Fig 3.21 D). This indicates directional selective calcium influx into VS cell axons. The results were reproduced in 4 consecutive trials (see Fig 3.21 D-G). All VS cell axons that we recorded from, exhibited directional selective calcium responses to large field motion in every single trial (see Fig 3.21 H&I). The responses recorded from axons of three different cells, that were found in every trial, were almost equal in amplitude and time course (Fig 3.21 H), indicating that the stimulus was large enough to excite all three cells to the same extent. The averaged VS cell responses in different trials however showed some variability (Fig 3.21 I). This was at least in part due to motion in the preparation, which hinders repeated imaging of the same structures at the exact same z-axis level. VS cells did not respond to horizontal motion of a vertically oriented moving grating of the same contrast frequency.

With a second preparation of a fly of the same genotype, we repeated these experiments. The results were qualitatively reproduced with this second animal (Fig 3.22 A): VS cell axons showed directional selective calcium influx in response to downward motion of horizontal gratings. The same cell did not respond to horizontal motion of a vertically oriented moving grating of the same contrast frequency ($\approx 1\ Hz$, data not shown). In another trial, we positioned the stimulus screen, centered in front of the fly. Instead of presenting vertical image motion, the grating was now rotated manually in front of the fly. VS cell axons exhibited directional selective fluorescence responses indicating calcium influx in response to clockwise image rotation. Image rotation counter clockwise did not elicit any fluorescence responses (Fig 3.22 C). We next observed fluorescence responses of VS cell dendrites during image motion (Fig 3.22 D). Again, we recorded calcium responses induced by downward motion. This was shown in five consecutive trials. The average responses are shown in (Fig 3.22 D). The VS cells' motion responses in the dendrite appeared transiently tuned to the onset of motion of the grating in a directional selective way. We did not make any efforts to precisely determine the identity of the imaged cells. This will be possible in the future, however, by filling of individual cells with synthetique dyes after the recordings.

These preliminary experiments demonstrate for the first time, that calcium imaging with GECIs is feasible in the central brain of a fruit fly *in vivo* on the level of individual identifiable cells. Moreover, we recorded for the first time optically from GECI expressing interneurons in the optic lobes close to the photoreceptors in *Drosophila*. We demonstrate directional selective motion responses with optical methods in *Drosophila* LPTCs. The amplitudes and signal-to-noise ratios of signals recorded at VS cell axons (ΔR/R = 19.1 $\pm$
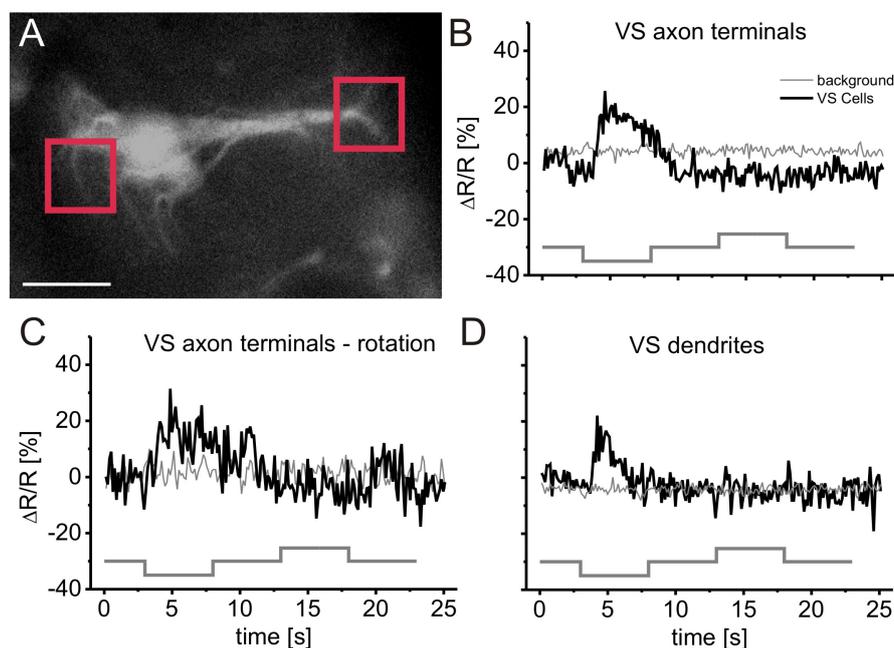
Figure 3.22: Directional selective calcium responses in VS cell axons and dendrites. (A) CCD camera image of a flybrain expressing TN-XXL in LPTCs under control of DB331-Gal4. Optical recordings using 2-photon microscopy were done on a VS cell axon in the central brain (right square, (B)-(C)) and a VS cell dendrite in the lobula plate (left square, (D)), while the fly was visually stimulated. (B-D) Fractional fluorescence changes are plotted as a function of time. (B) Fluorescence responses were recorded at VS cell axons during visual stimulation of the fly. A large field horizontal grating was moved first downward and then upward (indicated by the grey square trace: -30 = no motion, <-30 = downward motion, >-30 = upward motion). The averaged fluorescence response from 2 consecutive trials is plotted in black. The response to downward motion replicates the results shown in Fig 3.21(D)-(G). (C) Optical recordings from VS cell axons were done during alternative visual stimulation: The same grating that was shifted in (B) was now rotated in front of the fly (indicated by the grey square trace: -30 = no motion, <-30 = clockwise rotation, >-30 = counter clockwise rotation). Rotational speed was roughly 36 $°/s$. The rotational center was frontal to the fly. Clockwise rotation leads to downward motion of the pattern in front of the right eye and induces calcium influx in a VS cell axon. (D) Average fractional fluorescence changes, recorded at a VS cell dendrite in 5 consecutive trials are plotted in black. Visual stimulation as in (B). Downward motion induces a transient fluorescence response in a VS cell dendrite. Scale bar 50 μm.

2.8 %, signal-to-noise ratio = 3.8 ± 0.9) were sufficient to discriminate between different response shapes in axon termini and dendrites.

In future experiments, I plan to repeat the imaging experiments on LPTCs while genetically interfering with neural activity of visual interneurons presynaptic to LPTCs. Visual motion detection does most likely not rely on a single processing channel in the optic lobes of flies. Rather, parallel pathways convey signals that contribute to the processing of motion information [32]. Thus, the interference with individual cell types in the optic lobes, may not lead to abolished, but reduced or modified directional selective motion responses in LPTCs. The amplitudes and signal-to-noise ratios exhibited in directional selective motion responses of VS cell axons raise the hope that such modifications will be detectable with GECI based imaging using TN-XXL.

3.4 The Transgene Expression System LexA-pLOT

For such experiments, combined imaging and manipulation of neuronal activity in separate populations of cells, using transgenic tools for both, requires independent transgene expression. Since the Gal4-UAS system was introduced in 1993 [118], fly strains containing UAS- and Gal4-constructs have been established and are available for combination. I obtained several enhancer-trap flies from Lawrence Zipurski (University of California, Los Angeles, USA), that express Gal4 in diverse sets of columnar neurons. These will be used for the expression of proteins to block neural activity, like shibire ts.

To complement these, I started to adapt a second bipartite transgene system, for the expression of GECIs under the control of a bacterial operator. This operator is called LexAop as it is recognized by a transcription factor known as LexA. Two sorts of fly lines need to be established: First, fly strains that carry the desired GECI transgene under the control of LexAop. Second, fly strains that express the transcription factor LexA::VP16 under the control of genomic enhancers which drive expression in the desired sets of cells, like LPTCs.

3.4.1 Effector Strains: pLOT-GECI

According to the *in vivo* characterization of GECIs, Yellow Cameleon 3.60, D3cpv and TN-XXL were likely the most useful GECIs for imaging in the adult central nervous system. The applicability of TN-XXL in LPTCs was already demonstrated (see 3.3). I modified
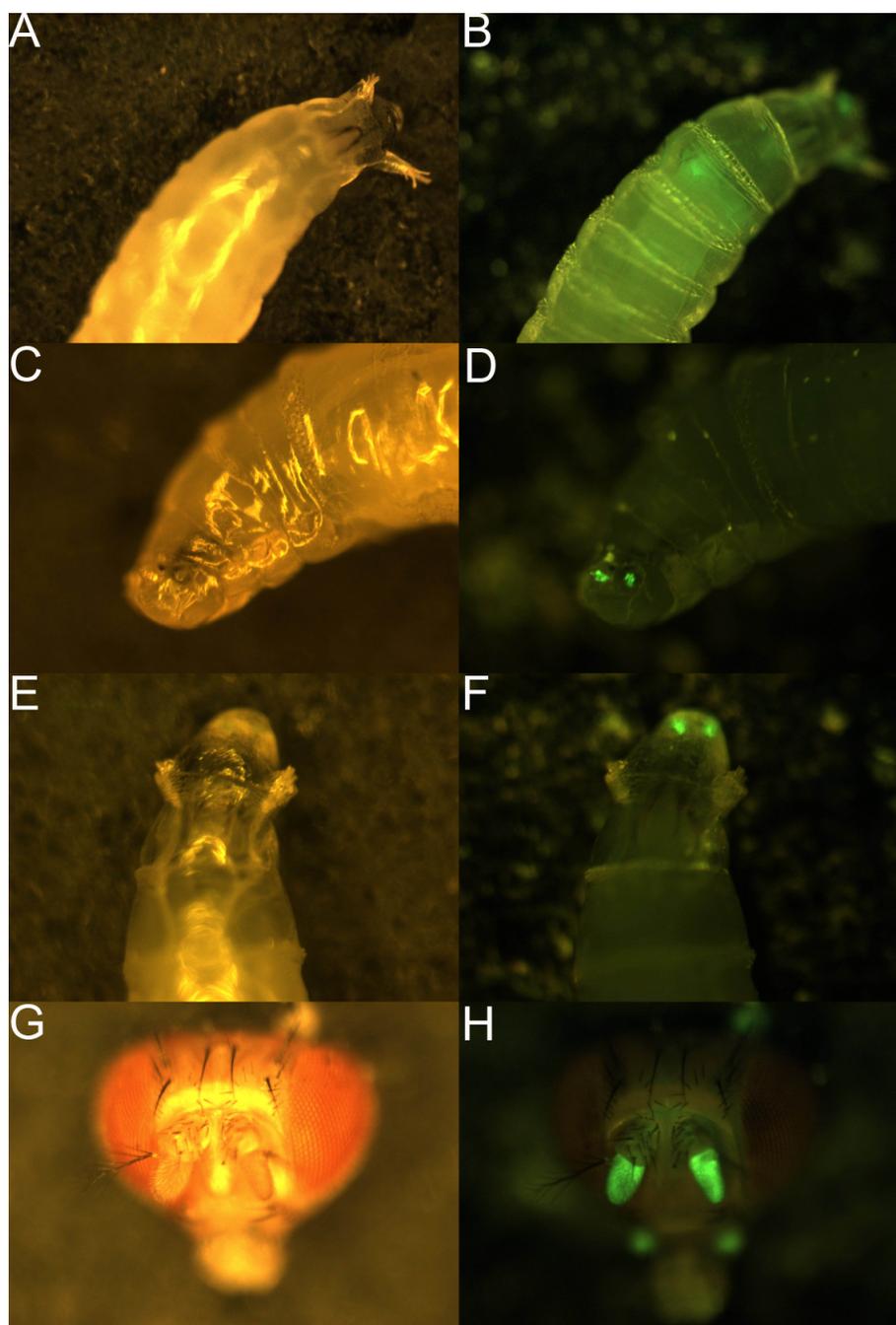
Figure 3.23: Larval and adult *Drosophila* expressing Yellow Cameleon 3.60 in olfactory organs under the control of the LexA-pLOT system. Pictures were taken under bright light (left) and under fluorescence excitation (right). (A)-(B) Frontal larval segments. Through the cuticle, weak fluorescence from the larval brain is visible. According to the described expression pattern of the line Or83b, the fluorescent structures are likely the larval antennal lobes where the axons of olfactory receptor neurons terminate. (C)-(D) Larval head. At the lower frontal end the paired dorsal organs show strong fluorescence. This is where the olfactory receptor neurons dendrites reside. (E)-(F) Same as (C)-(D), seen from above. (G)-(H) Adult head. 3rd antennal segment and the maxillary palps show strong fluorescence. Adult olfactory receptor neurons dendrites reside here (Maxillary palps are better visible in Fig 3.24).

Figure 3.24: Adult *Drosophila* expressing TN-XXL in olfactory organs under the control of the LexA-pLOT system. (A) Adult fly under bright light and fluorescence excitation. Fluorescence is detectable only from the olfactory organs of the fly, the 3rd antennal segment (funiculus) and maxillary palps. (B) Head of the same fly in higher magnification showing fluorescent maxillary palps and funiculi.

vectors for the expression of these GECIs under LexA control and generated the transgenic flies. At first this was done for TN-XXL and Yellow Cameleon 3.60.

I obtained the pLOT vector (Fig 2.5) from Tzumin Lee. I inserted the cDNAs for Yellow Cameleon 3.60 and TN-XXL, respectively, into the multiple cloning site of the pLOT vector, and generated transgenic flies by P element mediated germline transfection as described earlier. Flies transfected with pLOT can be identified on the basis of their red eyes. Stable lines were established for these transgenes.

To test for functional expression of GECIs flies were crossed to one of the few LexA driver lines available to date (OR83b-LexA::VP16) and progeny was screened for fluorescence. The driver flies express LexA::VP16 under the control of the genomic enhancer for an olfactory co-receptor gene known as OR83b. This enhancer is active in probably all olfactory receptor neurons in both larval and adult flies. I crossed these flies to newly generated LexAop-GECI flies. Progeny showed strong expression in olfactory accessory organs in both larva and adult for both GECIs. The larval terminal organ showed strong fluorescence (Fig 3.23 (A)-(F)) and weak fluorescence was detected in the larval brain; see (Fig 3.23 (A)-(B)) , probably originating from the larval antennal lobes. In adult flies, the third antennal segment and the maxillary palps showed strong fluorescence (Fig 3.23 (G)-(H) & (Fig 3.24 (A)-(B)). The labeled structures host all of the flies olfactory sensilla.

This confirmed (i) that the generated transgenes for GECI expression lead to functional expression of the transgenes, (ii) that the expression pattern of these genes is correctly localized and specified by the enhancer that controls LexA expression and (iii) that the resulting expression levels are high in double heterozygous flies, although this was not quantified.

3.4.2 Driver Constructs: Enhancer-LexA

For the generation of LexA driver lines I started to 'convert' existing Gal4 expression patterns into similar LexA expression patterns. For that purpose, I cloned putative genomic enhancers from identified relevant Gal4 enhancer-trap fly strains, to fuse these to LexA. Initially, we obtained 3 fly strains that express Gal4 in LPTCs (DB331, 3A and 1187) and 2 strains showing expression in many other classes of visual interneurons neurons, among others, a class of columnar cells implicated in motion vision, known as T4 cells (Shamprassad Raghu, unpublished data; NP2056, NP1372; see Table 2.1). I first mapped the P element insertions by iPCR (see 2.4.3), then amplified putatively corresponding enhancer regions from BAC clone DNA and tried to clone resulting fragments into an expression vector for LexA::VP16 (pCasper4-LexA::VP16) (see 2.4.4).

T4-Cell Driver NP2056

The enhancer trap line NP2056 expresses Gal4 broadly within the optic lobes and in structures of the central brain. The expression pattern is of special interest because it probably comprises a class of columnar neurons known as 'T4 cells', which have been implicated in motion perception (see Figs 1.3, 1.4, & 3.25). NP2056 was generated in a Gal4 mutagenesis screen in the laboratory of Kai Ito (National Institute of Basic Biology, Okazaki, Japan) (http://flymap.lab.nig.ac.jp/ dclust/getdb.html). The lines generated in this screen were already subject to iPCR but NP2056 and NP1372 could not be mapped there. For NP2056 I rescued genomic fragments by 5'iPCR with high sequence similarity to a wild-type genomic region on the right arm of the 2nd chromosome (Fig 3.26). The insertion lies within the first intron of the gene Fkbp13. Its molecular function is described as FK506 binding, it has peptidyl-prolyl cis-trans isomerase activity and maybe calcium ion binding. It may be involved in protein folding. 12 alleles are reported. It has 2 annotated transcripts and 2 annotated polypeptides. A second gene, neighbouring Fkbp13 is CG10496. Its 5' end lies 2 kb downstream of the NP2056 insertion. 5 alleles of this gene
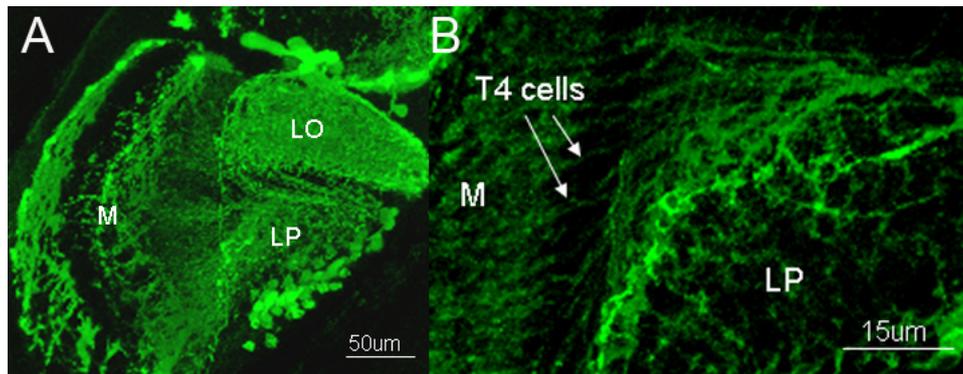
Figure 3.25: Gal4 expression pattern in the fly line NP2056 visualized by expression of UAS-mCD8:GFP and subsequent GFP-antibody staining. Maximum intensity projection of a confocal image stack. (A) Horizontal section through the optic lobe of a fly reveals strong staining of many neurons in the medulla (M), lobula (Lo) and the lobula plate (LP). Parts of the central brain are also stained (upper right). (B) Magnification showing T4 cells, indicated by arrows, in columnar organisation, projecting from the medulla to the lobula plate. Note that no LPTCs are contained in this expression pattern. Orientation: Left - lateral, top - central, lower/right rostral. Pictures kindly provided by Shamprassad Raghu.

have been reported but nothing is known about its function.

I designed primers and amplified a 3.7 kb fragment of genomic DNA from the BAC clone 13H23. This fragment spans the first two introns of Fkbp13 and the region between this gene and its 5' neighbor CG10496 (2R:17,382,800-17,386,500), assuming this region to contain the enhancer of interest. I subcloned this fragment into the bacterial vector pBSKII- but were until now not able to transfer it from there into pCasper4-LexA::VP16.

T4-Cell Driver NP1372

The enhancer trap line NP1372 was identified in the same screen as NP2056 and its genomic insertion site is unknown. Both strains show overlapping expression patterns. In NP1372 Gal4 expression probably comprises T4 cells and many other neurons within medulla, lobula and lobula plate (Fig 3.27). In my mapping efforts I yielded a 5' iPCR product. Genome blast of the sequencing results yielded highly significant sequence similarity with a *Drosophila* transposable element known as copia. These elements are highly abundant and widely distributed throughout the fly genome. It is thus impossible to infer from this the genomic site responsible for the NP1372 expression pattern. It may be possible to map this
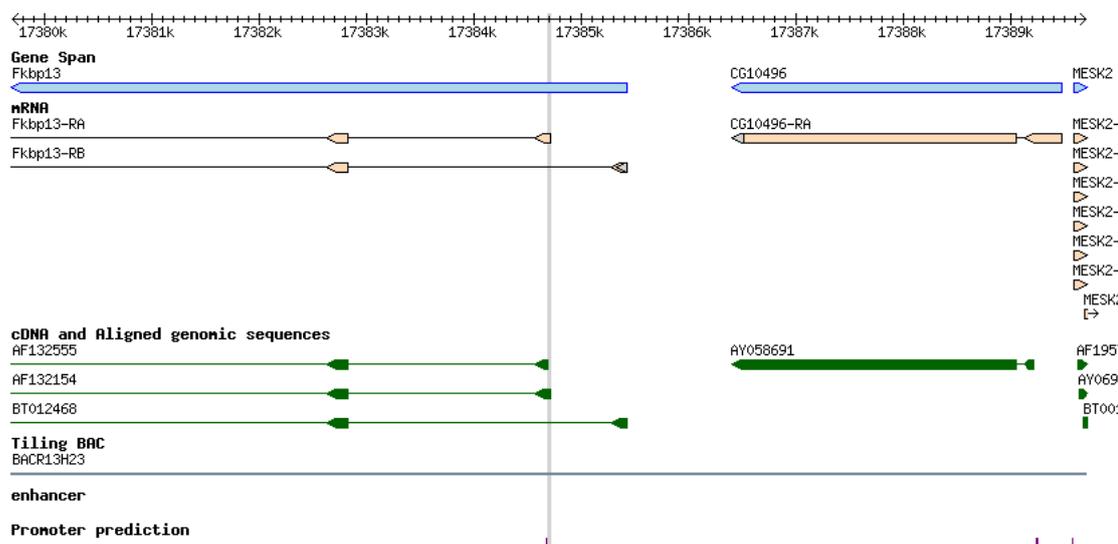
Figure 3.26: Genomic region 57E6 surrounding the Gal4 insertion of the enhancer trap line
NP2056 on the right arm of the 2nd chromosome. Grey line in the middle in-
dicates the insertion site. Many other transgene insertions have been mapped
to the same location indicating a hot spot for P element insertion. The inser-
tion hits a 2 kb intron of the gene Fkbp13, almost 1 kb from its start. The
next gene to the right is CG10496 (Map from http://flybase.bio.indiana.edu/;
version FB2007_03, released November 1, 2007).

insertion by means of the plasmid rescue method, in which larger genomic fragments are
isolated for sequencing. Thus, genomic sequence information outside the copia sequence
might be gained.

LPTC Driver DB331

The enhancer trap line DB331 was first described by Madelaine in the laboratory of Alexan-
der Borst. It is characterized by labeling of LPTCs comprising HS and VS cells, and also
by weaker labeling of columnar elements in the medulla (Fig 3.19). It was used to drive
GECI expression in the experiments described in 3.3. Its enhancer is thus of prominent
interest.

No iPCR fragments were yielded from either 5' nor 3' fragments. Ewa Koper and Gaia
Tavosanis kindly provided sequence information from plasmid rescue experiments on the
same flies. Plasmid rescue is an alternative strategy for P element mapping. In contrast
to the iPCR method, bigger fragments can be isolated here. These are amplified in bac-
teria instead of using PCR. According to these data, the insertion was mapped to the
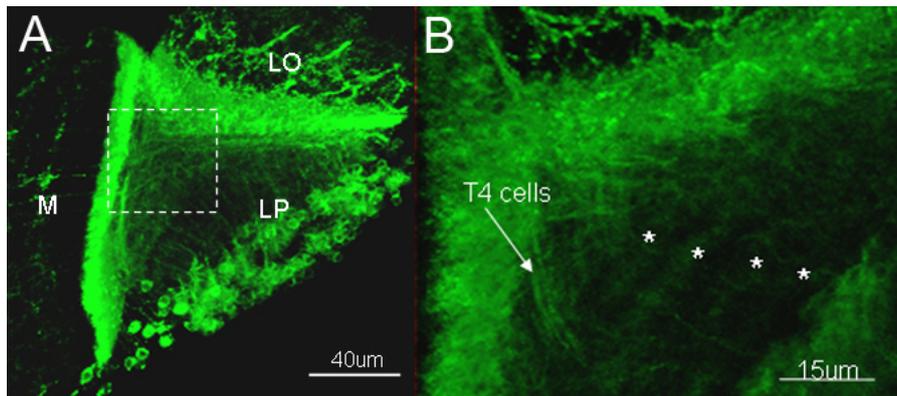
Figure 3.27: Expression pattern of the Gal4 enhancer trap line NP1372, visualized by GFP expression and subsequent GFP antibody staining. (A) Maximum intensity projection of a confocal image stack shows a horizontal section through the optic lobe and reveals staining in the medulla (M), the lobula (LO) and the Lobula Plate (LP). (B) A magnified area, presumably showing T4 cells. The asterisks indicate the four layers of the lobula plate. Orientation: Left - lateral, top - central, lower/right rostral. Pictures kindly provided by Shamprassad Raghu.
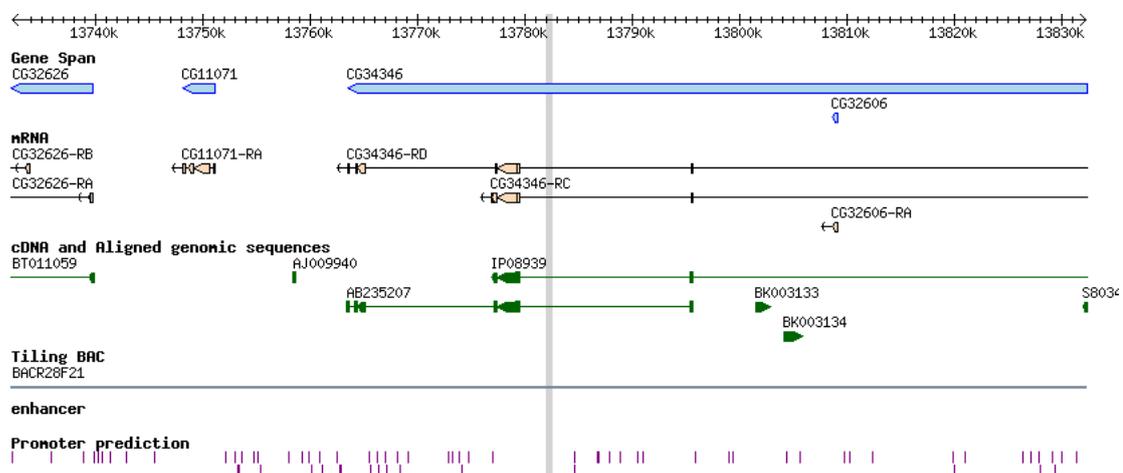
Figure 3.28: 100 kb Genomic region surrounding the Gal4 insertion of the enhancer trap line DB331 in region 12C8 on the X chromosome. Grey line indicates insertion site. Two other transgene insertions have been mapped to the same location. The insertion lies inside an intron of the 100 kb gene CG34346. The nearest neighboring gene lies 30 kb to the left. (Map from http://flybase.bio.indiana.edu/; version FB2007_03, released November 1, 2007)

region 12C8 of the X-chromosome (Fig 3.28). It lies inside an intron of the gene CG34346, which covers more than 100 kb. Its predicted functions are nucleic acid binding, protein binding and zinc ion binding. Biological processes in which it is involved are not known. It has 2 annotated transcripts and 2 annotated polypeptides (Information from http://flybase.bio.indiana.edu/; version FB2007_03, released November 1, 2007). According to an earlier annotation of the fly genome, the insertion seemed to hit a region between two genes that seemed likely to contain the desired enhancer region. Primers designed to amplify the correspondig genomic region from the BAC clone 28F21 yielded no stable products, probably as the sequence information was wrong. After the current annotation a new attempt to amplify a putative enhancer for the DB331 expression pattern has to be made.

LPTC Driver 3A
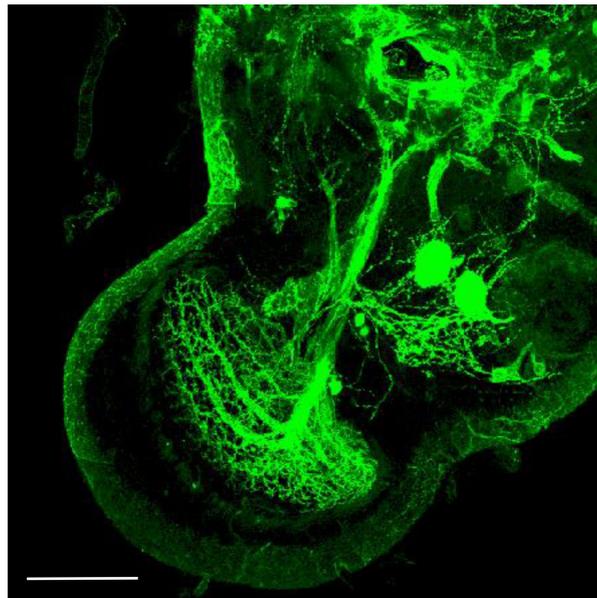
Figure 3.29: mCD8:GFP labeling in the optic lobe of a fly in a rostral view. A maximum intensity projection of a confocal image stack of a fly brain is shown, expressing UAS-mCD8:GFP driven by 3A-Gal4 and stained with a GFP antibody. Orientation: Lower/left - lateral, lower/right - dorsal, top/left - ventral, right - central. LPTCs dendritic network is stained and their axonal projection to the central brain. Scale bar 50 μm. Picture kindly provided by Shamprassad Raghu.

The expression pattern of the line 3A comprises LPTCs [35] and other structures both

within the optic lobes and in the central brain (Fig 3.29). The mapping information in the original publication turned out be false. No iPCR mapping had been made there (Thomas Raabe, personal communication). I did not succeed in mapping the insertion site of the P element in this line. Resulting iPCR fragments repeatedly produced poor sequencing results, independent of the restriction enzyme used in 3' and 5' iPCR. Such a problem may arise from highly repetitive genomic sequence.

LPTC Driver 1187

The enhancer trap line 1187 shows strongest expression in LPTCs (Fig 3.30) but also in columnar elements of the medulla and in structures of the central brain. iPCR on the 5' fragments of P element insertions yielded amplificates with highly significant sequence similaries to the region 25C6 on the left arm of the 2nd chromosome. The insertion lies in a 5 kb region between two genes (see Fig 3.31): (i) Msp300 (Muscle-specific protein 300) is functionally described as cytoskeletal protein binding, actin binding, double-stranded
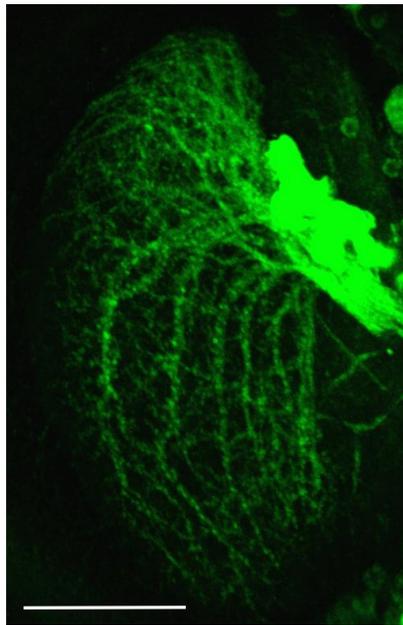
Figure 3.30: A maximum intensity projection of a confocal image stack of a fly's lobula plate is shown, expressing GFP under the control of 1187 and stained with a GFP antibody. Orientation: Left - lateral, top - dorsal, right - central. The bright structures are LPTC somata. To the left the dendritic arborizations of VS cells show GFP expression. Scale bar 25 μm Picture kindly provided by Shamprassad Raghu.
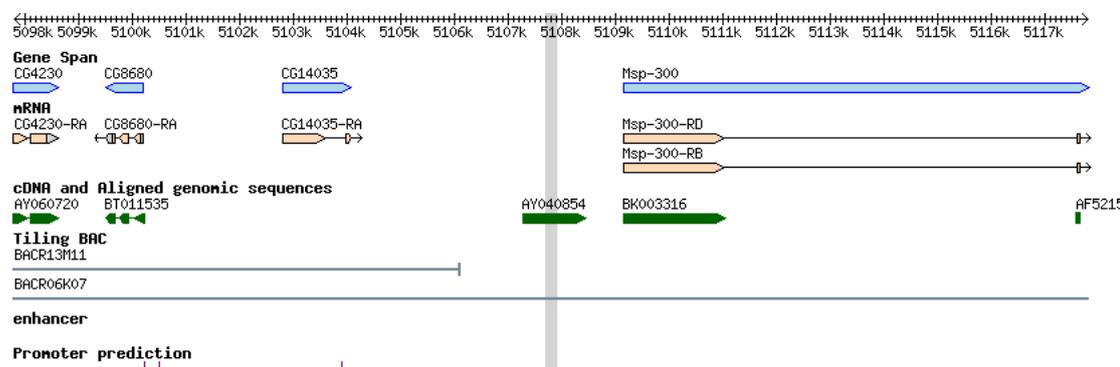
Figure 3.31: 20 kb genomic region 25C6-7 surrounding the 1187 insertion on the left arm of the 2nd chromosome. Grey bar indicates sequence similarity to iPCR product. The insertion lies between the two genes MSP-300 and CG14035 (Map and information from http://flybase.bio.indiana.edu/; version FB2007_03, released November 1, 2007).

RNA binding, centromeric DNA binding and nucleic acid binding. It is reported to be involved in diverse biological processes such as cytoskeleton organization, mesoderm development, cell cycle, chromosome segregation, cytokinesis, mitosis, cytoplasmic transport, establishment of nucleus localization and actin filament organization. 8 alleles are reported and 3 annotated transcripts and 3 annotated polypeptides are known. (ii) Nothing is known about the gene to the left of the insertion site CG14035 (information from http://flybase.bio.indiana.edu/; version FB2007_03, released November 1, 2007).

I designed primers to amplify the genomic region between the two genes from the BAC clone 06K07 and yielded the predicted 5 kb product. According to the current genome annotation this is the most likely region to contain the corresponding genomic enhancer for 1187 expression. The 5 kb fragment was subject to a control digest with HindIII. The control digest revealed 4 fragments of sizes between 200 bp and 2 kb, as predicted from the restriction map. Subsequently the full length fragment was cloned into the KpnI site of pCasper4-LexA::VP16 to yield pCasper4-1187-LexA::VP16. Correct sequence and orientation were checked by sequencing.

During my dorctoral work I did not get to test this putative enhancer construct. Next, I will generate transgenic flies using this construct and cross the resulting strain to pLOT-TN-XXL flies, to test for GECI expression in LPTCs. In parallel I will breed flies expressing shibire ts under Gal4-UAS control in various cell types of the optic lobes and test for the contribution of these cells to the direction selectivity of LPTCs. Combining these transgenes in the same animals will allow for an analysis of the functional role of individual

cell types in the motion detection circuit of the fly.

4 Discussion

The use of optophysiological recordings with GECIs promises to greatly accelerate the functional analysis of *Drosophila's* visual system. However, GECI development over the last ten years, did until now not provide sufficiently sensitive probes, that reliably report neural activity on the single cell level *in vivo*. Furthermore, functional analyses were hampered by the lack of a binary transgene expression system that could be used in parallel to, but independent of the Gal4-UAS system. The results presented in this thesis show that these tools are now at hand, and pave the way for the functional dissection of the visual motion detection system of fruit flies by means of genetic tools for parallel physiological observation and manipulation of distinct sets of neurons.

(i) A new method for the application of synthetic dyes to cellular compartments like presynaptic boutons of neuromuscular junctions was established. This allowed for a quantification of intracellular calcium levels at rest and various levels of prolonged neural activity. (ii) Expressing a variety of new and established GECIs at neuromuscular junctions I conducted a thorough comparative analysis of their *in vivo* response properties. This analysis revealed significant aberrations of GECI characteristics *in vivo* from their published characteristics as assessed in cuvettes. Based on *in vivo* measurements I identified the most suitable GECIs for imaging of neural activity in LPTCs. (iii) Using one of these, TN-XXL, allowed to measure, for the first, directional selective calcium responses with a genetically encoded sensor in visual interneurons in an intact animal. To allow future experiments in which transgenic tools will serve to both image and manipulate different subsets of visual interneurons in parallel, (iv) I adapted an alternative transgene expression system for *Drosophila* for my means.

4.1 Calcium Quantification with Synthetic Indicators

Two photon guided dye injection. To allow a quantitative analysis of GECI properties I first established an *in vivo* system with defined calcium concentrations. These were

quantified using synthetic calcium dyes. A previously applied method for application of synthetic dyes to motoneurons of larval neuromuscular junctions [112] requires very fast preparation and placement of the nerve because there, dyes are taken up through the severed nerve ends, which reseal within approximately five minutes after the cut [112]. Therefore, a new and reliable method of synthetic dye application was established by 2-photon microscopy guided iontophoretic dye injection in genetically labeled cells. A similar method has previously been described for bigger structures in [141, 142], where dyes were loaded into somata via patch pipettes. The dye injection with sharp electrodes works robustly, however, injected motoneurons do not always respond after injections. This is likely due to physical damage of the cells at the injection sites. Electrodes of 80-120 $M\Omega$ are required and the resting potential after injections should be below -15 mV. Given that, success rate of experiments was about 2/3. It proved critical to keep the dye free of calcium by pressure application to the electrode before iontophoretic injection. No special adjustments of the method were required for either of the dyes OGB-1, Magnesium Green and Fluo-4FF, except that Fluo-4FF revealed substantial heavy metal ion sensitivity. This made the use of Magnesium Green favorable as a low affinity complement to the high affinity sensor OGB-1. Injections of these 2 dyes enabled me to quantify calcium concentration changes inside nerve terminals.

Calcium Quantification with OGB-1 and Magnesium Green. I found steady-state calcium concentration changes between 0.1 μM up 1.8 μM in response to sustained activity (see Table 3.1), which is somewhat higher than previously described in the same system. Macleod et al. [134] found submicromolar calcium influx throughout: In response to 80 Hz action potential trains at 2 mM external calcium, the cytosolic calcium accumulated only up to 0.4 μM (here 0.9 μM at 80 Hz and 1.5 mM external calcium). In the same study, resting calcium was quantified as 65 nM and in a previous study by the same group [112] as 23 nM (31 nM here).

However, the bulk calcium concentration changes are relatively small, compared e.g. to the levels described in calcium microdomains underneath plasma membranes, that undergo spatially restricted (to hundreds of nm), large (over tens of μM), short lived (for hundreds of μs) fluctuations [104]. Also, the volume of type 1b boutons at neuromuscular junctions is relatively large ($\approx$ 2 to 70 μm^3 [103]), compared to e.g. boutons in the mouse brain (approximately 0.04 μm^3 [109]), which may further reduce volume averaged changes.

The most influential method for optical calcium quantification was introduced in 1985

[47] in the laboratory of Roger Y. Tsien and relies on ratiometric excitation of Fura-2. The ratioing cancels out optical path length, excitation intensity, and detector efficiency [137]. However dual excitation sources are difficult and expensive to implement in laser scanning microscopy. Moreover, small compartments produce noisy signals, and the ratioing further amplifies such noise. The method applied here was described by Maravall et al. in 2000 [137] in the laboratory of Karel Svoboda and offers some advantages, in particular at small compartments in intact tissue. Most importantly it does not require prior assumptions of resting calcium concentrations. The k_D of the indicator and the maximum fluorescence change *in situ* need to be measured only once. This is advantageous because the minimum fluorescence can only be determined by applying an excess of intracellular buffer, like BAPTA-AM - which is irreversible. The key parameter, that has to be determined is the fluorescence at saturating calcium. Using OGB-1 this was easy at the larval neuromuscular junction because 160 Hz stimulation saturated OGB-1 completely. Dyes of lower affinity can only be saturated *in situ* by the application of drugs like ionomycin, which is irreversible. Taken together, the applied method is the easiest and least error prone way to quantify calcium levels in the larval neuromuscular junction. The *in vivo* calibration of calcium indicators allowed to determine *in vivo* k_Ds for all GECIs, which will facilitate calculation of calcium from imaging experiments in the future.

4.2 GECI Function at the Neuromuscular Junction

GECI Improvements. The newer GECI variants differ from the older variants in several respects. Optimized circularly permuted GFPs were introduced for brighter fluorescence [82] and increased FRET in Yellow Cameleon 3.60 and 2.60 [67], D3cpv [71], TN-XL [66] and TN-XXL (Marco Mank, unpublished data). Engineering of the ion binding domains decreased FRET at resting calcium, changed the k_D and altered the response kinetics [67, 71, 66] (Marco Mank, unpublished data). In my *in vivo* experiments, at steady-state Yellow Cameleon 2.60 and 3.60, D3cpv and TN-XXL reported calcium changes of approximately 0.1 μM with signal-to-noise ratios > 2 (see Fig 3.11 & Table 3.1). However, no GECI allowed the detection of single or volleys of 2 action potentials (see Fig 3.17). This may either be due to the large diffusion volume of boutons and the accordingly low volume averaged concentration changes, or to slow GECI response kinetics.

OGB-1 responses to single action potentials (with peak $\Delta F/F$ 43.6 $\pm$ 2.5 % and signal-to-noise ratio > 10) show that the related volume averaged calcium changes can in principle

be detected with cytosolic indicators of high affinity. As transient fluorescence responses cannot easily be converted into calcium concentrations, it remains unclear whether GECIs fail to detect single action potentials because of low sensitivity or due to slow kinetics. TN-XL shows the fastest response kinetics in this study (see Table 4.1). These are comparable to those observed for some synthetic calcium sensors (time-constants for signal decay here: TN-XL = 200 ms, OGB-1 = 410 ms; literature: OGB-1, Fura-2, X-Rhod-5F: around 100 ms in [40]). However TN-XL lacks sufficient calcium sensitivity at low concentrations to report single action potentials.

probe	GFP variants[1]	functional sensor[2]	hill coefficient		K_D		max change		τ rise[9]	τ decay[0]
			in vitro[3]	in vivo[4]	in vitro[5]	in vivo[6]	in vitro[7]	in vivo[8]	(40Hz)	(40Hz)
YC3.3	ECFP/ Citrine	CaM/ M13	- -	2.5	- (1.5 µM)	0.47 µM 38 Hz	- (100%)	67%	1.41 s	1.05 s
YC3.60	ECFP/ cpVenus	CaM/M13 E104Q	2.24 (1.7)	1.67	0.63 µM (0.25µM)	0.36 µM 30 Hz	346% (560%)	136%	0.82 s	0.73 s
YC2.60	ECFP/ cpVenus	CaM/ M13	- (2.4)	1.84	- (0.04µM)	0.40 µM 32 Hz	- (560%)	194%	*0.88 s	*3.91 s
D3cpv	ECFP/ cpVenus	CaM/M13 redesigned	0.63 (0.74)	0.96	0.66 µM (0.53µM)	0.49 uM 41 Hz	190% (530%)	90%	0.36 s	1.84 s
TN-L15	ECFP/ Citrine	csTnC	1.29 (0.89)	2.59	0.72 µM (1.2 µM)	0.36 µM 30 Hz	82% (140%)	60%	0.81 s	1.49 s
TN-XL	ECFP/ cpCitrine	csTnC mut	1.9 (1.7)	2.74	2.20 µM (2.5 µM)	0.77 µM 65 Hz	252% (400%)	106%	0.59 s	0.20 s
TN-XXL	ECFP/ cpCitrine	csTnC 3/4dup	1.35	2.55	0.8 µM -	0.39 µM 30 Hz	- (230%)	149%	1.04 s	0.88 s
GC1.6	cpEGFP	CaM/M13	- (3.8)	2.34	- (0.15µM)	0.64 µM 54 Hz	- (490%)	162%	1.38 s	0.45 s
OGB-1	-	Bapta	0.97	1.48	0.24 µM (0.17µM)	0.26 uM 21 Hz	1100% (1400%)	316%	0.17 s	0.41 s

Table 4.1: Summary of GECI characteristics. [1] GFP variants lists the chromophores in GECIs. [2] Functional sensor indicates calcium binding and interaction moieties and respective modifications, described in the text (see 1.2.2). Hill coefficients are listed for [3] cuvette and [4] *in vivo* measurements. k_D values represent [5] cuvette and [6] *in vivo* measurements. *In vivo* k_Ds are given in absolute calcium concentration (top) and in stimulus frequencies (bottom). Max change represents [7] the maximum ΔR/R or ΔF/F in cuvette for a calcium concentration of 39.8 μM and [8] amplitudes at 160 Hz *in vivo*. [9] tau rise and [0] tau decay were determined from single exponential fits to rise and decay phase of indicator responses to 40 Hz. * 80 Hz for YC2.60. Values in brackets represent values from literature as cited in the text.

Considerable shortcomings of genetic probes *in vivo* have been described [38, 39, 40,

37]. As a major problem, GECIs' calmodulin and calmodulin binding peptide M13 likely interfere [37] with the highly abundant cellular calmodulin (10-100 μM in different cells) [143] and various calmodulin-regulated proteins of the cell (> 100 have been identified) [144]. Cameleons and GCaMPs function through an intramolecular interaction between two different moieties of the chimeric protein. However, this design may lead not only to the desired intramolecular interaction, that leads to a fluorescence signal, but could also allow intermolecular interactions between these moieties of different GECI molecules, which might inhibit signaling. Like intramolecular interactions, these intermolecular interactions may by calcium dependent.

Two approaches tried to solve these problems: complementary modification of relevant interaction sites within the binding interface of calmodulin and M13 [71], and replacement of calmodulin-M13 by troponin C [72, 95, 66, 80] (and Marco Mank, unpublished data) whose interaction partners are likely not expressed in neurons. Both designs of ratiometric GECIs are thought not to interact with wild-type neuronal proteins [95, 80].

In a comparison of *in vivo* and *in vitro* responses, those GECIs, that employ wild-type calmodulin-M13 as calcium sensor showed reduced dynamic range *in vivo* (Yellow Cameleon 3.60 and GCaMP 1.6) (see Fig 3.14 A&E). Troponin-based GECIs and D3cpv did not show this reduction. Instead, their *in vivo* responses exceeded their *in vitro* responses at high calcium changes (see Fig 3.14 B-D&F). This unexpected finding may be explained by unidentified interactions with components of the cytosol that promote FRET, like the presence of cofactors enhances the function of various enzymes. However, the good accordance of the *in vitro* and *in vivo* data for OGB-1 supports the applied method in principle, although this agreement does not prove the validity of the calcium quantification. Importantly however, independent of the exact cellular calcium concentrations, the principle difference between GECIs employing wild-type calmodulin (GCaMP 1.6 and Yellow Cameleon 3.60) and troponin-based GECIs and D3cpv on the other side remains. This is in agreement with the idea that homo- and heterophilic interactions of the calcium sensors in Cameleons limit these GECIs' *in vivo* performance, in a calcium dependent way. This problem is abolished in troponin-based GECIs, that do not rely on such interactions. A recent study also confirmed functionality of TN-L15 in transgenic mice [95].

Yellow Cameleon 3.60 responses in presynaptic boutons of motoneurons were comparable to those recorded with TN-XXL. In the imaging experiments experiments on LPTCs, however, I found no evidence of calcium signals from Yellow Cameleon 3.60. In the simplest case this might be due to a damaged preparation. Another possible answer lies in

the specificity of the proteome of every single class of cells in an organism. As outlined below, this is markedly true for the composition of calcium signaling proteins including channels, transporters, buffers and signaling partners. The environment in LPTCs might perturb calmodulin-based GECIs and favor troponin-based sensors, while the environment in motoneurons might influence GECI behavior more uniformly.

Comparison of the k_Ds *in vivo* and *in vitro* reveals a general shift towards higher calcium affinities (lower k_Ds) *in vivo*, independent of GECI composition (see Fig 3.15 A). For synthetic calcium indicators the opposite tendency has been observed: lowered *in situ* calcium affinities were found *in vivo* [145]. Factors such as osmolarity, pH, ionic strength and protein environment, that are known to influence calcium binding affinities [145] may influence GECIs and synthetic indicators differentially. Yellow Cameleon 2.60 (see Table 4.1) has not been tested in the cuvette here, simply because it did not seem to be a promising tool for imaging in LPTCs due to the extremely slow decay time-constants of its fluorescence responses. Moreover, the *in vivo* k_D, determined for Yellow Cameleon 2.60 is probably an overestimate, as responses to 20 and 40 Hz stimulation did not reach steady-state at the end of the 2 s stimulus period. Further prolonged stimulation would therefore likely reveal higher response amplitudes at low frequency stimulation, resulting in a higher calcium affinity.

The binding probability of ligands to a receptor that can bind more than one ligand can exhibit cooperativity: If the binding probability for a second ligand is higher than for the first, cooperativity is positive. If it is lower, cooperativity is negative [146]. In theory, receptors with no cooperativity show hyperbolic saturation curves, receptors with positive cooperativity show sigmoidal saturation curves. The steeper the slope of the linear phase of this sigmoidal curve, the higher the cooperativity. This is expressed in the hill coefficient $'n'$. Here, the determination of hill coefficients is based on FRET measurements, which makes an interpretation in terms of cooperativity complex: The hill coefficient of a FRET indicator does not reflect calcium binding dynamics but FRET dynamics. FRET is a function of the 6th power of the distance between 2 chromophores. In addition, the contribution of their relative orientation is unknown. Both distance and conformation maybe functions of calcium binding. 1 calmodulin binds up to 4 calcium ions. The contribution of each binding event to a conformational change accompanying the interaction with the M13-peptide is unknown. At both levels non-linear processes might occur.

Hill coefficients were determined as the slope of a linear fit to the double logarithmic plot of each GECIs saturation curves for both *in vivo* and cuvette measurements (see Table

4.1). A comparison of the hill coefficients, determined here *in vitro* or from the literature to those determined here *in vivo*, shows a marked difference between GECIs comprising calmodulin-M13 and GECIs employing other calcium sensor proteins: Troponin-based GECIs and D3cpv show increased hill coefficients *in vivo*. Yellow Cameleons and GCaMP 1.6 show decreased hill coefficients (see Fig 3.15 B). This difference between calmodulin-based GECIs on one side and troponin-based GECIs and D3cpv on the other side, suggests that interactions with native proteins reduce calcium binding cooperativity *in vivo*. If homophilic interactions contributed significantly to this shift, D3cpv should be affected in the same way as other Cameleons. This is not the case. The decrease in cooperativity may thus be explained by heterophilic interactions, like native calmodulin, binding to Cameleons when charged with calcium, and inhibiting the FRET conformation more efficiently, the more calcium is present.

Signal-to-Noise Ratio in Ratiometric and Single Chromophore GECIs. In ratiometric indicators, the division of two emission signals cancels out correlated noise in the two monitored signals, such as motion artifacts and brightness fluctuations of the excitation light source. This increases signal-to-noise ratios. But the division step in a ratiometric analysis amplifies noise that affects the two channels in an uncorrelated manner, i.e. photon noise. FRET efficacy in CFP/YFP pairs can reach values as high as 98 % [69]. In such a situation the denominator in the term R=YFP/CFP approaches zero, which leads to high signal values but also to high noise. This is the case in Yellow Cameleon 2.60 and 3.60 and D3cpv, which despite high signal amplitudes reached only moderate levels of signal-to-noise ratios at high calcium concentrations (see Fig 3.11 & Table 3.1). Notably, Yellow Cameleon 3.3 shows the highest maximum signal-to-noise ratio of all ratiometric GECIs despite low signal amplitudes. This maybe attributed to low maximum FRET efficacy.

The contribution of photon noise is the higher, the lower the total numbers of photons are. Accordingly, signal-to-noise ratio is a function of expression level and quantum yield, i.e. brightness. This leads to an interesting situation: Under photon limited conditions single chromophore GECIs might provide lower noise levels. However, low activity rates were only detected by Yellow Cameleon variants. A GCaMP variant with a low *in vivo* k_D might be of great benefit for low light conditions. When the number of photons is not limiting, GCaMP 1.6 should prove superior at high calcium levels, because the more calcium is bound, the higher its quantum yield and the higher the signal-to-noise ratio.

However, another factor influencing signal-to-noise ratios is the expression level. Indica-

tor concentration influences response kinetics and signal-to-noise ratios but does not affect fractional fluorescence change amplitudes at steady-state [39, 111]. Higher expression levels improve signal-to-noise, but also lead to more strongly perturbed measured kinetics. Qualitatively, the apparent expression levels were highest in Yellow Cameleon 3.3 and lowest in TN-L15. However, expression levels have not been systematically quantified. As fluorescence changes in Yellow Cameleon 3.3 were rather small, in particular at low activity rates, a high signal-to-noise ratio can only be achieved at high expression levels. The latter causes a slowdown of the response kinetics and substantial deviation from the unperturbed calcium signal due to additional buffering [147, 148, 149]. Two properties of GECIs are disadvantagous in this respect: They exhibit lower quantum yields than synthetic dyes. Therefore more molecules per volume are needed to yield sufficient signal-to noise ratios with GECIs. Moreover, each GECI molecule binds 4 calcium ions (for both calmodulin and troponin-based GECIs). Thus the external buffer added in GECI imaging is usually higher by an order of at least 4. This causes slow kinetics of the fluorescence responses [40]. Thus, GECIs may "miss" short lived events. The data reflect a trade-off between high temporal resolution and high sensitivity to small concentration changes, most obvious in two cases: Yellow Cameleon 2.60 displayed the highest overall fluorescence changes and a low k_D but also the slowest time-constants while TN-XL with no response to calcium changes below 40 Hz shows the fastest signal kinetics in this study (see Fig 3.12).

The External Buffer.   Calcium imaging using transgenetic sensors is sometimes claimed to allow for non-invasive experiments (e.g. [93, 77]). This statement needs some refinement. The calcium binding of an indicator may cause problems in an organism, pronounced in GECIs by the disadvantageous 4-to-1 stoichiometry. Apart from measurement artifacts as discussed in the previous paragraph, GECI expression might cause manifold side effects.

   Calcium is involved in the regulation of cellular processes in the most versatile timescales: In neurons at synapses it regulates exocytosis (μs scale). Muscle contractions are induced in the ms-range. Metabolism is regulated on the range of seconds, transcription over minutes and fertilization and proliferation are subject to calcium control over hours. Long lasting calcium events involve oscillations at various frequencies. To concert these processes, calcium regulates and is subject to regulation of a manifold cellular protein machinery. This regulatory machinery involves receptors (like mGlu1), transducers (like various forms of PLC and various G proteins), ion channels, IP3 receptors, buffers (like calbindin or parvalbumin), effectors (like troponin), enzymes (like NOS or adenylate cyclases) and

transcription factors (like CREB) as well as pumps and exchangers (like NCX and PMCA). This is a small selection from a long, yet certainly still incomplete list of participants [151]. On top of this, each cell has its own specific composition of fast and slow cytosolic calcium buffers (approximately 200 in the human genome) [151]. Hence, influencing calcium dynamics by adding or removing buffers can cause effects on any of the mentioned levels of biological regulation.

E.g. knock-out mice for the fast, mobile calcium buffer protein parvalbumin e.g. shown impaired relaxation in fast-twitch muscles, but they become fatigue resistant through a compensatory mechanism, in which mitochondrial calcium throughput is increased [152]. In the same way, the addition of cellular buffers by GECI expression can cause abnormalities: the cytosolic expression of GCaMP 2 or overexpression of calmodulin in cardiac myocytes can lead to increased heart size [74, 153]. In my experimental animals I did not observe any phenotypic abnormalities besides fluorescence. As biological regulatory mechanisms are usually evolved degenerate, first order effects maybe compensated and the compensations again may cause unexpected and undetected side effects.

A different problem is posed by the faithful translation of a fluorescence response into calcium changes, taking into account the possible influence of indicator presence. An effect of GECI concentration is obvious in the comparison of response kinetics at the neuromuscular junction of fly strains that express the same GECI at different levels: The higher the expression level, the slower the time course of the fluorescence responses [39]. However, such altered kinetics do not reflect altered kinetics of the true cytosolic calcium signal - but altered fluorescence response kinetics from a GECI. This can be analytically solved for linear and non-linear calcium signals [111]. Here, no efforts to reconstruct original calcium dynamics have been made, as all major conclusions are drawn from calcium amplitudes at steady-state, which are not influenced by indicator concentration. Thus, all conclusions are untouched by the expression levels of individual GECIs.

Together, these questions touch a general problem in descriptive sciences, which is the influence of the observation on the observed system. If the external buffer added to a cells intrinsic buffer systems were to compete with the latter, the influence could be severe - especially if we imagine a non-linear system, in which the observation e.g. in this case the additional calcium buffer, keeps the system below a certain threshold. Practically this can best be dealt with by applying bright indicators of low affinity at low concentrations.

Cytosolic vs. Targeted Calcium Reporters. Calcium microdomains underneath plasma membranes are of special interest as at synapses or close to calcium channels vesicle fusion is controlled by fast fluctuating ion concentrations (see above). A desired GECI would thus be targeted to e.g. the plasma membrane or to synaptic proteins and show fast kinetics, as calcium fluctuations vanish quickly due to localized and mobile buffers and diffusion through the cytosol. A membrane tethered calcium reporter has been presented in neurons using a combined approach, consistent of a synthetic calcium indicator and a transgenetic anchor protein (Calcium Green FlAsH). However, its use is limited by the requirement of an elaborate microscopy technique (TIRF) and by the mode of synthetic dye application [154]. In a transgenic approach the GECI SynapCam was targeted to the postsynaptic side of *Drosophila* neuromuscular junctions. Yet, this GECIs function has not been demonstrated in neuronal compartments [155]. The same is true for a chimeric membrane tethered variant of GCaMP 2 [156]. It is likely that the use of calmodulin-based GECIs is not feasible close to synapses because of the increased concentration of native calmodulin and calmodulin interaction proteins. D3cpv may prove useful in this respect. However even troponin-based GECIs showed reduced functionality when fused to targeting peptides in our laboratory (A. Ihring, unpublished data).

Wide Field vs. 2-Photon Microscopy. The GECIs were measured *in vivo* by 2-photon microscopy which offers advantages over wide field microscopy: lower scattering in tissue, essentially no scattered-excitation, reduced photo-damage, and superior background subtraction [157, 116]. This becomes apparent when the present results are compared to those obtained in a previous study using wide field microscopy [39]. In general, the response amplitudes obtained by 2-photon microscopy were increased by a factor of approximately 5 (although the same emission filter sets were used). Response kinetics were reproduced in this study.

Summarizing, I show that the major improvements in the new generation of GECIs were largely retained *in vivo*: in sensitivity (Yellow Cameleon 3.60 & 2.60, D3cpv, TN-XXL), in maximum amplitudes (Yellow Cameleon 3.60 & 2.60, TN-XXL and TN-XL) and in the time course (TN-XL) of the exhibited fluorescence changes. Distinct GECIs with distinct k_D, hill coefficient and fluorescence time course (see Table 4.1) are suited for different experimental preparations and demands. New GECIs are sensitive enough to report calcium changes related to brief bursts of action potentials, even when floating in the cytosol, where calcium fluctuations are strongly diluted compared to submembrane

compartments.

These insights have led to the first optical recordings of directional selective responses from neurons in fruit flies using the new troponin-based GECI TN-XXL.

4.3 Directional Selective Motion Responses in LPTCs

LPTCs have been extensively studied in blowflies (see 1.1). Imaging experiments revealed calcium currents in dendritic and axonal compartments of VS, HS, and CH cells e.g. [158, 12, 159, 160].

In two preliminary experiments I present here the first calcium measurements that demonstrate direction selectivity in VS cells of fruit flies using a novel genetically encoded probe. Axons of four different, yet unidentified VS cells showed steady-state responses of around 20 % ΔR/R. A dendritic compartment showed a transient, directional selective motion-on-response. These responses are reminiscent of transient calcium responses exhibited in higher order dendritic branches of a VS1 cell in response to a locally restricted moving grating [161]. It has been shown, that local motion responses in the dendrites of LPTCs are integrated in the axons [12]. However, the stimulus used here was not locally restricted but a large field grating. Thus, the local, motion induced calcium response should last throughout preferred direction motion stimulation. From former studies on blowflies local calcium signals in higher order branches of LPTC dendrites are expected to fluctuate with the temporal frequency of the stimulus grating [12]. In other studies on blowflies it was shown that synaptic input from local elementary motion detectors to VS cell dendrites may come through GABA receptors and nicotinic acetylcholin receptors [162, 163, 164]. The latter shape the local calcium fluctuations. Integrated axonal calcium signals are shaped by voltage gated calcium channels [159, 164].

In the presented experiments, the contrast frequency of the stimulus grating was roughly 1 Hz and motion was presented for 5 s in preferred and null direction. Thus, a local response to a single bar within the grating can also not account for the transient response. Behavioral experiments, measuring optomotor responses suggest a maximum response at 1 Hz in fruit flies [19]. The transient on-response found in the VS cell dendrite can thus not be explained by stimulus properties. Furthermore, the response decline is fast. Adaptation-like processes that might account for this response decay have not been described [165]. It will be interesting to see whether this transient response will be confirmed in further experiments with more precisely defined stimulus conditions.

The fluorescence signal measured with TN-XXL at VS cell axons during preferred direction motion reached $\approx 20\%$ Δ R/R in amplitude at steady-state. Extrapolating from the experiments at neuromuscular junctions, this relates to an increase of > 100 nM in axons. CCD-camera-based calcium imaging in blowflies yielded fluorescence change amplitudes of up to 10 % Δ F/F using calcium green, although with superior signal-to-noise ratio at 4 Hz sampling frequency [12]. Using 2-photon microscopy amplitudes of 50-100 % Δ F/F were measured [14]. Calcium was not quantified in these measurements. Null direction motion did not induce decrease in fluorescence response in our measurements, as found in *Calliphora* [12]. This is likely due to a lack of the GECIs sensitivity below the resting calcium concentrations of the VS cells.

Recent characterizations of VS cells in *Drosophila* support the assumption that general features of VS cells are shared by fruit flies and blowflies (Maximilian Joesch, unpublished observations): The 6 VS cells found in *Drosophila* are directional selective. They hyperpolarize in response to downward motion and depolarize in response to upward motion. The centers of their receptive fields are distributed along the flies azimuth. The width of the receptive fields is broader than expected from the receptive field of their dendrite, indicative of possible electrical coupling of VS cells as shown in blowflies [14]. VS cells, unlike a speedometer, display a temporal frequency tuning to moving gratings. This means that if a sine grating of spatial wavelength A, elicits a maximum VS cell response at speed B, then a grating of wavelength 2xA will elicit a maximum response at speed 2xB, because both result in the same contrast frequency. In *Drosophila* the VS cells are best tuned to a contrast frequency of 1 Hz. The velocity tuning is a major prediction, derived from the algorithmic model of a correlation type motion detector in action [5]. Also, the characteristic transient step-response shown in blowflies in agreement with the correlation-type motion detector model [166, 167] were reproduced in fruit fly VS cell recordings. Another prediction from the model, contrast invariance of the VS cell response to motion has also been demonstrated in blowflies and fruit flies (all: Maximilian Joesch, unpublished observations). Moreover, as had been proposed for blowflies, VS cells of *Drosophila* receive synaptic input at their dendrite via GABA receptors and nicotinic acetylcholine receptors. GABA receptors were also found on the axon terminals (Shamprassad V. Raghu, personal communication and [13]).

Together with morphological evidence [7], the first electrophysiological recordings from fruit fly VS cells and histological data on synaptic distribution on VS cells indicate that the motion detection system of flies is evolutionarily conserved between species. Thus, the rich

data acquired on blowfly LPTCs in decades of research can serve as working hypotheses for future experiments in LPTCs of fruit flies using GECI-based imaging.

4.4 Transgene Expression

In combination with the Gal4-UAS system, the LexA-pLOT system will allow for experiments, in which imaging of LPTCs can be done, while columnar cells in the medulla will be targeted with transgenes that inhibit neural activity. In principle, Gal4 independent transgene expression can be achieved using constructs that express a target gene, like a GECI under the direct control of a genomic enhancer. Bipartite expression systems via transcription factors like LexA and Gal4, however, amplify expression and allow flexible combinatorial use of various enhancers and transgenes. Both expression systems have been demonstrated to function well in the same animal in parallel, and expression levels, yielded with the new system LexA-pLOT reached or exceeded those achieved with Gal4-UAS [125]. The expression levels of GECIs under LexAop control, yielded with an enhancer that drives LexA expression in olfactory receptor neurons, was strong enough so that imaging experiments would be feasible (see Fig 3.23 & 3.24). Although expression levels depend on both driver and effector line, this shows that our pLOT-GECI effector lines will in principle be adequate for imaging experiments. Next, putative driver lines will be generated using the putative 1187 enhancer fused to LexA::VP16. Also, the genomic sequences surrounding the P element insertion sites of the enhancer-trap lines DB331 and NP2056 have been cloned and will be used to drive expression of LexA::VP16.

It should be mentioned however, that the genomic region containing a putative enhancer, responsible for the expression pattern of the enhancer-trap line 1187 may produce a pattern and level of gene expression, completely different from that found in the corresponding enhancer-trap line. As regulatory elements have been found to be spread over 300 kb [168], in exons of genes and both 5' and 3' from the promoters that they interact with, it is uncertain whether an enhancer responsible for 1187-like gene expression will be found. Enhancers cannot be recognized by genome maps or sequence analysis. If enhancers for specific genes are to be cloned, the general approach is, to amplify 2-10 kb of genomic DNA preceding the startcodon of this gene. In some cases this is sufficient to yield precisely the expression pattern that was desired [88]. However this depends on the complexity of the regulatory region of the specific gene.

Such non-coding sequences may contain complex arrays of long distance regulatory el-

ements. Well studied examples of complex gene expression regulation in *Drosophila* are the *bithorax* complex and the *antennapedia* complex. In the latter, the expression of the segmentation gene *fushi tarazu* is regulated by sequence elements in the 6 kb upstream of its promoter, containing at least 2 enhancers. On top of this, the whole transcription unit lies in between another gene, *sex combs reduced*, and its downstream enhancer that regulates expression of *sex combs reduced* but not of *fushi tarazu* although the promoter of the latter is in closer proximity than that of *sex combs reduced*. On the other hand, the promoter of *sex combs reduced* is protected from the *fushi tarazu* enhancers by an insulator or boundary element, which however does not seem to inhibit the effect of the *sex combs reduced* enhancer, that lies even further downstream. The *fushi tarazu* regulatory region comprises 6 kb 5' from its promoter. Expression analysis of this region reveals that parts of this sequence activate *fushi tarazu* expression at different times during development in different tissues [120, 169].

Thus, a fragment of genomic DNA preceding a gene, may produce expression patterns that are broader or finer than or distinct from the desired patterns, or may as well lead to no gene expression at all, because unexpected or no activating regulatory elements may be picked up [121]. A resulting pattern can be refined by using smaller or larger fragments of such sequences [120]. Once enhancers, specific for visual interneurons are found, the use of the second, Gal4 independent expression system LexA-pLOT will allow for some interesting experiments.

4.5 Outlook

The cellular implementation and the biophysical mechanism of motion detection in the fly's optic lobes is unknown. The analysis of its visual system has been hampered by one major limitation. Of the huge variety of cell types within each optical cartridge and column only cells in the lamina have been thoroughly characterized physiologically (L1, L2 and L3 [170, 171]). All other cells, specifically medullary neurons, have until now escaped electrophysiological characterization, mainly because of their small cell size. As shown, it is now possible to record optically from GECI expressing interneurons in the fruit fly's optic lobes. In our laboratory, we have a variety of Gal4 enhancer-trap fly strains at hand that allow to direct GECI expression to various subsets of visual interneurons. These flies have been generated in screens in the laboratories of Lawrence Zipurski (University of California, Los Angeles, USA) and Kei Ito (National Institute for Basic Biology Myodaiji,

Okazaki, Japan). The expression patterns of most of these have not yet been systematically analyzed, but many are characterized by expression in columnar elements. Examples are strains for transmedullary neurons such as Tm3 and other, unidentified cells. In 2-photon imaging experiments using GECIs, these fly strains will be subject to analysis of both cellular anatomy for identification of cell types and measurements of calcium responses to flickering light and motion stimuli.

Among the multitude of described cell types within each cartridge and column in the flies' optic lobes, a limited number is under suspicion to be part of the motion detection mechanism (see 1.1). Two parallel pathways were proposed (Fig 1.4). Each involves three cell types (L1 to Mi1 to T4, and L2 to Tm1 to T5) [27, 172], some of which (T4, T5) are labeled in known Gal4 enhancer-trap lines (NP1372 & NP2056). One other circuit was suggested, mainly based on morphology and histology and involves lamina amacrine (alpha) cells, L2 cells, T1 cells, Tm1, and the T5 cells, as well as Tm9 and a local interneuron at the level of T5 dendrites [173, 174]. It will require a major effort to identify enhancer-trap lines for all of these cell types and assess their responses to motion stimulation. According to a recent article [32] a critical role of T1 cells is unlikely. In this work enhancer-trap lines for lamina neurons have been described, that we also dispose of (L1, L1 & L2, L2, T1). Furthermore, a mutant fly strain was used there, that is deficient in the *ort* gene, which codes for a histamine receptor. In behavioral experiments these flies were shown to be almost completely motion-blind. Gal4-based rescue of the *ort* gene in different lamina monopolar cells and parallel imaging of columnar elements or LPTCs will provide insight into the wiring of visual interneurons.

After the optophysiological characterization of these lines the analysis can be taken one step further. Gal4 enhancer-trap lines will be used to express transgenes that interfere with neuronal activity. In the same flies GECIs will be expressed in LPTCs via the LexA-system. In such experiments the perturbation of columnar elements in the flies optic lobes in parallel to imaging in LPTCs will be tested for an effect on directional selectivity of LPTCs. The quality of the preliminary experiments demonstrated here, suggests that GECI imaging in LPTCs will not only allow detection of response abolishment but also of moderate reductions of motion sensitivity. In behavioral studies defects in neural circuits maybe masked by redundant mechanisms that compensate for defects. Physiological measurements may be more sensitive and pick up behaviorally ineffective deficiencies.

The combined genetic approach to optophysiology and manipulation of neural activity will provide insights into the neuronal circuits involved in motion vision in flies and will

help to solve a classical biological problem that has puzzled researchers since the 1950s [18, 175]. It will be interesting to see how motion detection systems in insects and mammals have evolved, whether the directional selectivity found in mammalian starburst amacrine cells [33, 34] is also used in visual interneurons of flies', and how mechanisms for motion detection are ultimately used for example to distinguish eye-movements from motion in the world outside.
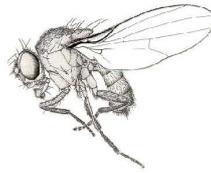
A Appendix

A.1 Abbreviations

AM	acetoxymethyl esther
CaM	calmodulin
CFP	cyan fluorescent protein
cp	circular permutation
dm	Drosophila melanogaster
EGFP	enhanced green fluorescent protein
GAD	Gal4-trans-activation domain
GECI	genetically encoded calcium indicator
GFP	green fluorescent protein
LPTC	lobula plate tangential cell
mDsRed	monomeric Discosoma spec red
OGB-1	oregon bapta green-1
TnC	troponin C
xl	Xenopus laevis
YC	yellow cameleon
YFP	yellow fluorescent protein

A.2 Matlab Scripts for Data Analysis

Data Analysis & Corrections

script for the analysis of single chromophore data
input: raw average fluorescence traces for roi (e.g. bouton) and roni (background)
output: ΔF/F traces, corrected for background fluorescence and bleaching
(analogous for ratiometric GECI analysis)

% Analysis of single data for single chromophore imaging data

% 0. generate x timescale
% 1. background subtract
% 1.1 exponential fit
% 1.2 subtract fit, add mean of first points
% 2. deltaF/F on raw traces - save and filter
% 3. deltaF/F on corrected traces - save filter
% 4. plot it all

% definitions

pathname = 'Pathname'; %where to save results
date = 'date'; %part of results filenames
geci = 'geciname'; %part of results filenames
number = 'experimentnumber'; %part of results filenames

% input files
stimulus = stimulusfile; %input file: stimulusprotocol
rawC = roi; %input file: recorded trace from region of interest
bgC = roni; %input file: recorded trace from region of NO interest

% deltaF variables (mean of frames p to q are basis for F(0))
p=1; %first frame for f(0)
q=15; %last frame for f(0)

% sampling time
d=0.128;

% smoothing (halfwidth of gaussian)
w=10;
filter = 'Gauss 10pt' % filtername for filename

% exponential fit on frames (m=first, n=last)
m=15; %stiumulus (frames m-n) will NOT be considered for bleach correction
n=20;

% 0. generate file with timeaxis and smooth raw traces with gaussian
$cfp\_t = [(rawC(:, 1). * d) + d, rawC(:, 2)]$; %timeaxis for ROI
$cfp\_t\_roni = [(bgC(:, 1). * d) + d, bgC(:, 2)]$; %timeaxis for RONI
$cfp1\_sm = conv(cfp\_t(:, 2), gausswin(w)./sum(gausswin(w)))$; %smoothing
$cfp2\_sm = cfp1\_sm(w/2 : end - w/2)$;
$raw\_cfp\_sm = [cfp\_t(:, 1), cfp2\_sm]$;
$save([pathname,' bs\_c\_sm', number],' raw\_cfp\_sm',' -ASCII')$; %save trace

% 1. background subtraction (rawdata minus mean background)
$cfp1\_bs = [cfp\_t(:, 1), cfp\_t(:, 2) - mean(cfp\_t\_roni(:, 2))]$;
$save([pathname,' bs\_cfp\_', number],' cfp1\_bs',' -ASCII')$; %save trace

% 1.1 exponential bleach correction - stimulus free trace

$cfpx\_first = (cfp1\_bs(1 : m, 1))$; %exclude stimulus period from trace
$cfpx\_last = (cfp1\_bs(end - n : end, 1))$;
$cfpx\_sf = [cfpx\_first; cfpx\_last]$;

$cfpy\_first = (cfp1\_bs(1 : m, 2))$; %exclude stimulus period from timeaxis
$cfpy\_last = (cfp1\_bs(end - n : end, 2))$;
$cfpy\_sf = [cfpy\_first; cfpy\_last]$;

$y0cfp = mean(cfp1\_bs(end - n : end));$

$cfp\_sf = [cfpx\_sf, cfpy\_sf];$

figure % plot stimulusfree trace

plot(cfp_sf(:,1),cfp_sf(:,2))

% 1.2 Exponential fit uses function: FitExponentialYishai (see below)

% fitting function parameter settings

options.MaxIter=10000;%maximum number of iterations

options.MaxFunEvals=10000;%maximum number of evaluations

% fit exponential to stimulus free trace and subtract fit from trace

$[a, b, c, fval, exitflag, output] = FitExponentialYishai(cfp\_sf(:, 2), cfp\_sf(:, 1), options)$

$cfp\_fit = [cfp1\_bs(:, 1), exp(a * cfp1\_bs(:, 1) + b) + c;];$

$cfp1\_c = [cfp1\_bs(:, 1), cfp1\_bs(:, 2) - cfp\_fit(:, 2) + mean(cfp1\_bs(m, 2))];$

save ([pathname, 'bs_c_cfp_', number] , 'cfp1_c', '-ASCII');% save trace

% 2. calculate deltaF/F on raw trace (uses a function 'deltaF')

$cfp2\_dF = deltaF(cfp1\_bs, p, q);$% calculate $\Delta F/F$

save ([pathname, 'df_cfp_', number] , 'cfp2_dF', '-ASCII');

$cfp1\_dF\_sm = conv(cfp2\_dF(:, 2), gausswin(w)./sum(gausswin(w)));$ % filter

$cfp2\_dF\_sm = cfp1\_dF\_sm(w/2 : end - w/2);$

$deltaF\_cfp\_sm = [cfp2\_dF(:, 1), cfp2\_dF\_sm];$

save ([pathname, 'df_cfp_sm_', number] , 'deltaF_cfp_sm', '-ASCII');%save

% 3. calculate deltaF: on corrected trace

$cfp2\_c\_dF = deltaF(cfp1\_c, p, q);$% calculate $\Delta F/F$

save ([pathname, 'df_cfp_c', number] , 'cfp2_c_dF', '-ASCII');

$cfp1\_c\_dF\_sm = conv(cfp2\_c\_dF(:, 2), gausswin(w)./sum(gausswin(w)));$% filter

$cfp2\_c\_dF\_sm = cfp1\_c\_dF\_sm(w/2 : end - w/2);$

$deltaF\_cfp\_c\_sm = [cfp2\_c\_dF(:, 1), cfp2\_c\_dF\_sm];$

save ([pathname, 'df_cfp_c_sm_', number] , 'deltaF_cfp_c_sm', '-ASCII');%save

% 4. plot it all
figure;
h=gcf;
set(h,'Position',[1600 80 700 840]);

%plot raw traces & exponential fit
subplot(2,1,1);
plot(cfp1_c(:,1), cfp1_c(:,2),'r',...
stimulus(:,1), stimulus(:,2).*5,'k-', cfp_t(1:end,1), cfp_t(1:end,2),'c',...
cfp_fit(:,1), cfp_fit(:,2)+mean(cfp_t_roni(1:end,2)),'k',...
cfp_t_roni(1:end,1), cfp_t_roni(1:end,2),'cx')
title ('raw (green and cyan)& bgsub, linear bleach corr (red)');

%plot raw & corrected ΔF/F
subplot(2,1,2);
plot(stimulus(:,1), stimulus(:,2).*5,'k-', cfp2_c_dF(:,1), cfp2_c_dF(:,2),'r',...
cfp2_dF(1:end,1), cfp2_dF(1:end,2),'c', cfp2_dF(:,1), cfp2_dF_sm,'k',...
deltaF_cfp_c_sm(:,1), deltaF_cfp_c_sm(:,2))
title('deltaF/F& lin bl corr (red)');

uicontrol('style','text','units','normalized','position',[0.35 0.95 0.3 0.05],...
'string', [geci, date, number]) % adds textbox 'name' to figure

saveas(gcf,[pathname, 'graph_', number],'m'); % save figure

clear % delete all variables from workspace

Data Analysis & Quantitative Evaluation

input: files with GECI traces after above analysis, corrections & smoothing
output: amplitudes, signal to noise, standard deviations and standard errors

% 'SNR_NMJ_1ch_multiTraceFile'
% Evaluation for one GECI, freq dep signals, from average traces file of
% form: 10HzMean_delta, sd, se, n, 20HzMean_delta, sd, ...
% output is one file (amp, sd, se, snr, sd, se, n)
% for each input file (each frequency)

pathname= 'pathname'; % where to save results

% amp from to
from=20; % define amplitude frames to average over
to=31;

% load input files from current folder to workspace
$for i = 15 : size(listoffiles, 1);$
$correl i = load(listoffiles(i, :));$
$filename = listoffiles(i, 1 : 6);$
$bt = correl i;$

$n = size(bt, 2);$
$lines = size(bt, 1);$

$Amps = mean(bt(from : to, :));$
$Amp = mean(Amps);$
$SdAmps = std(Amps);$
$SeAmps = SdAmps/sqrt(size(bt, 2));$

$SNRs = (Amps)./(std(bt(from : to, :)));$
$SNR = mean(SNRs);$
$SdSNR = std(SNRs);$
$SeSNR = SdSNR/(sqrt(size(bt, 2)));$

$Results = [Amp, SdAmps, SeAmps, SNR, SdSNR, SeSNR, n];$
$save([pathname, filename,' \_amp\&snr'],' Results',' -ASCII');$
end

clear Amp Amps SdAmps SeAmps SNR SNRs SdSNR SeSNR from to n lines b i
clear Results bt correl filename pathname

Function for Bleach Correction: Exponential Fit

The exponential fits used in afore scripts use two functions written and kindly provided by Yishai Elyada:

% 1. Function: ExpFitter

function [a,b,c, fval,exitflag,output] = ExpFitterYishai(V, t, varargin)

% [a,b,c, fval,exitflag,output] = ExpFitter(V, t)
% [a,b,c, fval,exitflag,output] = ExpFitter(V, t, options)

% Calculates exponential fit and offset for the values given in V, i.e. the model:

$$\% \ V = exp(a * t + b) + c$$

% the optional input variable options is the algorithm options for the optimization function.
% fval,exitflag,output are output from fminsearch

% Yishai Elyada 11.1.05
% MPI fuer Neurobiologie, Martinsried, Germany
% Department of Systems and Computational Neurobiology

```
    if nargin == 2,
options = optimset('fminsearch');
else
options = varargin1;
end
```

$$[Vars, fval, exitflag, output] = fminsearch(@(x)experror(x, V, t), [0, 0, mean(V)], options);$$

```
a = Vars(1); b = Vars(2);, c = Vars(3);
```

% 2. Function: experror

```
function E = experror(Vars, V, t)
```

% E = experror(Vars, V, t)

% Calculates the square error of a fit of the variable V to a shifted
% exponential described by the three variables in Vars. Vars(1) is the
% exponential coefficient, Vars(2) is the exponential offset and Vars(3) is
% the offset:
%
% V = exp(Vars(1)*t + Vars(2)) + Vars(3)
%
% Yishai Elyada 11.01.06
% MPI fuer Neurobiologie, Martinsried, Germany
% Department of Systems and Computational Neurobiology

```
a = Vars(1);
b = Vars(2);
c = Vars(3);
E = mean((V - (exp(a*t + b) + c)).^2);
```

Bibliography

[1] S. Martinez-Conde, S.L. Macknik, and D.H. Hubel. The role of fixational eye movements in visual perception. *Nat Rev Neurosci*, 5(3):229–240, 2004.

[2] M.A. Smith, N.J. Majaj, and J.A. Movshon. Dynamics of motion signaling by neurons in macaque area mt. *Nat Neurosci*, 8(2):220–228, 2005.

[3] K. Hausen. Funtional characterization and anatomical identification of motion sensitive neurons in the lobula plate of the blowfly *Calliphora erythrocephala*. *Z Naturforschung*, 31c:629–633, 1976.

[4] H. G. Krapp, B. Hengstenberg, and R. Hengstenberg. Dendritic structure and receptive-field organization of optic flow processing interneurons in the fly. *J Neurophysiol*, 79(4):1902–1917, 1998.

[5] J. Haag and A. Borst. Neural networks in the cockpit of the fly. *J Comp Physiol A*, 188(6):419–37, 2002.

[6] G. Miesenbock and I. G. Kevrekidis. Optical imaging and control of genetically designated neurons in functioning circuits. *Annu Rev Neurosci*, 28:533–563, 2005.

[7] K.F. Fischbach and A.P.M. Dittrich. The optic lobe of *Drosophila melanogaster* 1. A golgi analysis of wild-type structure. *Cell Tissue Res*, 258(3):441–475, 1989.

[8] R. Pierantoni. A look into the cock-pit of the fly. the architecture of the lobular plate. *Cell Tissue Res*, 171(1):101–122, 1976.

[9] R. Hengstenberg, K. Hausen, and B. Hengstenberg. The number and structure of giant vertical cells (vs) in the lobula plate of the blowfly *Calliphora erythrocephala*. *J Comp Physiol A*, 149:163–177, 1982.

[10] H. G. Krapp and R. Hengstenberg. Estimation of self-motion by optic flow processing in single visual interneurons. *Nature*, 384(6608):463–466, 1996.

[11] N. J. Strausfeld and J. K. Lee. Neuronal basis for parallel visual processing in the fly. *Vis Neurosci*, 7(1-2):13–33, 1991.

[12] S. Single and A. Borst. Dendritic integration and its role in computing image velocity. *Science*, 281(5384):1848–1850, 1998.

[13] S. V. Raghu, M. Joesch, A. Borst, and D.F. Reiff. Synaptic organization of lobula plate tangential cells in *Drosophila*: Gamma-aminobutyric acid receptors and chemical release sites. *J Comp Neurol*, 502(4):598–610, 2007.

[14] J. Haag and A. Borst. Neural mechanism underlying complex receptive field properties of motion-sensitive interneurons. *Nat.Neurosci.*, 7(6):628–634, 2004.

[15] K. Farrow, A. Borst, and J. Haag. Sharing receptive fields with your neighbors: Tuning the vertical system cells to wide field motion. *J Neurosci*, 25(15):3985–3993, 2005.

[16] K. Farrow, J. Haag, and A. Borst. Nonlinear, binocular interactions underlying flow field selectivity of a motion-sensitive neuron. *Nat Neurosci*, 9(10):1312–1320, 2006.

[17] H. Cuntz, J. Haag, F. Forstner, I. Segev, and A. Borst. Robust coding of flow-field parameters by axo-axonal gap junctions between fly visual interneurons. *Proc Natl Acad Sci U S A*, 104(24):10229–10233, 2007.

[18] B. Hassenstein and W. Reichardt. Systemtheoretische Analyse der Zeit, Reihenfolgen und Vorzeichenauswertung bei der Bewegungsperzeption des Rüsselkafers *Chlorophanus*. *Z Naturforsch*, 11(9-10):513–524, 1956.

[19] K. G. Goetz. Optomotorische Untersuchungen des visuellen Systems einiger Augenmutanten der Fruchtfliege *Drosophila*. *Kybernetik*, 2(2):77–92, 1964.

[20] K. G. Goetz. Die optischen Übertragungseigenschaften der Komplexaugen von *Drosophila*. *Kybernetik*, 2(5):215–221, 1965.

[21] M. Egelhaaf, A. Borst, and W. Reichardt. Computational structure of a biological motion-detection system as revealed by local detector analysis in the fly's nervous system. *J Opt Soc Am A*, 6(7):1070–1087, 1989.

[22] J. Haag, W. Denk, and A. Borst. Fly motion vision is based on reichardt detectors regardless of the signal-to-noise ratio. *Proc Natl Acad Sci U S A*, 101(46):16333–16338, 2004.

[23] N. J. Strausfeld. *Photoreception and Vision in Invertebrates*, chapter Functional Neuroanatomy of the Blowfly's Visual Sytem, pages 483–522. Plenum Publishing Corporation, 1984.

[24] J.K. Douglass and N.J. Strausfeld. Visual motion-detection circuits in flies: Peripheral motion computation by identified small-field retinotopic neurons. *J Neurosci*, 15:5596–5611, 1995.

[25] J.K. Douglass and N.J. Strausfeld. Visual motion-detection circuits in flies: Parallel direction- and non-direction-sensitive pathways between the medulla and lobula plate. *J Neurosci*, 16(15):4551–4562, 1996.

[26] C. Gilbert, D. K. Penisten, and R. D. DeVoe. Discrimination of visual motion from flicker by identified neurons in the medulla of the fleshfly sarcophaga bullata. *J Comp Physiol [A]*, 168(6):653–673, 1991.

[27] B. Bausenwein and K. F. Fischbach. Activity labeling patterns in the medulla of *Drosophila melanogaster* caused by motion stimuli. *Cell Tissue Res*, 270(1):25–35, 1992.

[28] M. Heisenberg and E. Buchner. The role of retinula cell types in visual behavior of *Drosophila melanogaster*. *J comp physiol*, 117:127–162, 1977.

[29] E. Buchner, S. Buchner, and I. Bulthoff. Deoxyglucose mapping of nervous activity induced in *Drosophila* brain by visual motion. *J Comp Physiol A*, 155:471–483, 1984.

[30] P. E. Coombe and M. Heisenberg. The structural brain mutant vacuolar medulla of *Drosophila melanogaster* with specific behavioral defects and cell degeneration in the adult. *J Neurogenet*, 3(3):135–158, 1986.

[31] M. Heisenberg, R. Wonneberger, and R. Wolf. Optomotor-blind (h31) - A *Drosophila melanogaster* mutant of the lobula plate giant neurons. *J Comp Physiol*, 124:287–296, 1978.

[32] J. Rister, D. Pauls, B. Schnell, C.-Y. Ting, C.-H. Lee, I. Sinakevitch, J. Morante, N.J. Strausfeld, and M. Heisenberg. Dissection of the peripheral motion channel in the visual system of *Drosophila melanogaster*. *Neuron*, 56:155–170, 2007.

[33] T. Euler, P.B. Detwiler, and W. Denk. Directionally selective calcium signals in dendrites of starburst amacrine cells. *Nature*, 418(6900):845–852, 2002.

[34] S.E. Hausselt, T. Euler, P.B. Detwiler, and W. Denk. A dendrite-autonomous mechanism for direction selectivity in retinal starburst amacrine cells. *PLoS Biol*, 5(7):e185, 2007.

[35] E.K. Scott, T. Raabe, and L.Q. Luo. Structure of the vertical and horizontal system neurons of the lobula plate in *Drosophila*. *J Comp Neurol*, 454(4):470–481, 2002.

[36] A. Miyawaki, J. Llopis, R. Heim, J.M. McCaffery, J.A. Adams, M. Ikura, and R.Y. Tsien. Fluorescent indicators for Ca^{2+} based on green fluorescent proteins and calmodulin. *Nature*, 388(6645):882–7, 1997.

[37] M.T. Hasan, R.W. Friedrich, T. Euler, M.E. Larkum, G. Giese, M. Both, J. Duebel, J. Waters, H. Bujard, O. Griesbeck, R.Y. Tsien, T. Nagai, A. Miyawaki, and W. Denk. Functional fluorescent Ca^{2+} indicator proteins in transgenic mice under tet control. *PLoS Biol*, 2(6):e163, 2004.

[38] T.A. Pologruto, R. Yasuda, and K. Svoboda. Monitoring neural activity and $[Ca^{2+}]$ with genetically encoded Ca^{2+} indicators. *J Neurosci*, 24(43):9572–9579, 2004.

[39] D.F. Reiff, A. Ihring, G. Guerrero, E.Y. Isacoff, M. Joesch, J. Nakai, and A. Borst. *In vivo* performance of genetically encoded indicators of neural activity in flies. *J Neurosci*, 25(19):4766–4778, 2005.

[40] T. Knopfel, J. Diez-Garcia, and W. Akemann. Optical probing of neuronal circuit dynamics: Genetically encoded versus classical fluorescent sensors. *Trends Neurosci*, 29(3):160–166, 2006.

[41] R. Araya, J. Jiang, K.B. Eisenthal, and R. Yuste. The spine neck filters membrane potentials. *Proc Natl Acad Sci U S A*, 103(47):17961–17966, 2006.

[42] G. Miesenbock, D.A. De Angelis, and J.E. Rothman. Visualizing secretion and synaptic transmission with ph-sensitive green fluorescent proteins. *Nature*, 394(6689):192–5, 1998.

[43] T. Kuner and G.J. Augustine. A genetically encoded ratiometric indicator for chloride: Capturing chloride transients in cultured hippocampal neurons. *Neuron*, 27(3):447–459, 2000.

[44] A. Minta and R. Y. Tsien. Fluorescent indicators for cytosolic sodium. *J Biol Chem*, 264(32):19449–19457, 1989.

[45] R.Y. Tsien. New calcium indicators and buffers with high selectivity against magnesium and protons - design, synthesis, and properties of prototype structures. *Biochemistry*, 19(11):2396–2404, 1980.

[46] R. Y. Tsien. Intracellular measurements of ion activities. *Annu Rev Biophys Bioeng*, 12:91–116, 1983.

[47] G. Grynkiewicz, M. Poenie, and R.Y. Tsien. A new generation of Ca^{2+} indicators with greatly improved fluorescence properties. *J Biol Chem*, 260(6):3440–3450, 1985.

[48] F. Lanni and H.E. Keller. *Imaging in Neuroscience and Development*, chapter 95, pages 740–741. CSHL Press, 2005.

[49] R.Y. Tsien. The green fluorescent protein. *Ann Rev Biochem*, 67:509–544, 1998.

[50] S. B. Savvin. Photometric estimation of thorium and uranium with the arsenazo ii reagent. *Doklady Akademii Nauk SSSR*, 127:1231–1234, 1959.

[51] J. E. Brown, P. K. Brown, and L. H. Pinto. Detection of light-induced changes of intracellular ionized calcium concentration in limulus ventral photoreceptors using arsenazo iii. *J Physiol*, 267(2):299–320, 1977.

[52] A. Minta, J. P. Kao, and R. Y. Tsien. Fluorescent indicators for cytosolic calcium based on rhodamine and fluorescein chromophores. *J Biol Chem*, 264(14):8171–8178, 1989.

[53] O. Shimomura, F. H. Johnson, and Y. Saiga. Extraction, purification and properties of aequorin, a bioluminescent protein from the luminous hydromedusan, aequorea. *J Cell Comp Physiol*, 59:223–239, 1962.

[54] D. G. Moisescu, C. C. Ashley, and A. K. Campbell. Comparative aspects of the calcium-sensitive photoproteins aequorin and obelin. *Biochim Biophys Acta*, 396(1):133–140, 1975.

[55] F. H. Johnson, O. Shimomura, and Y. Saiga. Action of cyanide on cypridina luciferin. *J Cell Comp Physiol*, 59:265–272, 1962.

[56] D. C. Prasher, V. K. Eckenrode, W. W. Ward, F. G. Prendergast, and M. J. Cormier. Primary structure of the aequorea victoria green-fluorescent protein. *Gene*, 111(2):229–233, 1992.

[57] M. Chalfie, Y. Tu, G. Euskirchen, W. W. Ward, and D. C. Prasher. Green fluorescent protein as a marker for gene expression. *Science*, 263(5148):802–805, 1994.

[58] H. Morise, O. Shimomura, F. H. Johnson, and J. Winant. Intermolecular energy transfer in the bioluminescent system of aequorea. *Biochemistry*, 13(12):2656–2662, 1974.

[59] F. Yang, L. G. Moss, and G. N. Phillips. The molecular structure of green fluorescent protein. *Nat Biotechnol*, 14(10):1246–1251, 1996.

[60] M. Ormo, A. B. Cubitt, K. Kallio, L. A. Gross, R. Y. Tsien, and S. J. Remington. Crystal structure of the aequorea victoria green fluorescent protein. *Science*, 273(5280):1392–1395, 1996.

[61] O. Griesbeck, G.S. Baird, R.E. Campbell, D.A. Zacharias, and R.Y. Tsien. Reducing the environmental sensitivity of yellow fluorescent protein. mechanism and applications. *J Biol Chem*, 276(31):29188–29194, 2001.

[62] T. Nagai, K. Ibata, E. S. Park, M. Kubota, K. Mikoshiba, and A. Miyawaki. A variant of yellow fluorescent protein with fast and efficient maturation for cell-biological applications. *Nat Biotechnol*, 20(1):87–90, 2002.

[63] R. Heim and R. Y. Tsien. Engineering green fluorescent protein for improved brightness, longer wavelengths and fluorescence resonance energy transfer. *Curr Biol*, 6(2):178–182, 1996.

[64] A. Miyawaki. Innovations in the imaging of brain functions using fluorescent proteins. *Neuron*, 48(2):189–199, 2005.

[65] M. A. Rizzo, G. H. Springer, B. Granada, and D. W. Piston. An improved cyan fluorescent protein variant useful for fret. *Nat Biotechnol*, 22(4):445–449, 2004.

[66] M. Mank, D.F. Reiff, N. Heim, M.W. Friedrich, A. Borst, and O. Griesbeck. A fret-based calcium biosensor with fast signal kinetics and high fluorescence change. *Biophys J*, 90(5):1790–1796, 2006.

[67] T. Nagai, S. Yamada, T. Tominaga, M. Ichikawa, and A. Miyawaki. Expanded dynamic range of fluorescent indicators for Ca^{2+} by circularly permuted yellow fluorescent proteins. *Proc Natl Acad Sci USA*, 101(29):10554–10559, 2004.

[68] V. A. Romoser, P. M. Hinkle, and A. Persechini. Detection in living cells of Ca^{2+}-dependent changes in the fluorescence emission of an indicator composed of two green fluorescent protein variants linked by a calmodulin-binding sequence. a new class of fluorescent indicators. *J Biol Chem*, 272(20):13270–13274, 1997.

[69] S. Shimozono, H. Hosoi, H. Mizuno, T. Fukano, T. Tahara, and A. Miyawaki. Concatenation of cyan and yellow fluorescent proteins for efficient resonance energy transfer. *Biochemistry*, 45(20):6267–6271, 2006.

[70] A.E. Palmer and R.Y. Tsien. Measuring calcium signaling using genetically targetable fluorescent indicators. *Nat Protoc*, 1(3):1057–1065, 2006.

[71] A.E. Palmer, M. Giacomello, T. Kortemme, S.A. Hires, V. Lev-Ram, D. Baker, and R.Y. Tsien. Ca^{2+} indicators based on computationally redesigned calmodulin-peptide pairs. *Chem Biol*, 13(5):521–530, 2006.

[72] N. Heim and O. Griesbeck. Genetically encoded indicators of cellular calcium dynamics based on troponin c and green fluorescent protein. *J Biol Chem*, 279(14):14280–14286, 2004.

[73] M. Ohkura, M. Matsuzaki, H. Kasai, K. Imoto, and J. Nakai. Genetically encoded bright Ca^{2+} probe applicable for dynamic Ca^{2+} imaging of dendritic spines. *Anal Chem*, 77(18):5861–5869, 2005.

[74] Y.N. Tallini, M. Ohkura, B.R. Choi, G. Ji, K. Imoto, R. Doran, J. Lee, P. Plan, J. Wilson, H.B. Xin, A. Sanbe, J. Gulick, J. Mathai, J. Robbins, G. Salama, J. Nakai, and M.I. Kotlikoff. Imaging cellular signals in the heart *in vivo*: Cardiac expression of the high-signal Ca^{2+} indicator gcamp2. *Proc Natl Acad Sci USA*, 103(12):4753–4758, 2006.

[75] A. Miyawaki, O. Griesbeck, R. Heim, and R.Y. Tsien. Dynamic and quantitative Ca^{2+} measurements using improved cameleons. *Proc Natl Acad Sci U S A*, 96(5):2135–40, 1999.

[76] G.S. Baird, D.A. Zacharias, and R.Y. Tsien. Circular permutation and receptor insertion within green fluorescent proteins. *Proc Natl Acad Sci U S A*, 96(20):11241–11246, 1999.

[77] D.A. Clark, C.V. Gabel, H. Gabel, and A.D.T. Samuel. Temporal activity patterns in thermosensory neurons of freely moving *Caenorhabditis elegans* encode spatial thermal gradients. *J Neurosci*, 27(23):6083–6090, 2007.

[78] A.E. Palmer, C. Jin, J.C. Reed, and R.Y. Tsien. Bcl-2-mediated alterations in endoplasmic reticulum Ca^{2+} analyzed with an improved genetically encoded fluorescent sensor. *Proc Natl Acad Sci USA*, 101(50):17404–17409, 2004.

[79] A. M. Gordon, E. Homsher, and M. Regnier. Regulation of contraction in striated muscle. *Physiol Rev*, 80(2):853–924, 2000.

[80] O. Garaschuk, O. Griesbeck, and A. Konnerth. Troponin c-based biosensors: A new family of genetically encoded indicators for *in vivo* calcium imaging in the nervous system. *Cell Calcium*, 42(4-5):351–361, 2007.

[81] D. Yu, G.S. Baird, R.Y. Tsien, and R.L. Davis. Detection of calcium transients in *Drosophila melanogaster* mushroom body neurons with camgaroo reporters. *J Neurosci*, 23(1):64–72, 2003.

[82] T. Nagai, A. Sawano, E.S. Park, and A. Miyawaki. Circularly permuted green fluorescent proteins engineered to sense Ca^{2+}. *Proc Natl Acad Sci USA*, 98(6):3197–3202, 2001.

[83] V. Robert, P. Gurlini, V. Tosello, T. Nagai, A. Miyawaki, F. Di Lisa, and T. Pozzan. Beat-to-beat oscillations of mitochondrial $[Ca^{2+}]$ in cardiac cells. *EMBO J*, 20(17):4998–5007, 2001.

[84] S. Shimozono, T. Fukano, T. Nagai, Y. Kirino, H. Mizuno, and A. Miyawaki. Confocal imaging of subcellular Ca^{2+} concentrations using a dual-excitation ratiometric indicator based on green fluorescent protein. *Sci STKE*, 2002(125):L4–, 2002.

[85] J. Nakai, M. Ohkura, and K. Imoto. A high signal-to-noise Ca^{2+} probe composed of a single green fluorescent protein. *Nat Biotechnol*, 19(2):137–141, 2001.

[86] Y. Peng and A. Guo. Novel stimulus-induced calcium efflux in *Drosophila* mushroom bodies. *Eur J Neurosci*, 25(7):2034–2044, 2007.

[87] D. Yu, A.C. Keene, A. Srivatsan, S. Waddell, and R.L. Davis. Drosophila dpm neurons form a delayed and branch-specific memory trace after olfactory classical conditioning. *Cell*, 123(5):945–957, 2005.

[88] J.W. Wang, A.M. Wong, J. Flores, L.B. Vosshall, and R. Axel. Two-photon calcium imaging reveals an odor-evoked map of activity in the fly brain. *Cell*, 112(2):271–282, 2003.

[89] G. Ji, M.E. Feldman, K.Y. Deng, K.S. Greene, J. Wilson, J.C. Lee, R.C. Johnston, M. Rishniw, Y. Tallini, J. Zhang, W.G. Wier, M.P. Blaustein, H.B. Xin, J. Nakai, and M.I. Kotlikoff. Ca^{2+}-sensing transgenic mice: Postsynaptic signaling in smooth muscle. *J Biol Chem*, 279(20):21461–21468, 2004.

[90] J. Diez-Garcia, W. Akemann, and T. Knopfel. *In vivo* calcium imaging from genetically specified target cells in mouse cerebellum. *Neuroimage*, 34(3):859–869, 2007.

[91] M.I. Kotlikoff. Genetically encoded Ca^{2+} indicators: Using genetics and molecular design to understand complex physiology. *J Physiol*, 578(Pt 1):55–67, 2007.

[92] A. Fiala, T. Spall, S. Diegelmann, B. Eisermann, S. Sachse, J.M. Devaud, E. Buchner, and C.G. Galizia. Genetically expressed cameleon in *Drosophila melanogaster* is used to visualize olfactory information in projection neurons. *Curr Biol*, 12(21):1877–84, 2002.

[93] D.F. Reiff, P.R. Thiel, and C.M. Schuster. Differential regulation of active zone density during long-term strengthening of *Drosophila* neuromuscular junctions. *J Neurosci*, 22(21):9399–409, 2002.

[94] R. Kerr, V. Lev-Ram, G. Baird, P. Vincent, R. Y. Tsien, and W. R. Schafer. Optical imaging of calcium transients in neurons and pharyngeal muscle of *C. elegans*. *Neuron*, 26(3):583–594, 2000.

[95] N. Heim, O. Garaschuk, M.W. Friedrich, M. Mank, R.I. Milos, Y. Kovalchuk, A. Konnerth, and O. Griesbeck. Improved calcium imaging in transgenic mice expressing a troponin c-based biosensor. *Nat Methods*, 4(2):127–129, 2007.

[96] H. Keshishian, A. Chiba, T. N. Chang, M. S. Halfon, E. W. Harkins, J. Jarecki, L. Wang, M. Anderson, S. Cash, and M. E. Halpern. Cellular mechanisms governing synaptic development in *Drosophila melanogaster*. *J Neurobiol*, 24(6):757–787, 1993.

[97] A. Prokop and I.A. Meinertzhagen. Development and structure of synaptic contacts in *Drosophila*. *Semin Cell Dev Biol*, 17(1):20–30, 2006.

[98] L. Y. Jan and Y. N. Jan. Properties of the larval neuromuscular junction in *Drosophila melanogaster*. *J Physiol*, 262(1):189–214, 1976.

[99] K. S. Broadie and M. Bate. Development of the embryonic neuromuscular synapse of *Drosophila melanogaster*. *J Neurosci*, 13(1):144–166, 1993.

[100] K. Broadie and M. Bate. Innervation directs receptor synthesis and localization in *Drosophila* embryo synaptogenesis. *Nature*, 361(6410):350–353, 1993.

[101] A. Prokop, M. Landgraf, E. Rushton, K. Broadie, and M. Bate. Presynaptic development at the *Drosophila* neuromuscular junction: assembly and localization of presynaptic active zones. *Neuron*, 17(4):617–626, 1996.

[102] H. Keshishian, T. N. Chang, and J. Jarecki. Precision and plasticity during *Drosophila* neuromuscular development. *FASEB J*, 8(10):731–737, 1994.

[103] B. Hoang and A. Chiba. Single-cell analysis of *Drosophila* larval neuromuscular synapses. *Dev Biol*, 229(1):55–70, 2001.

[104] R. Schneggenburger and E. Neher. Presynaptic calcium and control of vesicle fusion. *Curr Opin Neurobiol*, 15(3):266–274, 2005.

[105] J.W. Barclay, H.L. Atwood, and R.M. Robertson. Impairment of central pattern generation in *Drosophila* cysteine string protein mutants. *J Comp Physiol A*, 188(1):71–78, 2002.

[106] H. M. Gerschenfeld. Chemical transmission in invertebrate central nervous systems and neuromuscular junctions. *Physiol Rev*, 53(1):1–119, 1973.

[107] L. Y. Jan and Y. N. Jan. L-glutamate as an excitatory transmitter at the *Drosophila* larval neuromuscular junction. *J Physiol*, 262(1):215–236, 1976.

[108] T. Schikorski and C. F. Stevens. Quantitative fine-structural analysis of olfactory cortical synapses. *Proc Natl Acad Sci U S A*, 96(7):4107–4112, 1999.

[109] T. Schikorski and C.F. Stevens. Quantitative ultrastructural analysis of hippocampal excitatory synapses. *J Neurosci*, 17(15):5858–5867, 1997.

[110] B.L. Sabatini, T. G. Oertner, and K. Svoboda. The life cycle of Ca^{2+} ions in dendritic spines. *Neuron*, 33(3):439–452, 2002.

[111] A. Borst and H. D. I. Abarbanel. Relating a calcium indicator signal to the unperturbed calcium concentration time-course. *Theor Biol Med Model*, 4:7, 2007.

[112] G.T. Macleod, M. Hegstrom-Wojtowicz, M.P. Charlton, and H.L. Atwood. Fast calcium signals in *Drosophila* motor neuron terminals. *J Neurophysiol*, 88(5):2659–2663, 2002.

[113] G.A. Lnenicka, J. Grizzaffi, B. Lee, and N. Rumpal. Ca^{2+} dynamics along identified synaptic terminals in *Drosophila* larvae. *J Neurosci*, 26(47):12283–12293, 2006.

[114] W. Denk, J.H. Strickler, and W.W. Webb. Two-photon laser scanning fluorescence microscopy. *Science*, 248(4951):73–76, 1990.

[115] W.R. Zipfel, R.M. Williams, and W.W. Webb. Nonlinear magic: Multiphoton microscopy in the biosciences. *Nat Biotechnol*, 21(11):1369–1377, 2003.

[116] K. Svoboda and R. Yasuda. Principles of two-photon excitation microscopy and its applications to neuroscience. *Neuron*, 50(6):823–839, 2006.

[117] A.C. Spradling and G.M. Rubin. Transposition of cloned p elements into *Drosophila* germ line chromosomes. *Science*, 218(4570):341–347, 1982.

[118] A.H. Brand and N. Perrimon. Targeted gene expression as a means of altering cell fates and generating dominant phenotypes. *Development*, 118(2):401–15, 1993.

[119] J. Bischof, R.K. Maeda, M. Hediger, F. Karch, and K. Basler. An optimized transgenesis system for *Drosophila* using germ-line-specific phic31 integrases. *Proc Natl Acad Sci U S A*, 104(9):3312–3317, 2007.

[120] L. Pick, A. Schier, M. Affolter, T. Schmidt-Glenewinkel, and W. J. Gehring. Analysis of the ftz upstream element: Germ layer-specific enhancers are independently autoregulated. *Genes Dev*, 4(7):1224–1239, 1990.

[121] L. Sipos and H. Gyurkovics. Long-distance interactions between enhancers and promoters. *FEBS J*, 272(13):3253–3259, 2005.

[122] T. Lee and L. Luo. Mosaic analysis with a repressible cell marker for studies of gene function in neuronal morphogenesis. *Neuron*, 22(3):451–461, 1999.

[123] S. E. McGuire, P. T. Le, A. J. Osborn, K. Matsumoto, and R. L. Davis. Spatiotemporal rescue of memory dysfunction in *Drosophila*. *Science*, 302(5651):1765–1768, 2003.

[124] D. Szuts and M. Bienz. Lexa chimeras reveal the function of *Drosophila* fos as a context-dependent transcriptional activator. *Proc Natl Acad Sci U S A*, 97(10):5351–5356, 2000.

[125] S.L. Lai and T. Lee. Genetic mosaic with dual binary transcriptional systems in *Drosophila*. *Nat.Neurosci.*, 9(5):703–709, 2006.

[126] A. Keller, S.T. Sweeney, T. Zars, C.J. O'Kane, and M. Heisenberg. Targeted expression of tetanus neurotoxin interferes with behavioral responses to sensory input in *Drosophila*. *J Neurobiol*, 50(3):221–33, 2002.

[127] T. Kitamoto. Conditional modification of behavior in *Drosophila* by targeted expression of a temperature-sensitive shibire allele in defined neurons. *J Neurobiol*, 47(2):81–92, 2001.

[128] M. Schwaerzel, M. Monastirioti, H. Scholz, F. Friggi-Grelin, S. Birman, and M. Heisenberg. Dopamine and octopamine differentiate between aversive and appetitive olfactory memories in *Drosophila*. *J Neurosci*, 23(33):10495–502, 2003.

[129] R. A. Baines, J. P. Uhler, A. Thompson, S. T. Sweeney, and M. Bate. Altered electrical properties in *Drosophila* neurons developing without synaptic transmission. *J Neurosci*, 21(5):1523–1531, 2001.

[130] B. H. White, T. P. Osterwalder, K. S. Yoon, W. J. Joiner, M. D. Whim, L. K. Kaczmarek, and H. Keshishian. Targeted attenuation of electrical activity in *Drosophila* using a genetically modified k(+) channel. *Neuron*, 31(5):699–711, 2001.

[131] D.M. Lin and C.S. Goodman. Ectopic and increased expression of fasciclin ii alters motoneuron growth cone guidance. *Neuron*, 13(3):507–523, 1994.

[132] S. Kerscher, S. Albert, D. Wucherpfennig, M. Heisenberg, and S. Schneuwly. Molecular and genetic analysis of the *Drosophila* mas-1 (mannosidase-1) gene which encodes a glycoprotein processing alpha 1,2-mannosidase. *Dev Biol*, 168(2):613–626, 1995.

[133] S. Hayashi, K. Ito, Y. Sado, M. Taniguchi, A. Akimoto, H. Takeuchi, T. Aigaki, F. Matsuzaki, H. Nakagoshi, T. Tanimura, R. Ueda, T. Uemura, M. Yoshihara, and S. Goto. Getdb, a database compiling expression patterns and molecular locations of a collection of gal4 enhancer traps. *Genesis.*, 34(1-2):58–61, 2002.

[134] G.T. Macleod, L. Marin, M.P. Charlton, and H.L. Atwood. Synaptic vesicles: Test for a role in presynaptic calcium regulation. *J Neurosci*, 24(10):2496–2505, 2004.

[135] M. Wachowiak, W. Denk, and R.W. Friedrich. Functional organization of sensory input to the olfactory bulb glomerulus analyzed by two-photon calcium imaging. *Proc Natl Acad Sci USA*, 101(24):9097–9102, 2004.

[136] G.H. Patterson, D.W. Piston, and B.G. Barisas. Forster distances between green fluorescent protein pairs. *Anal Biochem*, 284(2):438–440, 2000.

[137] M. Maravall, Z.F. Mainen, B.L. Sabatini, and K. Svoboda. Estimating intracellular calcium concentrations and buffering without wavelength ratioing. *Biophys J*, 78(5):2655–2667, 2000.

[138] G.T. Macleod, M.L. Suster, M.P. Charlton, and H.L. Atwood. Single neuron activity in the *Drosophila* larval cns detected with calcium indicators. *J Neurosci Methods*, 127(2):167–178, 2003.

[139] B. Chanda, R. Blunck, L.C. Faria, F.E. Schweizer, I. Mody, and F. Bezanilla. A hybrid approach to measuring electrical activity in genetically specified neurons. *Nat Neurosci*, 8(11):1619–1626, 2005.

[140] J. M. Fernandez, R. E. Taylor, and F. Bezanilla. Induced capacitance in the squid giant axon. lipophilic ion displacement currents. *J Gen Physiol*, 82(3):331–346, 1983.

[141] S. Komai, W. Denk, P. Osten, M. Brecht, and T.W. Margrie. Two-photon targeted patching (tptp) *in vivo*. *Nat Protoc*, 1(2):647–652, 2006.

[142] T.W. Margrie, A.H. Meyer, A. Caputi, H. Monyer, M.T. Hasan, A.T. Schaefer, W. Denk, and M. Brecht. Targeted whole-cell recordings in the mammalian brain *in vivo*. *Neuron*, 39(6):911–918, 2003.

[143] Z.G. Xia and D.R. Storm. The role of calmodulin as a signal integrator for synaptic plasticity. *Nat Rev Neurosci*, 6(4):267–276, 2005.

[144] M.X. Mori, M.G. Erickson, and D.T. Yue. Functional stoichiometry and local enrichment of calmodulin interacting with Ca^{2+} channels. *Science*, 304(5669):432–435, 2004.

[145] D. Thomas, S. C. Tovey, T. J. Collins, M. D. Bootman, M. J. Berridge, and P. Lipp. A comparison of fluorescent Ca^{2+} indicator properties and their use in measuring elementary and global Ca^{2+} signals. *Cell Calcium*, 28(4):213–223, 2000.

[146] J.N. Weiss. The hill equation revisited: Uses and misuses. *FASEB J*, 11(11):835–841, 1997.

[147] D.W. Tank, W.G. Regehr, and K.R. Delaney. A quantitative analysis of presynaptic calcium dynamics that contribute to short-term enhancement. *J Neurosci*, 15(12):7940–7952, 1995.

[148] F. Helmchen, K. Imoto, and B. Sakmann. Ca^{2+} buffering and action potential-evoked Ca^{2+} signaling in dendrites of pyramidal neurons. *Biophys J*, 70(2):1069–1081, 1996.

[149] H.J. Koester and B. Sakmann. Calcium dynamics associated with action potentials in single nerve terminals of pyramidal cells in layer 2/3 of the young rat neocortex. *J Physiol*, 529 Pt 3:625–646, 2000.

[150] K.L. Rogers, S. Picaud, E. Roncali, R. Boisgard, C. Colasante, J. Stinnakre, B. Tavitian, and P. Brulet. Non-invasive *in vivo* imaging of calcium signaling in mice. *PLoS ONE*, 2(10):e974, 2007.

[151] M.J. Berridge, M.D. Bootman, and H.L. Roderick. Calcium signalling: Dynamics, homeostasis and remodelling. *Nat Rev Mol Cell Biol*, 4(7):517–529, 2003.

[152] B. Schwaller, J. Dick, G. Dhoot, S. Carroll, G. Vrbova, P. Nicotera, D. Pette, A. Wyss, H. Bluethmann, W. Hunziker, and M. R. Celio. Prolonged contraction-relaxation cycle of fast-twitch muscles in parvalbumin knockout mice. *Am J Physiol*, 276(2 Pt 1):C395–C403, 1999.

[153] J.M. Colomer, M. Terasawa, and A.R. Means. Targeted expression of calmodulin increases ventricular cardiomyocyte proliferation and deoxyribonucleic acid synthesis during mouse development. *Endocrinology*, 145(3):1356–1366, 2004.

[154] O. Tour, S.R. Adams, R.A. Kerr, R.M. Meijer, T.J. Sejnowski, R.W. Tsien, and R.Y. Tsien. Calcium green flash as a genetically targeted small-molecule calcium indicator. *Nat Chem Biol*, 3(7):423–431, 2007.

[155] G. Guerrero, D.F. Reiff, G. Agarwal, R.W. Ball, A. Borst, C.S. Goodman, and E.Y. Isacoff. Heterogeneity in synaptic transmission along a *Drosophila* larval motor axon. *Nat Neurosci*, 8(9):1188–1196, 2005.

[156] M.Y. Lee, H. Song, J. Nakai, M. Ohkura, M.I. Kotlikoff, S.P. Kinsey, V.A. Golovina, and M.P. Blaustein. Local subplasma membrane Ca^{2+} signals detected by a tethered Ca^{2+} sensor. *Proc Natl Acad Sci USA*, 103(35):13232–13237, 2006.

[157] W. Denk and K. Svoboda. Two-photon upmanship: Why multiphoton imaging is more than a gimmick. *Neuron*, 18(3):351–357, 1997.

[158] A. Borst and M. Egelhaaf. *In vivo* imaging of calcium accumulation in fly interneurons as elicited by visual motion stimulation. *Proc Natl Acad Sci U S A*, 89(9):4139–4143, 1992.

[159] J. Haag and A. Borst. Spatial distribution and characteristics of voltage-gated calcium signals within visual interneurons. *J Neurophysiol*, 83(2):1039–1051, 2000.

[160] S. Single and A. Borst. Different mechanisms of calcium entry within different dendritic compartments. *J Neurophysiol*, 87(3):1616–1624, 2002.

[161] A. Borst and S. Single. Local current spread in electrically compact neurons of the fly. *Neurosci Lett*, 285(2):123–126, 2000.

[162] T. M. Brotz and A. Borst. Cholinergic and gabaergic receptors on fly tangential cells and their role in visual motion detection. *J Neurophysiol*, 76(3):1786–1799, 1996.

[163] T. M. Brotz, E. D. Gundelfinger, and A. Borst. Cholinergic and gabaergic pathways in fly motion vision. *BMC Neurosci*, 2:1, 2001.

[164] T. G. Oertner, T. M. Brotz, and A. Borst. Mechanisms of dendritic calcium signaling in fly neurons. *J Neurophysiol*, 85(1):439–447, 2001.

[165] A. Borst, V. L. Flanagin, and H. Sompolinsky. Adaptation without parameter change: Dynamic gain control in motion detection. *Proc Natl Acad Sci U S A*, 102(17):6172–6176, 2005.

[166] A. Borst, C. Reisenman, and J. Haag. Adaptation of response transients in fly motion vision II: Model studies. *Vision Res*, 43(11):1309–1322, 2003.

[167] C. Reisenman, J. Haag, and A. Borst. Adaptation of response transients in fly motion vision. i: Experiments. *Vision Res*, 43(11):1291–1307, 2003.

[168] R. K. Maeda and F. Karch. The abc of the bx-c: The bithorax complex explained. *Development*, 133(8):1413–1422, 2006.

[169] V.E. Belozerov, P. Majumder, P. Shen, and H.N. Cai. A novel boundary element may facilitate independent gene regulation in the antennapedia complex of *Drosophila*. *EMBO J*, 22(12):3113–3121, 2003.

[170] S.B. Laughlin and D. Osorio. Mechanisms for neural signal enhancement in the blowfly compound eye. *J Exp Biol*, 144:113–146, 1989.

[171] R. C. Hardie and M. Weckstrom. Three classes of potassium channels in large monopolar cells of the blowfly *Calliphora vicina*. *J Comp Physiol A*, 167:723–736, 1990.

[172] B. Bausenwein, A. P. Dittrich, and K. F. Fischbach. The optic lobe of *Drosophila melanogaster* II. sorting of retinotopic pathways in the medulla. *Cell Tissue Res*, 267(1):17–28, 1992.

[173] C.M. Higgins, J.K. Douglass, and N.J. Strausfeld. The computational basis of an identified neuronal circuit for elementary motion detection in dipterous insects. *Vis Neurosci*, 21(4):567–586, 2004.

[174] I. Sinakevitch and N. J. Strausfeld. Chemical neuroanatomy of the fly's movement detection pathway. *J Comp Neurol*, 468(1):6–23, 2004.

[175] H.B. Barlow and W.R. Levick. The mechanism of directionally selective units in rabbit's retina. *J Physiol*, 178(3):477–504, 1965.

Acknowledgement

Many people helped in many different ways to get this work done - by teaching techniques, sharing materials or experience, or by doing things I couldn't do, or by means that are only indirectly linked to work. The list of people I mention here is neither complete nor does the sequence express how much I appreciate these peoples contributions.

I want to thank my supervisor and friend Dierk Reiff for hiring me for a project in which almost every technique was new to me and thus for all support, advice, teaching and development, generosity in sharing figures for talks and this thesis and also for everything outside the institute. I want to thank my Doktorvater Alexander Borst for giving me the opportunity to work in such a splendid social and scientifically superb atmosphere, for his help in many things, his loyalty as a group leader, for discussions, and his superfast programming services.

I thank Wolfgang Essbauer for a lot of cloning work and teaching, for his time, nerve and involvement and for flycare, and Christian Theile for flycare, iPCRs and garlic.

I want to thank Marco Mank and Oliver Griesbeck for a collaboration, that made this work conclusive, and enabled the experiments we care most about. I thank Gaia Tavosanis for helpful advice and being part of my thesis committee and Ewa Koper in her lab for sharing data. I want to thank Florain Büsch and Thomas Carell for synthesizing the Dipikrylamin, that was unfortunatly poisonous and Eva-Maria Jahn for sharing another potential voltage sensor.

I want to thank Yihai Elyada, Friedrich Forstner, Deusdedit Spavieri, Virginia Flannagin, Nina Maack and Franz Weber for teaching, help and code in Matlab and LaTex, both of which I would not have learned without them. Also I want to thank Alexandra Ihring for teaching me the larval preparation, Shamprassad Raghu for sharing pictures and flies, his help and his smile, Ilona Kadow for some very good cloning advice and Takashi Suzuki for sharing flies, plasmids and knowhow.

I want to thank Max Joesch for his energy, rocks, apperitivos, south america and the fly prep for the most exciting experiment in this thesis, Karl Farrow for advice and making

Curriculum Vitae

Thomas Hendel, geboren 15. Oktober 1975 in Buchen / Odw.

06/1995 Abitur	am Simon Marius Gymnasium in Gunzenhausen
10/1995-12/1996 Zivildienst	bei der Caritas e.V. Freiburg i.Br.
10/1997-04/2003 Studium der Biologie	an der Julius Maximilian Universtität in Würzburg
bis 04/2003 Diplomarbeit	in Genetik & Neurobiologie bei Prof. Martin Heisenberg und Dr. Bertram Gerber: "Appetitive, but no aversive olfactory learning in fruit fly larvae."
05/2003-08/2003 Gastforscher	an der University of Toronto at Mississauga bei Prof. Marla Sokolowski
09/2003-03/2004 Doktorarbeit	im Lehrstuhl für Genetik & Neurobiologie bei Prof. Martin Heisenberg und Dr. Bertram Gerber: "Olfactory Re-cognition in *Drosophila*."
seit 04/2004 Doktorarbeit	am MPI für Neurobiologie, Abteilung fuer Neuronale Informationsverarbeitung, bei Prof. Alexander Borst und Dr. Dierk F. Reiff

Versicherung

Ehrenwörtliche Versicherung

Ich versichere hiermit ehrenwörtlich, dass die vorgelegte Dissertation von mir selbständig und ohne unerlaubte Hilfe angefertigt ist.

München, den

(Unterschrift)

Erklärung

Hiermit erkläre ich, dass die Dissertation nicht ganz oder in wesentlichen Teilen einer anderen Prüfungskommission vorgelegt worden ist und dass ich mich anderweitig einer Doktorprüfung ohne Erfolg nicht unterzogen habe.

München, den

(Unterschrift)